POLITECNICO DI TORINO

Corso di Laurea Magistrale

in Ingegneria Biomedica

Tesi di Laurea Magistrale

Repair, impact behaviour and fracture toughness in shells of Patella vulgata

Relatore

Prof. Cristina Bignardi

firma del relatore

. . . .

Candidato

Riccardo Mala

firma del candidato

. . . .

A.A. 2017/2018

Dedication

To my mother, my father and my little brother,

shamefully neglected but so desperately loved.

Table of contents

List of Figures

List of Tables

1 Sommario

La storia dell'uomo è costellata da tentativi di imitazione della natura e dei suoi principi. La storia dell'aviazione rappresenta un lampante esempio di tale fenomeno. Grazie agli studi compiuti da Leonardo Da Vinci sulle ali di pipistrello e a quelli dei moltissimi che lo hanno seguito con studi e sperimentazioni nel campo del volo, oggi possiamo usufruire di aerei in grado di volare ben più in alto e per molto più tempo di quanto sia in grado di fare un qualsiasi uccello. In natura nulla è dato al caso. Alcuni studiosi del secolo scorso se ne sono accorti, riscoprendo un mondo di infinite opportunità celato dietro al concetto di biomimetica e spendendo sempre più ore a studiare ad esempio perché la natura si sia evoluta in una certa direzione piuttosto che in una altra o perché le strutture biologiche abbiano sviluppato certe caratteristiche e proprietà specifiche.

Fra le infinite strutture le cui proprietà hanno attratto l'attenzione nel campo dell'ingegneria, ci sono anche le conchiglie dei Molluschi, ed in particolare un materiale noto come madre perla che costituisce uno degli strati interni di alcune specie di Gasteropodi e Bivalvi. Tale materiale è in grado di combinare fragilità a elevati valori di carico rottura e tenacità a frattura. Tale comportamento costituisce la ragione per cui in letteratura si possono trovare numerosi studi mirati a realizzare materiali innovativi in grado di replicarne l'organizzazione interna. Si ritiene infatti sia quest'ultima la causa principale delle ottime prestazioni del materiale. In realtà, tuttavia, le conchiglie della maggior parte delle specie di Gasteropodi e Bivalvi non contengono alcuno strato di madre perla. Al suo posto è presente una complessa struttura gerarchica basata sull'alternanza di calcite e aragonite, entrambe forme di carbonato di calcio. Risulta interessante, studiare il comportamento meccanico di tali strutture al fine di comprendere il motivo che ha condotto la natura a preferirle rispetto a quelle basate su madre perla, considerando le migliori le prestazioni meccaniche di queste ultime. Fra le specie prive di madre perla compare la Patella vulgata.

Lo scopo della conchiglia di Patella vulgata, specie analizzata nel presente studio, è quello di proteggere i tessuti molli dell'animale, tenendolo al riparo da attacchi predatori, disidratazione e traumi accidentali. Questa specie è la più comune fra quelle che popolano le coste Irlandesi ed è caratterizzata da una struttura fortemente eterogenea, oltre che da un efficace sistema di auto-riparazione del danno. L'analisi delle più rilevanti caratteristiche meccaniche della conchiglia, quali l'abilità di autoripararsi, la sua risposta a impatto (singolo o multipli) e la tenacità a frattura,

sono analizzate facendo ricorso sia ad un approccio sperimentale che ad uno computazionale. Valutazioni precedenti sono state effettuate da Taylor([47], [52]), in merito a resilienza, comportamento a fatica per impatti successivi e tenacità a frattura in direzione circonferenziale.

La prima parte del lavoro è concentrata sull'abilità delle conchiglie di Patella vulgata di ripristinare la loro resilienza iniziale, dopo essere state danneggiate meccanicamente in vario modo. Un'indagine aggiuntiva è portata avanti su come la creazione di un foro nella regione apicale della conchiglia e la sua posizione condizionino la resilienza dell'intera struttura. Sebbene dopo due mesi il processo di riparazione sia avvenuto con successo in termini di risposta all'impatto in tutte le tipologie di danno procurato, differenti sono le dinamiche di recupero osservate. Le conchiglie perforate in zona apicale sperimentano tutte una caduta improvvisa nelle prestazioni meccaniche, senza però produrre significative differenze in funzione della posizione del foro.

Un ulteriore argomento di studio è rappresentato delle prestazioni a fatica delle patelle, in funzione dell'applicazione di impatti consecutivi e impatti ciclici. Questi ultimi sono particolarmente rilevanti in quanto simulano molto meglio il comportamento naturale delle patelle, che in condizioni normali non vengono colpite in sequenza. Più realisticamente impatti successivi avvengono a giorni o settimane di distanza fra loro; tempo sufficiente per mettere in atto meccanismi di autoriparazione. Il risultato per impatti successivi conferma lo scarso comportamento a fatica del materiale già osservato in uno studio precedente[47]. L'applicazione di impatti ciclici sembra invece indicare un miglioramento delle prestazioni a fatica, nonostante le pesanti limitazioni nello studio effettuato.

Al fine di validare i risultati ottenuti mediante compressione ed impatto, simulazioni statiche e dinamiche sono state effettuate facendo ricorso al metodo degli elementi finiti (FEM). Il modello realizzato si è dimostrato affidabile nel descrivere il comportamento della struttura, non solamente fornendo un valido supporto alla descrizione dei meccanismi di generazione del danno e successivo fallimento, ma anche trovando una corrispondenza con forma e disomogeneità tipiche delle conchiglie. Le simulazioni effettuate mostrano inoltre come alcuni parametri di modello, quali lo stato di attrito fra conchiglia e supporto, influenzino considerevolmente il comportamento della struttura.

Nell'ultima parte dello studio si pone invece l'attenzione sulla tenacità a frattura delle patelle, facendo uso di due differenti approcci: il primo mira a valutare la tenacità a frattura in termini di delaminazione, mentre il secondo propone una stima in direzione radiale facendo nuovamente uso dell'approccio computazionale tramite FEM. Se il primo metodo ha consentito di ottenere un valore di G_c pari a $142.61 J/m^2$, il secondo invece ha prodotto una sovrastima del valore reale, risultando per tanto inaffidabile. Se tuttavia quest'ultimo approccio non ha consentito di ottenere un risultato quantitativo affidabile, da un punto di vista qualitativo è invece osservabile un buon livello di corrispondenza con i risultati sperimentali.

2 Abstract

Human history is littered with attempts to imitate nature and its principles. Aviation history is a major example. The interest of Leonardo Da Vinci in bat wings, followed by several studies and experimentation brought us the present planes, able to fly higher and longer than any existing bird. Nature, in every little detail, has developed in a certain way for a reason. Scientists in modern age realized the infinite opportunities that lie behind the world of biomimetics, spending more and more time in understanding why nature evolved in a certain direction and why biological structures developed specific features and properties.

One of the countless examples of structures that earned the attention of engineers is represented by Molluscs shell, and in particular a material called nacre that constitutes the internal layer of some species of Gastropoda and Bivalvia. Mostly known as mother of pearl, it is a composite material that combines high brittleness with enhanced strength and toughness. These are the reasons why it is widely studied and several attempts have been made to replicate its structure, which is responsible for all its interesting properties. Most of the Gastropoda and Bivalvia shells however, do not count on a nacreous layer in their shell; a complex hierarchical structure based on calcite and aragonite is present instead. It is interesting then to investigate the mechanical properties of one of these molluscs that do not contain nacre in their structure in order to understand why nature preferred them for the majority of the species, despite the apparent lower performances.

The purpose of the shell of Patella vulgata limpet, the species chosen for the present study, is to protect the animals soft tissues, concealing it from external dangers like predation, dehydration and accidental trauma. Characterized by an extremely heterogeneous structure and by an efficient repairing ability from accidental damage, this specie is the most common mollusc populating Irish coasts. Both experimental and computational approaches are adopted in order to better investigate some of the most interesting features of the shell, such as: repairing ability, impact behaviour (single or multiple impacts) and fracture toughness. All the data related to these topics were obtained by Professor Taylor([47], [52]), mostly regarding impact strength, impact fatigue and circumferential toughness.

The first part of this work is focused on the abilities of limpets damaged in different ways, to

heal themselves in terms of ability to restore their initial impact strength. Further investigations are then addressed upon how a hole pierced in the apex region and its exact location affects the impact performance of the specimen. The recovery of the mechanical properties after two months shows different dynamics for different damages; all of them however show effective healing process and highlights how impact strength is step by step restored. Pierced specimens on the other hand, experienced a sudden drop in the impact performances, but no meaningful difference is observed modifying is location.

The second part is focused on the impact fatigue performances of limpets shells as consecutive or cyclical strikes are applied. The last is an effort to better simulate natural conditions, since limpets in their environment are not used to experience many impacts in a row; some time passes between an impact and the following one, so that repairing can eventually affect the results of the test. The results for the consecutive impact tests simply confirmed limpets' poor behaviour already seen in previous study[47]. The results for the cyclical impact tests instead move in the direction of improved fatigue performances, although they are affected by relevant limitations.

The implementation of a FEM static and a dynamic model is performed in order to validate the experimental findings obtained during impact and compression tests. The model proved to be reliable in terms of structure behaviour when loaded both in static and dynamic conditions, not only identifying the damage and failure mechanisms but even nicely matching with shell irregular shape and heterogeneity. No relevant information are obtained by the comparison between the static and the dynamic condition. The model showed a great sensibility on some parameters of the system, like the friction coefficient adapted for the contact between shell and support.

Finally the last part is related to further investigations of shell toughness following two separate approaches. The first one aims to correct the delamination toughness assessment performed in an earlier stage of the study, while the second required the use of a computational model in order to retrieve an estimate for the toughness in the radial direction. If the first method allowed to obtain a reliable value of G_c of $142.61 J/m^2$, the second one produced a physically meaningful but unrealistic value. It can be therefore concluded that this approach does not give useful solutions. If a quantitative evaluation is not possible, a qualitative one shows interesting results that matches with the experimental findings.

3 Introduction

The subject of the present work is to investigate from an engineering point of view some of the most interesting mechanical properties of Patella vulgata. *"Why has it has been chosen to study these shells?"* This might be the question arising while reading the title of this study. In order to give an answer to such a question it is required to take one step back to properly introduce the field of biomimetics that is at the base of the whole work.

3.1 Overview

Biomimetics can be defined as the science that studies nature's methods, mechanisms and processes[1] and tries to replicate them. As many scientific terms biomimetics comes from the combination of two Greek words: *"bio"* that means life and *"mimesis"* that means to imitate[2]. The concept behind it is simply that human history compared to the one of planet earth is only the last brief chapter. In millions of years before human race even existed, nature gained a tremendous advantage in developing complex structures able to solve the most extreme tasks. Even though human technologies made giant step forwards in the last century, nature still represents a benchmark for a wide variety of behaviours.

In the present work biomimetics is discussed strictly for its engineering applications, it is however a genuinely interdisciplinary subject, heavily studied nowadays for architectural and design purposes too. The term biomimetics has been coined by the physics and electrical engineer Otto Schmitt in 1957, who first used it in his paper "Some interesting and useful biomimetic transformation" in 1969. Considered a prominent figure in the field, Schmitt experimented himself the principles of biomimetics studying nervous systems of living creatures (squid) and giving birth to devices like the Shmitt trigger, a comparator circuit adopted in many electrical devices[3].

The subject of biomimetics, on the other hand has much older roots. Even before Galileo described the scientific method as we know it today, history brought us examples of genuine applications of its principles applied on field of biomimetics. An inspiring example is represented by the notorious "flying machine" (Figure1a) drafted a hundred years before by the genius of Leonardo Da Vinci, and inspired by the structure of bat wings[4]. Another early example comes from the Korean admiral Yi Sun-shin, contemporary to Galileo this time but on the other side of the planet, that developed a new battleship called "turtle ship" (Figure1b), whose structure mimicked the shape of a turtle and proved its efficiency allowing the Korean fleet to fend off the Japanese invasion in spite of the outnumbered fighting vessels (1592-1598)[5].

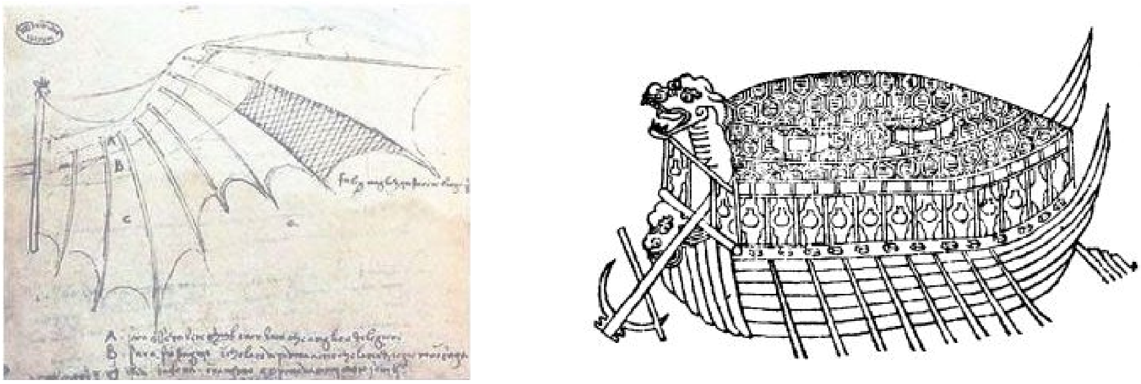

(a) **(b)**

Figure 1: Early examples of biomimetics: (1a) sketch belonging to Leonardo Da Vinci of a bat wing designed for his flying machine, from Renee[4]; (1b) illustration of a turtle ship from "The complete book of Admiral Yi Sun-shin"[5].

Naval and aeronautical engineering for historical reasons are comprehensibly the first fields of application of biomimetics. The history of aviation from the Wright brothers to the modern planes is entirely modelled on the principle used by birds to detach from the ground and defy gravity. As time went by, more and more interesting natural features became attractive and inspired a lot of researches and technologies; some them even by pure chance as for Velcro®.

A general awareness of biomimetics relevance and its potential implications rose in the past thirty years leading to an impressive increase in the number of publications since the early 90's until these days (Figure2). The increasing academic interest in this subject is testified by the outstanding number of world wide publications per year (over 2500) as well as by the number of conferences, journals and lectures organized every year specifically on the topic of biomimetics[6]. It is impossible nowadays that a freshman in a engineering school does not face several times during his academic career topics regarding field of biomimetics.

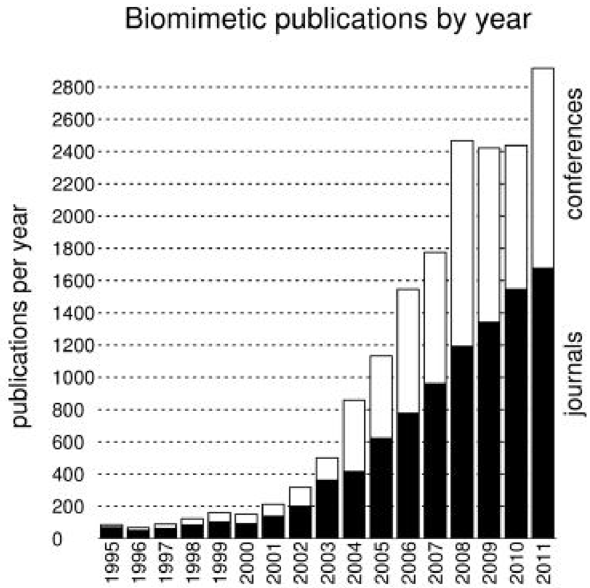

Figure 2: Trend of accademic pubblications: number of journals and conference papers published on biomimetic subject from 1995 to 2011, from Lepora et al.[6].

Both fauna and flora are under investigation for many unique characteristics that would be extremely useful in both present and future engineering applications. Biomimetic process is mainly composed of two different stages: the study of the natural phenomena and the attempt to replicate, or even improve, them. Physics, chemistry and biology knowledge as well technological progress are required for both steps. Following this approach several studies are nowadays performed to analyze animals and plants behavour and various technological applications are explored for these findings. Recent examples are listed below: geckos feet enhanced adhesive ability [7] and its application for climbing devices[8] or medical skin patch[9]; shark scales antibacterial effect and ability to reduce drag force[10] and its application for atibacterical surfaces and for high performance swimsuits[11]; lotus leaves ultra-hydrophobicity[12] and its application for self cleaning surfaces[13]; KingFisher beak shape able to minimize the water ripples generated as it dives in the water, and its application for high speed trains[2].

Because of the study of biological structures has been going on for decades, different studies have reached different stages. Some of them are still in a very early stage trying to understand how does nature implement a certain solution; others already entered in the market with a great success. Some commercial products are available for instance, for the studies listed before like: Speedo®

made a swimsuit that replicates the shark scale morphology in order to enhance the performances; Sharklet technologies® realized an antibacterial material (Sharklet™) that imitates shark skin texture; Shinkansen is the name of the high speed Japanese train that imitates the kingfisher beak shape to reduce noise and air resistance (Figure3). The market for applied biomimetics is considerably increasing too, so that due to the increasing interest of worldwide companies in this field a market that counted \$1.5 billion in between 2005 and 2008 is expected to reach \$1 trillion in 2025[2].

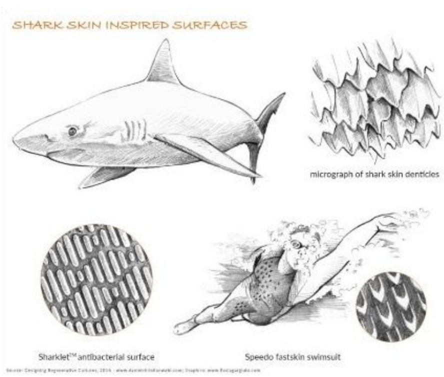

(a)

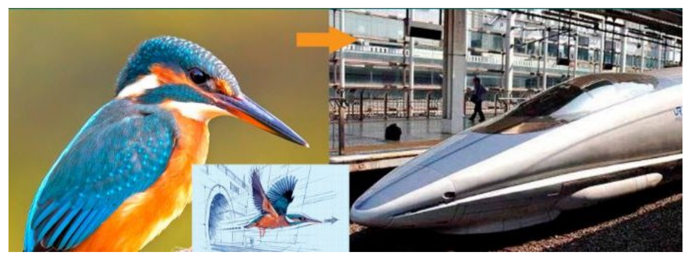

(b)

Figure 3: Applied biomimetics: (3a) shark scales morphology replied on high performance swimsuit in order to reduce drag force, from Whal[14]; (3b) beak shape of the Japanese "bullet train" (Shinkansen) able to reduce noise and improve aerodynamics, from the web[15].

Biomedical applications are considerably spreading in biomimetics field, gecko skin patch and Sharklet antibacterial texture are indeed related to biomedical world. Many more studies however are on the go as for a PLMC scaffold that combines electrospinning technique with SMA materials for bone repair and regeneration[16] or drug delivery micro-needles mimicking the proboscis of mosquito[17].

Nature is an endless source of inspiration. Many different biological structures are studied for their unique abilities in order to learn how to improve specific properties for man-made engineering tools (Figure4). Composite materials represent one of the main fields of study in terms of biomaterials. Most of the tissues in living being are actually made of these materials, and the rising interest on such a materials is justified by their mechanical properties that far exceed the ones of their constituents[18].

For the purpose of the present study, the property we are interested in is mechanical strength. Enhanced strength is observed within animals' hard tissues like bones, teeth and sea shells. Despite the fact these tissues play very different roles in the respective organisms, there are many similarities between the three structures. As matter of fact each of them can be considered a composite material, which means that their structure can be defined on a macroscopic scale as composed of two or more different materials[19]. Similarities are not limited to the type of structure; all three materials contain indeed a mineral phase, an organic matrix and a defined content of water. The mineral phase for all the structures is based on calcium: hydroxyapatite in bones and teeth, calcium carbonate in seashells. The organic content is instead mainly protein: collagen for teeth and bones, undefined for seashells since it varies with the species. Considering their role as hard tissues in living organisms, they will need to have good values of strength, toughness and life fatigue which are quite typical for a composite material, as well as an enhanced anisotropy and a great dependency on its microstructure[19].

The first great difference encountered is represented by the proportion of these three phases: mineral and water content fairly increase progressively in bones, teeth and shells; the opposite behaviour is observed for the organic content. This characteristic heavily influences the properties of the three structures. Since location, function, size, loading condition and surrounding tissues are very different microstructure developed very differently, so too did the overall mechanical behaviour.

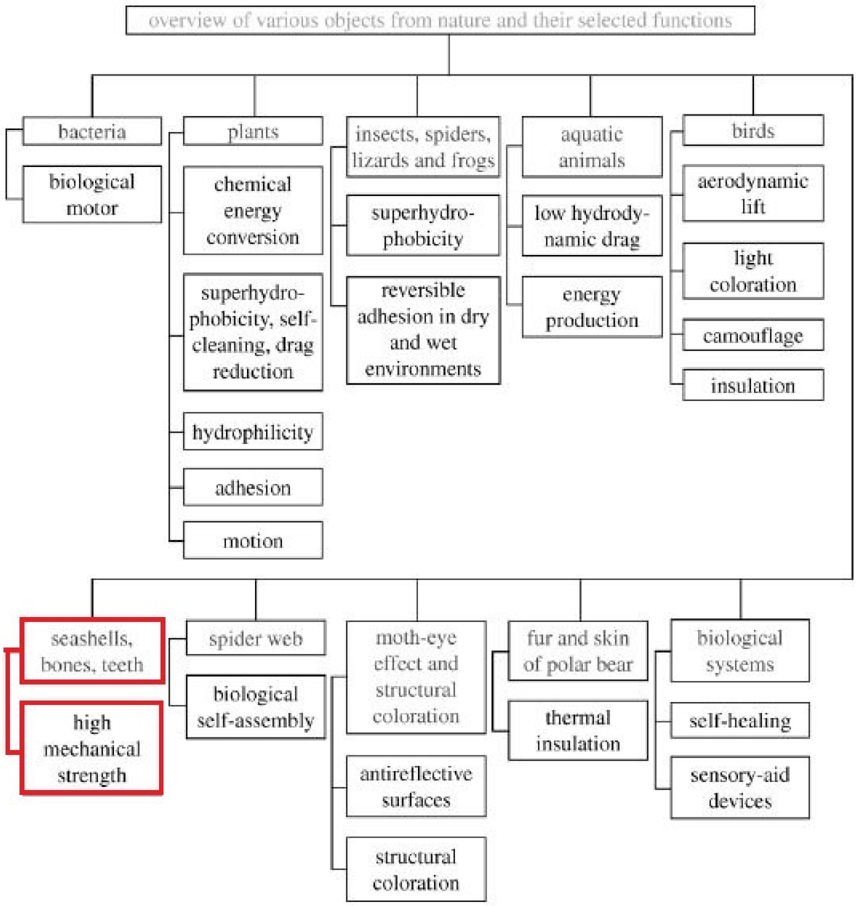

Figure 4: Overview of bioinspired features: biomimetic properties and their source of inspiration, from Bhushan[20]. In red the interesting part for the present study.

For a very long time bones drew the attention of the scientific community. In orthopedic field for instance, to learn how a broken femur is stressed during a daily activity, like walking or running is extremely important. Many features of human bones have been studied. Repair mechanism and enhanced fatigue behaviour are fairly connected to presence of microcracks within it[21], providing impressive fatigue life[22], which is not common for all composite structures. Teeth and bones however are not the subject of the present work, so no further analysis will be done.

Another structure studied that represents a sort of bridge between bone and seashell is the insect cuticle. It is the insect exoskeleton material and it represents the second most common composite material (after wood) in the world. Its structural role is somehow comparable to the one of bone since they have similar functionalities, although the structure is mostly organic (chitin and protein). The major interest of such a structure is provided by its ability to repair, and even improve its mechanical abilities when severely damaged[23] as well as its relevant fracture toughness[24]. Nature therefore implemented different solutions in different structures including bones, cuticles and many other to avoid failure by crack propagation in materials with structural roles[25].

The last and most important set of living beings mostly studied for their strength are mollusc shells. It is important however to make a distinction within it. Several classes of molluscs and great variability in mechanical properties is observed within them due to their microstructure [26]. Speaking of biomimetics the most interesting material is nacre. Also known as mother of pearl it is an easily recognizable iridescent material that forms parts of the shell of notorious mollusc species like abalone (Gastropoda class) and oyster pearl (Bivalvia class). The great ability of such a structure is represented by its toughness, around $4.5MPa\sqrt{m}$[27], and its strength although extremely anisotropic. As already pointed out this ability is in conflict with the small presence of organic material (below 5%)[28]. The secret behind the enhanced mechanical performances is found in the microscopical *Brick and mortar* arrangement, with aragonite tablets, one of the forms of calcium carbonate ($CaCO_3$), ordered in layers with the organic material that fills the spaces within the material[28]. In such a structure various mechanisms are involved to enhance toughness like microcracking, channel cracking, interlocking, ligament bridging aragonite fiber bridging and crack deflection[29], resulting in a very tough material.

The effect of the hierarchical structure is proved comparing the measured toughness for nacre structures with pure aragonite (around 3000 times better[30]) or eggshell($0.3MPa\sqrt{m}$)[31]. As result nacre structures represent a perfect compromise between the brittleness of $CaCO_3$ and the enhanced fracture behaviour of bones (Figure5). Further information are proposed by Currey et al.[32], who compared nacre with bovine bone and highly mineralized bone (rostral bone of Mesoplodon densirostris) finding that nacre shows analogue performances to the common bone in terms of fatigue and fracture toughness while the highly mineralized bones appears much more brittle and sensitive to multiple stresses.

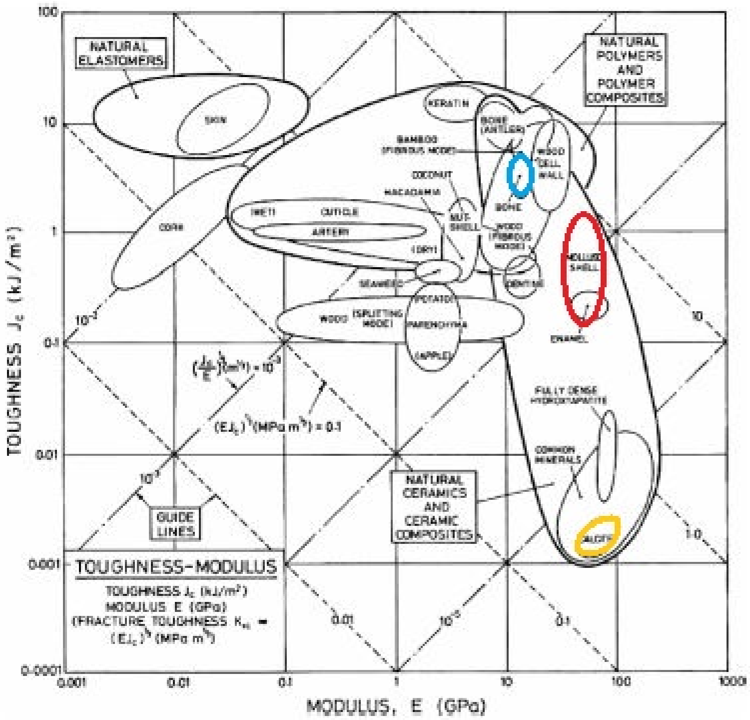

Figure 5: Materials toughness map: toughness and Young modulus plotted for ceramic materials and biological soft and hard tissues, from Barthelat et al[33]. Mollusc shell, bone and calcite are highlighted in red, blue and yellow respectively.

Many attempts have been performed in order to replicate nacre properties by mimicking its microscopic structure. Several procedures have been tested including freezing, MEMS (Micro-elettromechanical systems) or mimicking the macroscopical arrangement[33]. Ice casting technique has been further successfully developed to obtain materials with enhanced compressive and tensile strength[34]. Finally, layer by layer deposition technique has been adopted to replicate the cross-lamellar structure typical of the majority of the seashells[35].

In the end, in order briefly summarize this overview on the concept of biomimetics, its history and the present and future applications it is a good thing to quote Leonardo Da Vinci for a never more current warning on the matter of nature imitation: “Those who takes for their standard anyone but nature, the mistress of all masters, wary themselves in vain”[36].

3.2 Previous works

Nacre is only one of several available structures for mollusc shells, even whithin the same specimen. Mollusc phylum counts a remarkable number of species, mostly belonging to the Gastropoda class (35000 species) and the Bivalvia one (10000 species) that lives in different environment and developed a certain structural variability. Examples of shell microstructures are: columnar nacre, sheet nacre, foliated, prismatic, cross-lamellar, complex cross lamellar, homogeneous. All of these structures are based on $CaCO_3$, present alternatively or together in its two most common forms: calcite and aragonite. The study of species do not containing a nacreous layer inside is becoming more and more common. The reason why this is happening is to investigate the reasons why nature chose for the majority of the molluscs a shell that does not contain nacre, which is found to have impressive mechanical abilities. Mechanical parameters measured for cross-lamellar structures have not been able to match with the nacre one so far[37]; nevertheless it is hypothesized that an increased isotropy could play a decisive role in promoting non nacreous structure[30].

The present work is focused on one of the numerous species of living Gastropods, Patella vulgata limpet. As its name suggests, it is the most common sea snail that populates tidal regions of Northern European Atlantic coasts. The soft body off the animal is characterized by a strong muscular foot able to keep the animal firmly attached to the rock underneath, and a shell that completely conceals the animal protecting the soft tissues. The shell presents a conical shape and radial ridges moving from the apex towards the rim on the external surface. Never reaching size larger than $60mm$, they grow accordingly into rock topography in order to enhance locking. Since they spend half of their time under water and half outside they are subjected to dangers of both situations. For this reasons they developed characteristics features to adhere to the rock either out or under water, when they graze, as well as a functional shell able to protect it.

As for all the Gastropods, the shell is characterized by a strongly hierarchical structure, made of layers of $CaCO_3$, present in both forms calcite and aragonite. A very strong heterogeneity is encountered considering different areas of the shell. Ortiz and al. gave a very comprehensive description of the layered structure of Patella vulgata (Figure6) where the M layer (the myostracum) is the one muscles are attached to, and all the other layers (above and below) are named adding or subtracting the number of layers that separate it from the myostracum itself. This description is extremely relevant considering that each layer is characterized by a specific form of $CaCO_3$, a typical arrangement and orientation of the microstructure[38]. For the purpose of the study it is important to underline that calcite is not present everywhere inside the shell, it is concentrated around apex and rim regions instead[38].

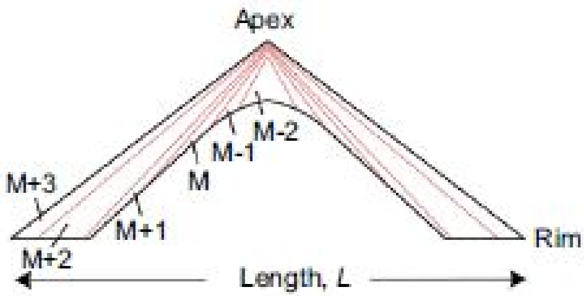

Figure 6: Shell internal structure: illustration showing the layered structure present within Patella vulgata shells, from Ortiz[38].

Seashore is a very complex environment; shells have to deal with many dangers like predation, dehydration and occasional impacts. In order to survive their own environment limpets shells had to develop good mechanical performances. The mechanical behaviour of Patella vulgata has been studied under both static and dynamic conditions. Compression tests have been performed on limpets shells in quasistatic condition[39], which means that the load was applied very slowly so that the static condition could be assumed respected ($2mm/min$[39] or $1mm/min$[40]). A FEM model was realized too in order to compare limpet deformation in terms of shape of different species.

However interesting it is not very realistic for a limpet to be subjected to a steady compression. Impact are much more common to occur to limpet than high static loads, as proved by several studies. In particular it has been found that impacts are not only possible but also dangerous for limpets integrity, eventually even for their life. Damage has been found to happen as consequence of powerful waves[41] as well as wave born boulders (moving rocks and pebbles)[42] and ice scouring(for limpets living in the Antarctic region)[43],[44]. While Shanks and Wright correlated the amount of impact on a fixed target with the presence of pebbles, movable rocks and high waves in the area, Harper correlated the damage occurrence with the amount of scouring ice in the area.

Evidence of repair mechanism has been observed in some of the damaged specimens collected during these studies[43],[44]. Mineral patches were found in the specimens, and proved to be able to restore strength for the single damage but no cumulative strengthening. The same behaviour was found comparing healthy and repaired shells under compression condition[40]. In depth analysis was then performed on artificially damaged limpets (hole drilled from side to side) using various techniques as histological and SEM analysis on one side[45], RNA-sequencing and a semi-quantitative PCR on the other[46] and finding meaningful repair to happen after only two months.

Together with the repairing mechanism, the other interesting property for limpet is how they actually respond to impact. From this point of view, one step ahead was done by Professor Taylor[47]. What he did was to impact Patella vulgata shells in different conditions in order to describe their impact behaviour. Limpets were impacted one by one, with a given energy (E_{app}), using a falling weight and recording size and if failure occurred during the first strike. The outcome of the impacts were approximated by a step function (Figure7), where the step occurs at a given length called from now on critical length (L_{cr}). Such a value represents the minimum size required for the specimen to fail and was obtained minimizing the error made by the step function approximation.

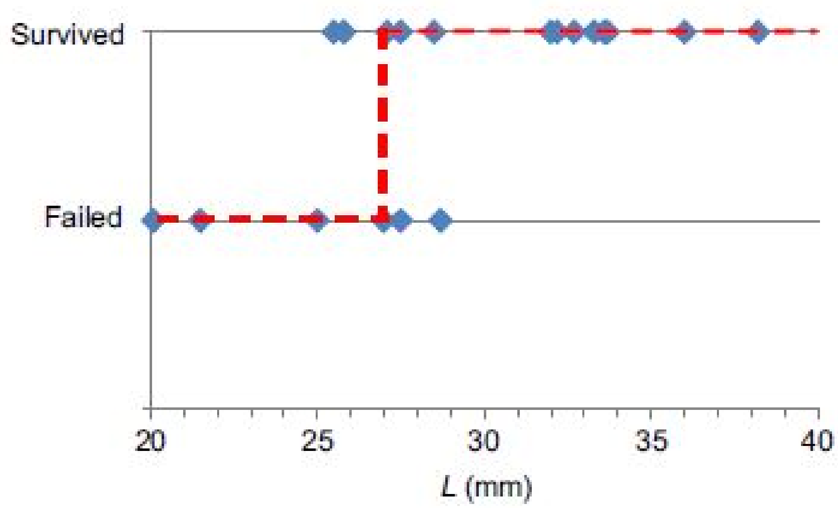

Figure 7: Step function: function approximating the fate of limpet shells subjected to a single impact, from Taylor[47].

The E_{app} was therefore nothing but the minimum energy required for a specimen of size L_{cr} to fail during a single impact. The impact strength was defined normalizing the E_{app} for the specimen size as follows:

$$E_{cr} = E_{app}/L_{cr}^{4.6} \tag{1}$$

Results obtained as before showed that the presence of the animal flash as well as the impact surface are not as important as during the compression tests since no difference in impact strength could be seen.

In order to characterize Patella vulgata limpet mechanics, fatigue behaviour is a very important engineering parameter. As matter of fact it is one of the most important defining property a composite material, since there is a great life fatigue variability depending on the arrangement of different phases and the materials involved. Because of in their environment limpets are found to be more likely being impacted than being statically compressed, we are mostly interested in a impact fatigue characterization (typical for composite materials[48],[49]).

Previous results on this matter are once more given by Taylor[47] who performed consecutive impacts on several Patella vulgata specimens, once again obtaining unexpected results (Figure8). Results where expressed in terms of the energy applied (normalized with the same procedure used for the critical value) and the total amount of energy applied, evaluated as follows:

$$Accumulated\ E_n = \sum_{i=1}^{n} E_n(i) \cdot Nf(i) \tag{2}$$

Where N_f is the number of impact required to reach failure. Poor fatigue performance were observed in all the tests, even the ones performed in situ which represented the optimal condition, since specimens' organic and water content as well as the support are the natural ones. In detail, failure was used to happen as the total accumulated energy approached the impact strength of the undamaged situation.

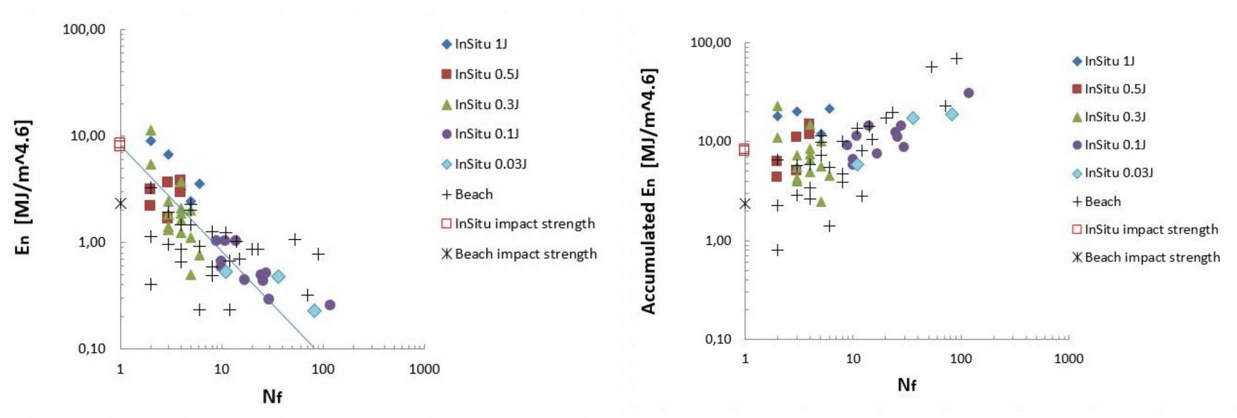

(a) (b)

Figure 8: Fatigue tests: (8a) applied normalized energy over the number of impact to reach failure; (8b) accumulated normalized energy over the number of impact to reach failure. Images obtained from Taylor[47].

Since the main property of nacre is the toughness, it would be interesting to evaluate it within the Patella vulgata structure as well. An early toughness estimate was given in a previous work in terms of delaminations cracks. As for many composite materials delamination (Figure9) is one of the principal damage mechanisms to be observed, and it is characterized by smooth cracks running along the edges between different layers[48]. The adopted procedure required to impact two separate groups of shells using two different subcritical energies (10% and 20% of the E_{cr}). The number of cracks within the cross-section of each shell was counted and the total crack area (A) assessed. The fracture toughness was then evaluated in terms of strain energy release rate (G_c), and since delamination cracks are showed to be parallel to the shell structure, the equation experimentally adopted for trough-thickness cracks[50] was modified as follows:

$$G_c = \frac{\Delta E_{app}}{\Delta A} \qquad (3)$$

Where ΔE_{app} and ΔA are nothing but the energy and the crack area variation between the two impact conditions (10% and 20% of the E_{cr}). The fracture toughness obtained was equal to $553.42 J/m^2$ which corresponds to a critical stress intensity factor (K_c) of $3.16 MPa\sqrt{m}$. The value of K_c is obtained using $K_c = \sqrt{G_c \cdot E}$ [50], where E is the Young modulus of the limpet shell obtained from Currey[51]. The procedure followed had however a big problem since the energy involved in the crack generation was considered equal to the total applied energy. This assumption is clearly not true as a good percentage of the applied energy is most certainly transferred to the pavement beneath the shell.

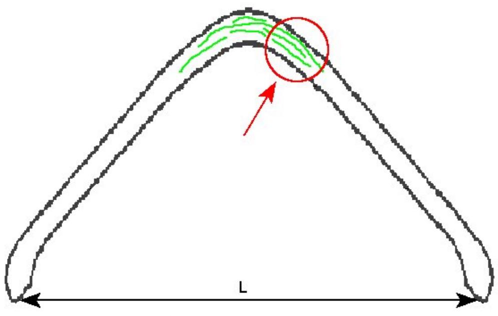

(a)

(b)

Figure 9: Delamination cracks: (9a) illustration of the cross section of a limpet shell showing delamination cracks; (9b) optical microscopy image showing actual delamination cracks.

One more approach was followed by Taylor[52], who assessed a value of toughness through bending tests. In this case it was not used an entire shell for but only a rectangular specimen with a sharp notch cut through the thickness in circumferential direction, like for some of the cracks observed in impacted specimens. A K_c of 0.98 ($\pm$0.23) $MPa\sqrt{m}$ was then obtained[52].

3.3 Preconditions

Before describing the aims of the study and the body of the work it is important to make few clarifications:

- Inside the body of the work many references are done to radial, circumferential and vertical directions within the shell structure. Figure10 shows the principal directions over the picture of a limpet shell in order to avoid misunderstanding and simplify the discussion.

(a) **(b)**

Figure 10: Directions definition: (10a) vertical and radial directions; (10b) circumferential direction.

- All the shells analysed during the work came from the same site (5317'18"N; 66'42"W), in Dublin county (Figure11a). The area showed to be a good compromise between convenience and reduced human presence. On one hand, an half hour journey from the city centre with public transportation enable the place to be reached on a weekly base, especially to perform fatigue tests without excessive waste time. On the other hand, the area is not used for fishing activity and the presence of more attractive sites for bathing and rock diving nearby ensures a limited number of visitors confined to the edge of the area for sightseeing activities. The low rocky shore (Figure11b), completely covered during the high tide, makes the site a perfect environment for the growth of limpet shells.

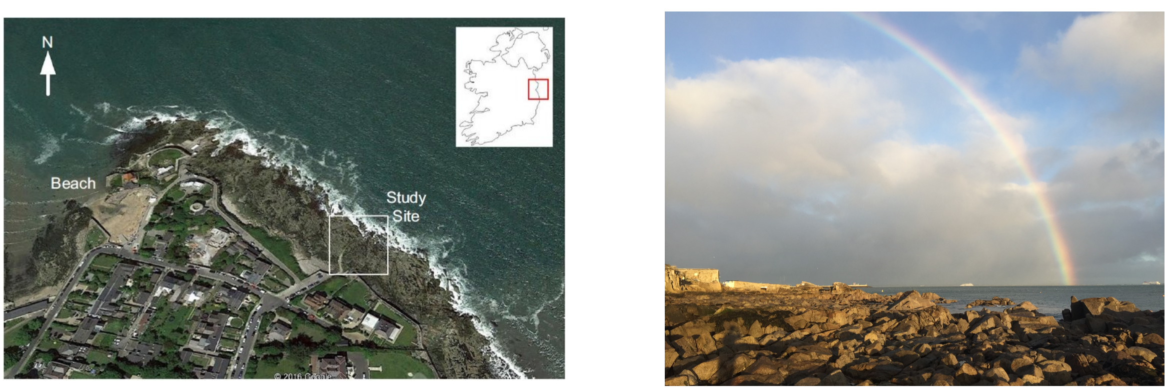

(a) **(b)**

Figure 11: Collection site: (11a) map of the collections site together with the the location of the site within Ireland map, from Taylor[47]; (11b) picture of the rocky collection site.

- Limpets damage and failure during impact test are mainly related to the delamination and spalling phenomena. The first one is nothing but the separation of internal layers of the structure as consequence of the interlaminar stresses arising as the structure is impacted[19]. It is a major problem in composite materials made of several layers and seashells are no exception. On the other hand, spalling phenomenon involves the detachment of flakes of material from the material surface during the impact[47]. It is partially related to the first one since it is may originate from delamination cracks formed within the structure.

- The term fatigue is going to be used in the rest of the study as a synonym of impact fatigue. Although the difference with the normal fatigue is not too big, it is important to make clear which one we are referring to.

- In order to validate experimental findings, the Finite Element Method (FEM) is used to simulate both impact and compression tests. Coined in the 60's it finds its origin in a group of researches performed the 40's, mostly in the aerospace and civil engineering[53]. Although widely used in many branches of the engineering and for various analysis (solid structural, fluid dynamics, heat transfer, etc.) for the purpose of this study, it is used to perform structural simulations of the shell behaviour in both static and dynamic conditions. The basic principle behind the method is that the complexity of the reality of continuous can be discretized in a certain number of components (called elements) mono or multidimensional, on which the analysis is performed assuming a certain number of boundary conditions. Then force-displacement relation is solved for each element, the solution is than applied to different elements connections (called nodes) and finally extended to the whole system [54]. Numerically the FEM requires to reverse constitutive matrices as complicated as the assumptions made on material and geometry complexity, so that the use of computers abilities are essential. Both implicit and explicit solver are adopted in order to obtain reasonable results in a reasonable computational time, taking care of the different observation time required for static compression (where there is no time effect) and impact[55].

- When the term toughness is used in this study it is always referred to the so called fracture toughness which is nothing but the ability of a material to withstand crack propagation. This is a relatively new concept that is widely used in many engineering fields including biomedical one to understand and possibly predict failure in material characterized by high strength and stiffness as glasses or ceramics[50].

3.4 Objectives of the study

The aim of the present study is to further investigate shells of Patella vulgata limpets attempting to give a full description of some of the most characterizing mechanical properties (repair mechanism, fatigue behaviour, and toughness) together with a computational description of its behaviour under impact. Even though the whole work has unique interest in improving the knowledge of the mechanical behaviour of a non nacreous structure, separate experiments are carried out, leading to unique conclusions on the structure behaviour. The work body is therefore divided in four separate sections, proceeding in parallel to each other, in detail: impact strength, fatigue, computational modelling and toughness.

3.4.1 Impact strength

Impact strength measured like Taylor[47] using equation1 is used in order to assess the repairing mechanism implemented by the limpets in order to restore its mechanical properties. Experimental findings on damaged specimens (impacted, abraded and pierced) left in situ for two months are gathered with data collected in previous studies for shorter repairing time[63]. The repairing mechanism is therefore studied both in terms of repairing time and in terms of damage typology.

Missing data among pierced specimens impacted at zero days is filled by performing more impact tests, paying great attention on the effect of the hole location. Besides the repair mechanism, impact strength is used to give a complete description of the decreasing in the mechanical properties as consequence of different types of damages, including apex hole and near apex hole in the comparison.

Several question are waiting for an answer at the beginning of the work. Because two separate topics are discussed in this section (repairing effect and piercing effect) these questions are split in two groups as follows:

- Is two months a period long enough to see the mechanical response to impact completely restored? What significant differences can be seen considering different repairing times? Does different damage typologies lead to different repairing abilities?
- Comparing it to other damage typologies, how much does the presence of a small hole

throughout the apex affect impact strength of the specimens tested? Does the location significantly affect the impact behaviour of the shells?

3.4.2 Fatigue

Pre-damaged shells left in situ for two months are subjected to impact fatigue tests analogous to the ones performed by Taylor[47] in order to analyse whether different types of damages and the repairing mechanism ,that is taking place, still cause the poor performances already observed.

Nevertheless the application of multiple consecutive strikes is not a good approximation of the natural behaviour. Fatigue impact tests are performed using different energies and time intervals between different sessions to investigate a more realistic condition.

Questions are split here too in two groups, regarding consecutive and cyclical impacts, as follows:

- Do the tested shells show the same poor fatigue performance or are they enhanced? Are there any significant difference between different groups? Considering the fixed energy applied for all the specimens, are the results obtained reliable?

- As cyclical impacts are applied how does the overall fatigue behaviour change? Are the achieved solutions reliable? How does the damage appear inside the structure of the surviving specimens?

3.4.3 Computational modelling

To further investigate the stress and strain distribution inside the shell the finite element method is adopted. The impact procedure is the one under investigation since it is the one proved to be the principal source of damage in limpets shells. Compression is modelled too in order to compare the two loading conditions and validate the Young modulus adopted. A general overview of how the structure is affected by the applied load is required. To do so, a simplified model is used neglecting the sources of anisotropy and asymmetry in the shell. The attention is focused on the apex region where the major damages are observed, keeping under control body contacts and geometric relations.

The simulations performed are finally aimed to answer the following questions:

- Are the simulations performed able to describe the damaging and failure process observed experimentally? Are the results able to justify local variabilities in shape and microstructure? How do the approximations affect results? Which parameters are critical for the computational solution and how? Are the parameters used able to predict experimental crash test solution? Do static and dynamic simulations show clear differences?

3.4.4 Toughness

A simple bending test is not feasible in order to evaluate fracture toughness in directions different from the one already tested. It has been observed however that delamination is a major thing, while cracks growing from rim defects in direction are commonly observed in compression tests. Two different approaches are therefore used to describe quantitatively the toughness of Patella vulgata limpet. A first way aimed to adjust the delamination toughness already obtained[63] by assessing the amount of applied energy that is really involved in crack generation during an impact. As matter of fact, part of the energy applied travels along the shell and is transferred to the support underneath. The basic principle adopted is that damaged specimens (impacted) when compressed show a lower stiffness, in other words the amount of energy required to be deformed of the same quantity is reduced by the presence of the damage within the structure[49].

On the other side, toughness in radial direction is investigated by means of the FEM model already used, with the simple adaptation of a notch in the rim region. Results are then used to validate the experimental observations done by Professor Taylor[52], performing compression tests on $30.25mm$ average size specimens including a $6mm$ notch caved at the rim.

The goals of the study is to give an answer to the following questions about the delamination and radial toughness evaluation procedures:

- What is the amount of energy involved in the crack formation? Does the corrected value of toughness gives a realistic description of the delamination process?

- Is it possible to obtain a realistic estimate of toughness in radial direction using the implemented model? Are the behaviours seen in the computational and in experimental results comparable?

4 Materials and methods

4.1 Impact strength

The procedure used for this section is analogous to the one already performed in Taylor work[47]. Impact test have been performed on limpet shells using a basic equipment made of a stainless steel tube 1 metre height and a weight of 123 grams (Figure12). The mass was held by a steel stick through one of the ten holes drilled in the tube and spaced 83 (± 0.56) mm from each other. The diameter of the tube was slightly larger to avoid friction between its internal walls and the falling body.

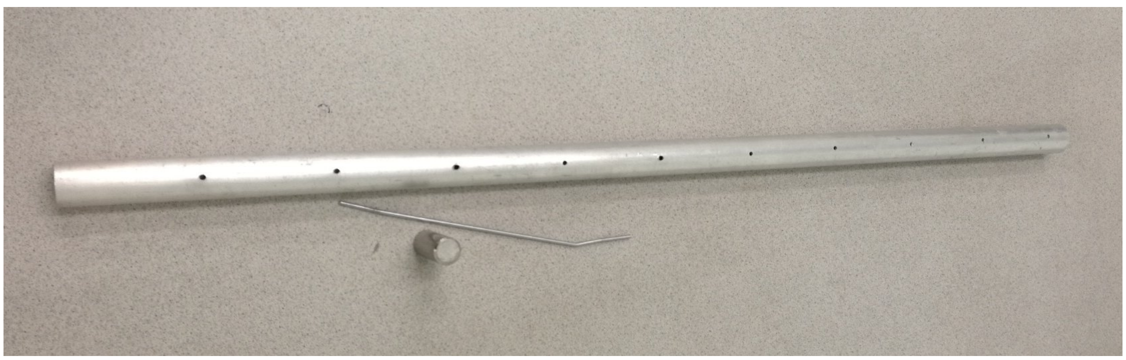

Figure 12: Original impact experimental set up: tube, stick and weight adopted for the impact tests.

A single 0.50 ($\pm 0,01$) J impact was performed on dry shells on a flat pavement in atmospheric conditions. The impacts themselves were performed holding the tube in vertical position centred above the specimen apex and dropping the weight from a height proportional to the required impact energy. The applied energy was considered simply as the potential energy of the weight mass (m) at the initial height (h), considering a constant gravitational acceleration (g) of $9.81 m/s^2$, as shown by equation4. The applied energy are always expressed with a variability measurement containing the uncertainty due to the mass, the holes position and the air resistance (almost negligible for this application).

$$E_{app} = m \cdot h \cdot g \tag{4}$$

Each impact has two possible outcomes: survival or failure. The failure is defined considering the damage magnitude. Only damages big enough to jeopardize the survival of the animal inside are assimilated to failure like: big hole formation at the apex, detachment of considerable portion of the shell wall, specimen splitting in half or collapse of the whole structure (Figure13). Pierced shells already had a hole in the apex; a hole widening is considered equally deathly. Most of these damage do not involve a sudden death of the animal which perish as combination of multiple factors in the following days or weeks, as observed by Taylor[47].

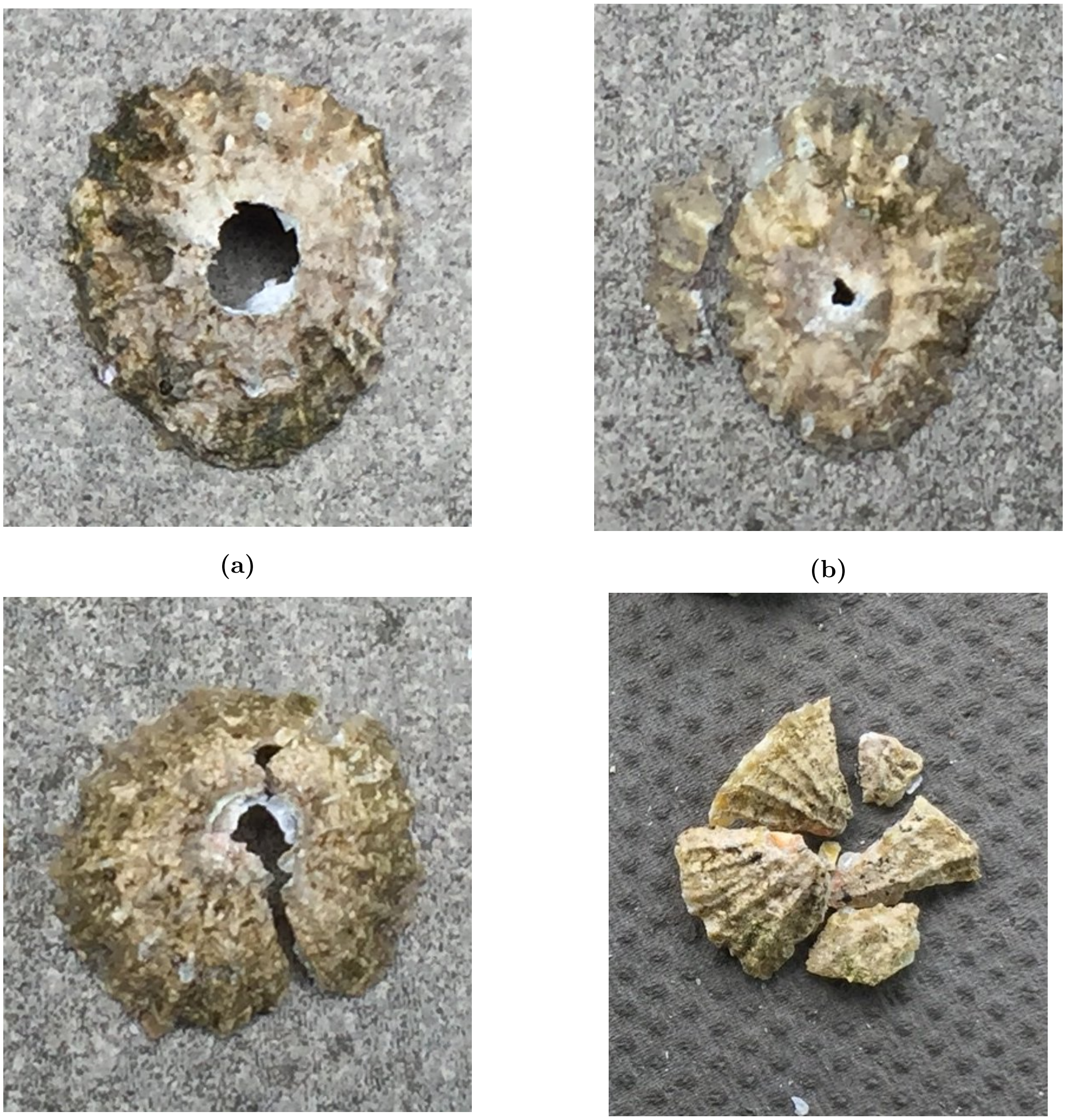

(a) (b) (c) (d)

Figure 13: Failure mechanisms: (13a) apex hole formation; (13b) detachment of a large piece of shell from the rim; (13c) splitting of the shell in half with a crack crossing the apex; (13d) collapse of the whole specimen, generating multiple pieces with relatively homogeneous size.

The specimens impacted can be divided in three different groups, depending on the pre-damages operated:

1. Abraded;
2. Impacted;
3. Pierced.

The abrasion process involves the removal of some material in the apex region using a file; the impact was applied as described but with an energy of 0.30 ($\pm$0.01) J; finally the piercing was obtained gently tapping the apex with a nail.

To study the repairing mechanism in situ, shells have been damaged and collected: 25 abraded shells and 34 impacted shells were collected after 63 days; 17 pierced specimens were collected at different times (52, 63 and 74 days) but considered as a unique group because only few of them could be used for impact strength evaluation.

An additional group of fresh shells has been collected and then pierced using a nail and the weight as hammer (Figure14). In order to investigate the effect of the hole position on impact strength 20 and 21 shells were pierced at the apex and in the surrounding area respectively.

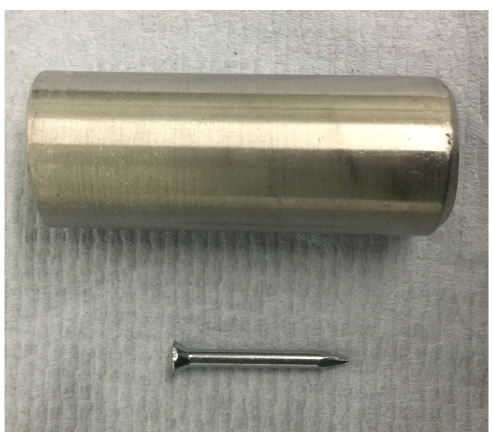

Figure 14: Equipment used for the piercing procedure: nail used to pierced the shell and weight adopted as a hummer.

Critical length and consequently critical energy were calculated for each group using equation1. In order to avoid oversight and speed up the calculation a Matlab® optimization algorithm was written and compiled for all the groups. The algorithm is iterative and aims to minimize the total error (e), error generated by the the step function approximation (Figure7), changing the value of

L over time of a quantity that is reduced every time e increases, until a precision of 0.01mm is reached. In order to avoid local minimum, the same optimization process is repeated five times choosing initial length values equally spaced between the smallest and the biggest shell size not lying on the step function already described.

To ease the process, the input data are loaded directly from the Excel® file containing all the results in the form: failed specimen in the first column and survived specimen in the second column. The output of the algorithm contains, for a given data set, the critical length, the number of specimen having non-null error, the total error and the standard deviation calculated as described by Taylor[47].

4.2 Fatigue

4.2.1 Consecutive impacts

All the specimens that survived the single impact where then adopted for the study of their fatigue behaviour. More and more strikes were performed on each survivor until one of the failure mechanisms previously described occurred. No modifications were done to the experimental set-up adopted for the single strike (Figure12), the same energy was used, 0.5 ($\pm$0.01) J, for all the impacts and the number of impact required to reach failure was recorded.

Results were then compared to the ones already obtained by Taylor[47] in terms of normalized critical energy evaluated using equation1 and total accumulated energy using equation2 over the number of cycles at failure (N_f).

4.2.2 Cyclical impacts

These tests were carried out in situ using 10% and 20% of the critical energy, obtained simply reversing equation1.

During a four months long study, from September 2017 to December 2017, 221 Patella vulgata limpets have been used. The amount of subcritical energy applied and the time interval between two consecutive strikes were modified, such that the entire limpet population considered can be divided into four separated groups:

1. 57 limpets were impacted every week at 10% of their critical energy;

2. 54 limpets were impacted every week at 20% of their critical energy;

3. 63 limpets were impacted every two weeks at 20% of their critical energy;

4. 46 limpets were not impacted but monitored during the whole experiment.

In order to ease the impact to happen orthogonally to the apex, only limpets living on horizontal surface were considered. The size distribution was homogeneous within a range between $26mm$ and $46mm$ for each group. Finally all the shell tested belonged to a group of rocks (Figure15) a few metres away from each other so that the location was not a source of variability itself. It is assumed that limpets relatively close to each other have the same probability of experiencing pebbles and waves impact as well as predatory attacks[42]. It happens sometimes that in situ limpets are covered by sea weed, typically in the apex area. Their presence in terms of mechanical behaviour has not been studied yet, it is however reasonable to think that it could introduce some unexpected dumping behaviour, modifying the response of the structure itself.

Figure 15: Group of rocks chosen for the fatigue test: all the limpets tested belonged to rocks in a $5m$ radius area.

Choosing to apply a percentage of the critical energy, the amount of energy to be applied was different according to the size of the limpet, and was obtained by simply reversing equation1. The accuracy of the procedure used is affected by two main problems: one is the practical difficulty of performing accurate size measurement on in situ shells; the other is the low accuracy of the equipment used.

The first problem was solved by measuring length to the nearest millimetre and considering a systematic error equal to $0.5mm$ in the uncertainty computation. The equipment accuracy was heavily improved drilling in the tube new holes 20.75 ($\pm 0,81$) mm apart from each other and by using four stainless steel weights of different height and 28.9, 57.9, 115.6 and 231.3 (± 0.2) g masses (Figure16). Finally, the resultant uncertainty of the impact performed was smaller than 1% of E_{cr}.

The choice of using several weights is due to the fact that having a lighter mass increases the system accuracy but has limitations in applicable energies since the tube has a fixed length. Each shell was measured before every impact session instead of measuring it only once the first time, as further precaution to avoid systematic errors. In order to speed up the impacting procedure, it was used a table containing the range of useful sizes (rounded to the nearest millimetre) and the relative subcritical impact energies (10% and 20%).

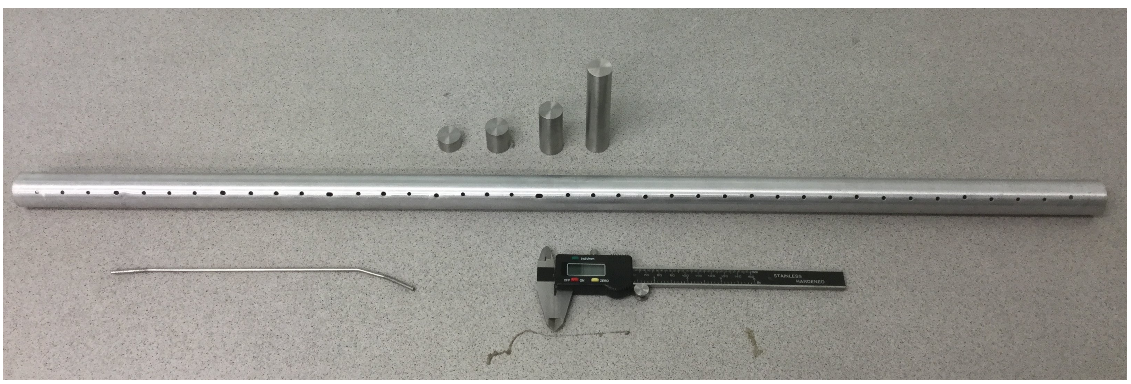

Figure 16: Fatigue experimental set-up: 20.75 ($\pm 0,81$) mm holes are drilled in the tube and four weight of different sizes are used to improve the system accuracy, respectively 28.9, 57.9, 115.6 and 231.3 (± 0.2) g.

After every impact session limpets were classified in: survived if nothing happened; missing if they could not be found; found broken if there was a hole at the apex before being hit; and failed if a relevant damage that could compromise the survival of the shell was generated.

Finally at the end of the study some of the remaining shells was brought to the lab to have a close look to the appearance of the internal structure using Scanning Electron Microscopy (SEM) technique. Before being inserted inside the SEM machine (Zeiss Utra Plus, Figure17d) the specimens were reduced in size, cut across the apex area and finally coated by conductive material. Having a smaller specimens was very useful to reduce the coating time. The specimens were therefore ground by holding the shell flat on the rotating silicon-carbide abrasive paper disk of the grinder (Struers Knuth-rotor, Figure17a) until around five millimetres of material were removed from the rim. Removal of the outermost area of the shell is not a problem since it is not interesting for the aim of the study. The cut was operated along the main axis by means of a handsaw (Tactix, Figure17b), keeping always the rig-hand half for the following steps. Finally a silver-palladium nano-coating was applied thanks to a high resolution sputter coater (208HR Cressington, Figure17c) on the shell stuck on a circular metal holder using carbon based cement.

(a)

(b)

(c)

(d)

Figure 17: Equipment:(17a) Struers Knuth-rotor grinding machine; (17b) handsaw; (17c) Crossington HR208 from Cressington website[56]; (17d) Zeiss Ultras Plus machine from Zeiss website[57].

4.3 Computational modelling

The CAD system used to implement all the geometries was ANSYS® Design Modeler. The platform used for finite element analysis models was ANSYS® Workbench 18.0.

Two different analysis were performed:

1. Dynamic analysis to model what happens during the impact test;

2. Static analysis to model what happens during the compression test.

In order to simulate an impact lasting only a few milliseconds an explicit solver was used to model the dynamic condition. For the static one an implicit solver was preferred.

4.3.1 Geometry

An approximated geometry was adopted to model the experimental situations. Three bodies were used for both dynamic and static analysis: shell, support and weight. The weight is equivalent to the falling body used during the dynamic analysis. It is however used without any changes to model the piston in the static model, where inertia effects are not considered and a body with circular base fairly approximate the compression machine piston. The approximations adopted allowed to introduce two symmetry planes in the system, so that only a quarter of the entire system was used in the simulations and the computational costs were heavily reduced(Figure18).

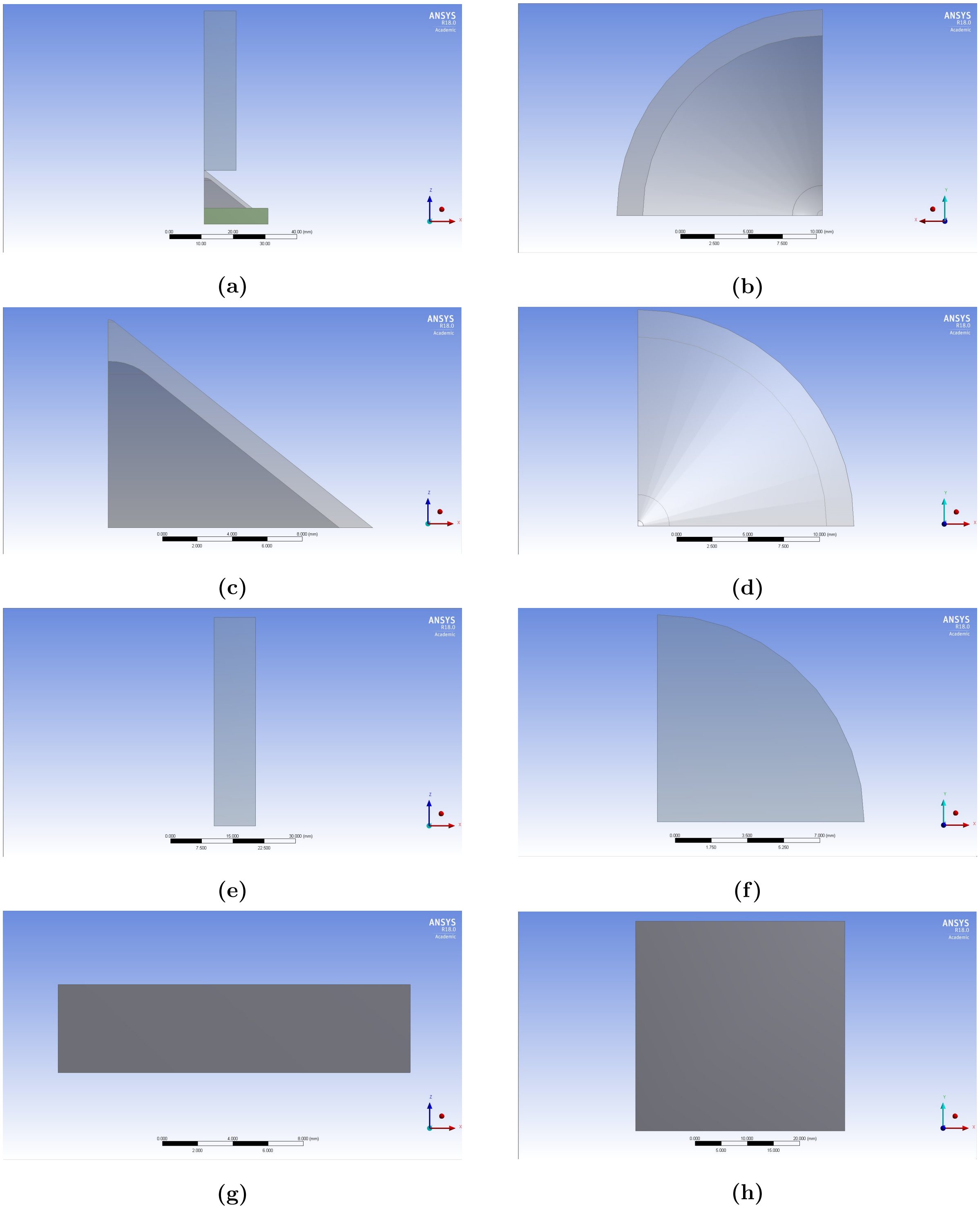

Figure 18: Sempified geometry modelled: (18a) full model; (18d), (18c), (18b) shell from above, the cross section and below respectively; (18e) and (18f) weight cross section and from below respectively; (18g),(18b) support cross section and from above respectively.

A 123g circular base cylinder was used to replicate weight geometry. A 10mm base radius and 50mm height are the characteristic dimensions; stainless steel is the material assigned to the body. The support is modelled as a stainless steel parallelepiped, 5mm thick and slightly larger than the shell rim to ensure a full contact even when the shell is crushed. The shell body had the only complex geometry in the whole system. The aim of the this body was not to replicate the limpet shell one, but to simplify it setting a limited number of parameters easily revisable (Figure19).

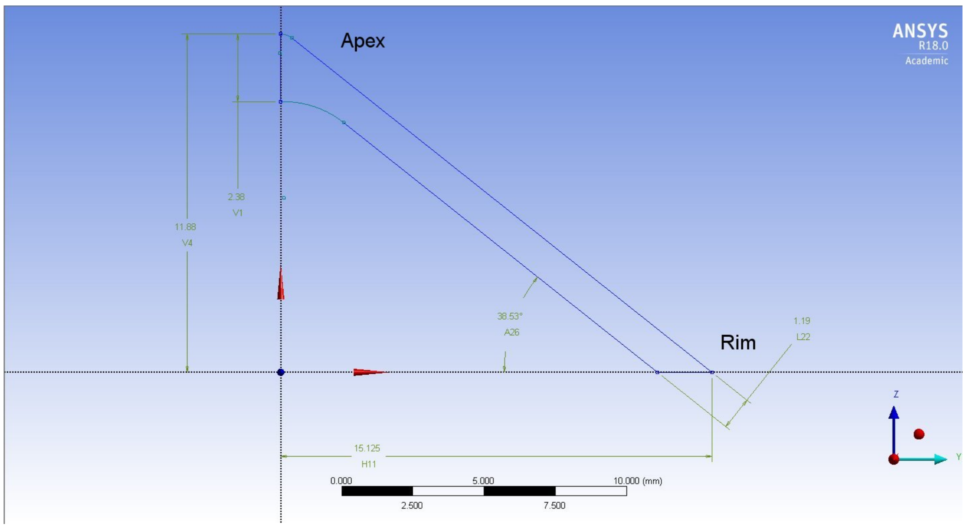

Figure 19: Shell sketch: semplified model reducing the complexity of limpet shell geometry to a few parameters including base radios, hight, wall and apex thickness.

First of all the complexity was reduced performing a series of simplifications:

1. Shell base ellipticity (Figure20a), ratio between the major and minor dimensions of the base, is approximated to unity (circular base);
2. Shell base eccentricity (Figure20a) is considered as null (centered apex);
3. The outer surface is smoothed, neglecting its uneven appearance filled by ridges (whose role is not known);
4. Wall thickness is considered as constant. Real limpets shows thin walls in the aragonite made region and gets thicker in proximity of apex and rim regions, or calcite made regions (Figure20b).

Rim radius of the shell was chosen averaging the major and minor base diameters of a 33mm limpet. Shell size (equivalent to the main dimension) was chosen as the median size of the whole population of tested shells during the experiments. The minor dimension of the rim was calculated from the main dimension using the typical base ellipticity quantified by Cabral[58] as 0.799 ($\pm$0.042)[1]. Shell height once again has been obtained relying on Cabral conicity value[58], ratio between height and main dimension of a limpet, of 0.356 ($\pm$0.059)[1].

The thickness has not been considered constant everywhere. Two different values have been used, one for apex region and one the rest of the shell. From the value given by Cabral[58] relative to a 30mm shell it was derived by linear regression the sideways wall thickness as 1.29mm. Thickness value at the apex was much more difficult to assess. In a parallel work, apex thickness measurements have been performed on fresh shells using a digital callipers. The measurements where conducted on the specimens cut in half across the apex. The values obtained were however partially distorted by considerable loss in material around the apex during the cutting process. In addition the results obtained showed enhanced variability, making the measurements even less reliable. Nevertheless choosing a thickness at the apex twice the one at the walls seemed a reasonably good approximation.

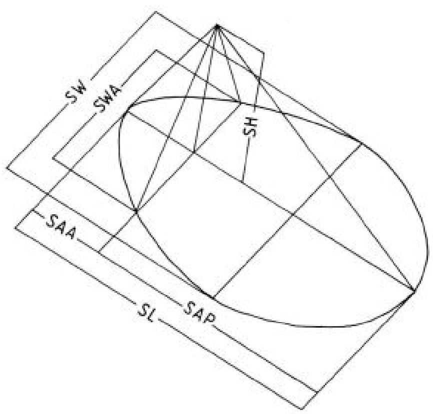

(a)

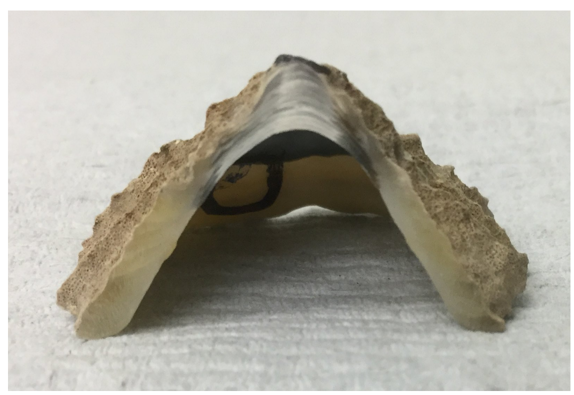

(b)

Figure 20: Model approximations: (20a) shell draft showing the base eccentricity defined as the shell width at the apex over the shell width (SWA/SW), the base ellipticity as the shell width over the shell length (SW/SL) and the conicity as the shell hight over the shell length (SH/SL), from Cabral[58]; (20b) thickness variation along the walls, with maximum reached close to the apex and the rim and minimum in the region where M, M+1 and M-1 layers are placed (aragonite structure)[38].

[1]Standard deviation

4.3.2 Mesh

The mesh adopted in the two analysis are different as function of the different solver adopted.

In the dynamic condition the impact happens on a very localized region, therefore the choice of a hexahedral mesh with reduced integration elements would have lead to hourglassing phenomena. This is a non physical behaviour of the elements which have an excessive flexibility of the hexahedal elements producing zero-energy deformation modes (Figure21) and leading to meaningless results. The use of a less coarse mesh could reduce the propagation of the effect but does not avoid it completely. On the other side the use of a full integration mesh would reduce the computational efficiency, other than introducing shear locking due to the enhanced stiffness of the element itself[59]. On this application overall hourglass energy exceeded three times the maximum recommended value (10% of the internal energy energy)[60].

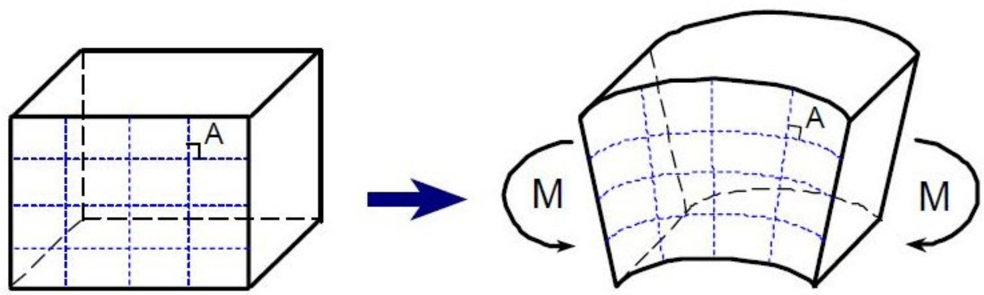

Figure 21: Zero energy deformation: hourglass effect on eight nodes integration hexaedral element. Misleading bending is observed within the flexible hexahedral elements, illustration from Sun[59].

The solution adopted is to generate a tetrahedral mesh in the bodies involved in the impact (weight and shell) and a hexahedral one anywhere else (Figure22).

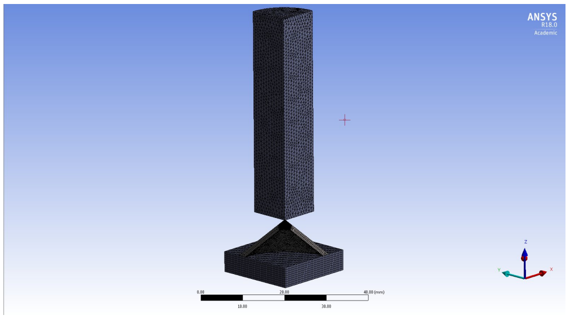

(a)

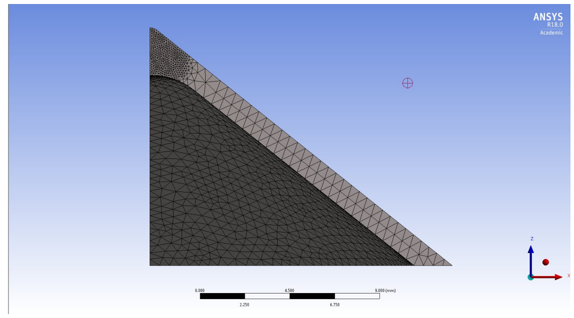

(b)

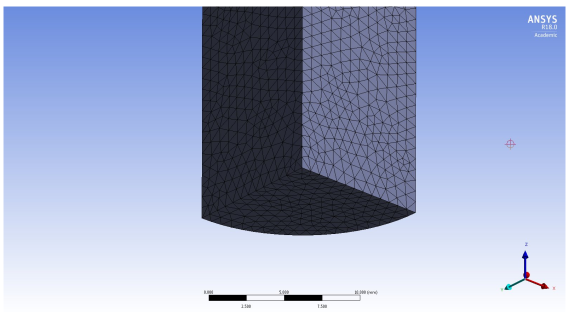

(c)

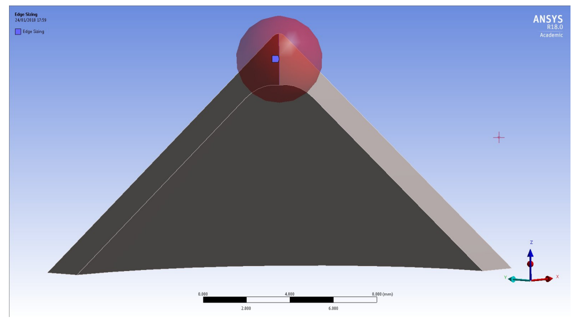

(d)

Figure 22: Dynamic model mesh: (22c) whole model; (22b), (22c) tetrahedral mesh generated on weight and shell; (22d) $2mm$ radius refined area around the apex.

Brick mesh was preferred in the static model. Surface quadratic elements swept through the whole volume have been used to fill entirely the solid (Figure23). This type of mesh has a series of benefits:

1. Restricted computational costs, as the number of elements (and nodes) is considerably reduced;
2. Emphasised stress patterns over the model, as sizing and inflations procedures are enabled and enhanced;
3. Enhanced element compliance with the adopted geometry chosen, as the elements aspect ratio is automatically modified to better follow the shape of the body.

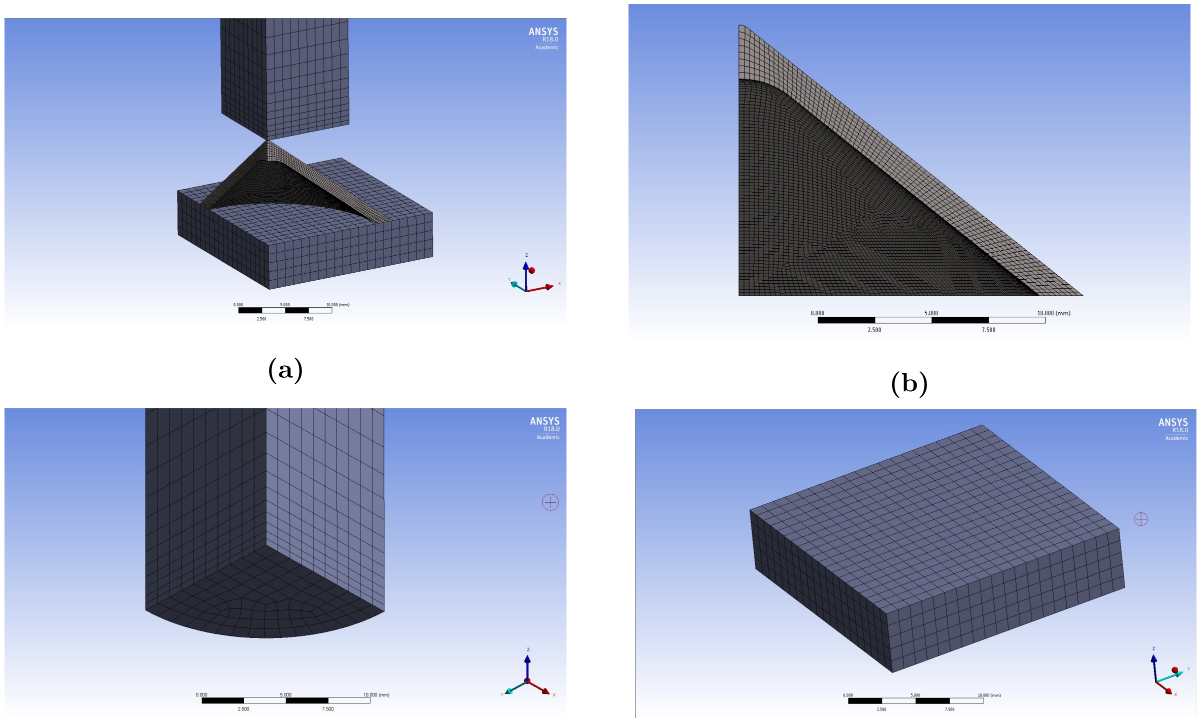

(a) **(b)** **(c)** **(d)**

Figure 23: Static model mesh: (23c) is whole model; (23b) shell hexahedral mesh; (23c) vertical biased sizing in proximity to the contact region of the weight; (23d) support regular mesh.

4.3.3 Parameters

All simulations were supposed to happen at room temperature. Within the analysis set-up a few approximations have been adopted regarding material properties, body contacts, and loading conditions.

Weight and support are considered as made of stainless steel, whose properties were already included in ANSYS® library. Limpet shell structure has already been described as mainly calcium carbonate in the forms of calcite and aragonite, localized in different regions and forming a layered structure[38]. As consequence it is expected a highly inhomogeneous and anisotropic material. Because of the aim of the model is to respect the main geometric features of the shell in order to evaluate its effect on stress distribution inside the structure, the material is assumed as homogeneous and linear elastic isotropic material. Its properties are summarized in Table1 together with the stainless steel ones. Density value was obtained from a study performed on the shell of Nocella concinna[61]; Poisson ratio was the same as the one used by Cabral[58] in his study; while the young modulus was obtained by Currey[51].

Material	Limpet shell	Stainless steel
Density(ρ) $[Kg/m^3]$	2600	7850
Young modulus(E) $[GPa]$	18	200
Poisson ratio(ν)	0.2	0.3
Bulk modulus(B) $[GPa]$	10	167
Shear modulus(G) $[GPa]$	7.5	77

Table 1: Material properties for limpet shell and stainless steel. Limpet shell density, Young modulus (E) and Poisson ratio (ν) are obtained from literature, while Bulk and Shear modulus are generated from the values of E and ν; Stainless steel properties are included in ANSYS® library.

Two body contacts can be distinguished in the model between: shell-weight contact and shell-support contact. In the last one, friction is modelled between the two contact surfaces, such that there is a dynamic friction coefficient (μ_d) of 0.4[62] and a static one (μ_s) of 0.7. Because no information in literature has been found for the static condition, μ_s considered was obtained simply arbitrary increasing the value of the dynamic one. To have an idea of how the results are affected by this parameter different values of μ_s are used, in detail: 0 (fixed), 0.3, 0.5 and ∞ (frictionless).

The shell-weight contact was modelled differently in the static and dynamic conditions for understandable reasons. In the compression model the number of degree of freedom allowed between the two bodies is irrelevant. No sliding or rotation happens even if they are allowed since the compression force applied is impressive, the piston inferior surface is flat and centred on the testing shell and the eccentricity of the shell itself is considered null. The dynamic condition is more complicated as the contact surface changes over time; it is therefore allowed the software to detect during every cycle the amount of surface involved in the contact considering the vertical trajectory of the falling weight.

For the compression simulation it was considered a load of $1000N^2$ on the upper surface of the weight and directed downwards. The compressive force applied was not chosen arbitrarily but

[2] 125N for the quarter model

resulted from experimental tests performed previously. The load-displacement curves obtained for most of the specimens tested (dry fresh shells) showed a sharp reduction in steepness after $1000N$ (Figure24). This behaviour is due to damage accumulating inside the structure, in terms of crack formation and propagation.

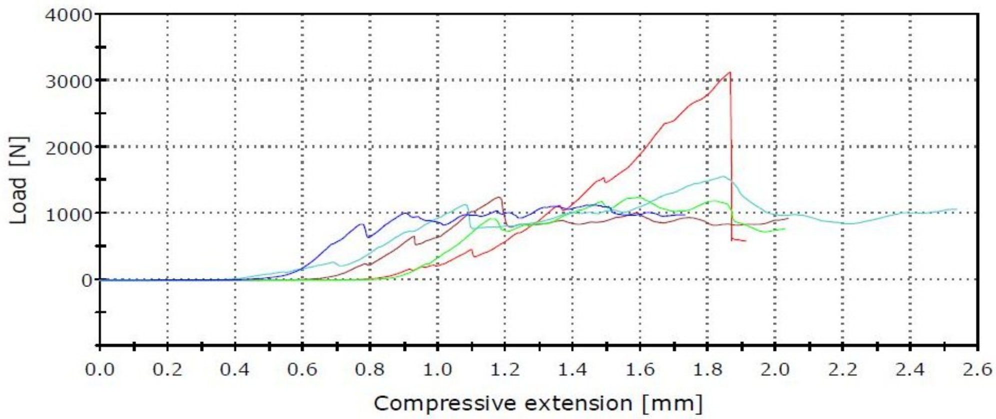

Figure 24: Load-displacement curve for several limpets tested in compression: As the compressive load approaches to $1000N$, some sort of damage is created inside the shell structure since the applied load remains steady while the piston keep moving downwards at $1mm/min$ speed. Such a low speed is advisable to consider the test as quasistatic.

In the impact model the load applied to the shell is applied by the falling weight. In order to speed up the calculations and avoid meaningless informations it was not modelled the weight being dropped from a certain height and the whole fall after that. The simulation started with the weight touching the shell with at given vertical velocity instead. Similarly the final part of the impact, when the two bodies move apart and the weight bounces back (flight phase), was neglected. It was chosen a simulation end time of $0.4ms$, which is enough to see the what happens in the contact phase.

An initial velocity of $2.85m/s$ was evaluated reversing equation4 to model a $0.5J$ impact. Since it has a major contribution in the dynamic of the process the gravitational acceleration was considered during the whole impact. The applied energy was chosen using the value adopted in most of the experimental tests performed. Its modulus has been modified in some more tests choosing both critical and subcritical values[3] in order to see if any macroscopical changes can be

[3]The critical energy considered is the one relative to a shell of $33mm$ size

observed in the stress distribution within the structure, as shown in table2.

% of critical energy [%]	10	20	100
Energy applied [J]	0.12	0.24	1.22
Weight velocity at the impact [m/s]	1.40	1.98	4.45

Table 2: Subcritical and critical tests parameters: impact energy and relative weight initial velocity for 10%, 20% and 100% of the E_{cr}.

The value of Young modulus already presented is very similar to the bone one and was obtained for wet specimens during bending tests. Values twice and three times as the one used here were found for most of the other limpets species, making the Patella vulgata one of the less stiff shells. The maximum deformation obtained in the model (at the shell apex) was compared with the one obtained with Young modulus of $50GPa$ and the one obtained experimentally.

A weak point in the model geometry is represented by the thickness at the apex, which is very variable and not easy to detect without compromising the measure itself. For this reason a couple of additional simulations were performed for apex thickness 2.5 and 1.5 times the thickness of the walls.

4.4 Toughness

Two procedures were followed to assess toughness in terms of stress intensity factor (K_c) and strain energy release rate (G_c). The second one comes directly from Griffith's approach to fracture, and it is more suitable for comparisons with other materials like nacre[50]. The second one is easily evaluated from the stress field in the defect neighbourhood, following Irwin's approach. The value obtained are then compared to the one obtained by Taylor[52].

4.4.1 Delamination crack

Twelve shells between 26 and $40mm$ were collected and impacted once at subcritical energy. Impact was performed at approximately 10% of the critical energy on the same pavement used for the other experiments, in order to avoid other source of variability. E_{cr} adopted is $8.8MJ/m^{4.6}$, which is nothing but the impact strength found by Taylor[47] for empty shells. The impact equipment adopted was the same as the one used for the cyclic impacts on site (Figure16).

Compression tests were performed both before and after the impact test on each specimen using a compression machine (Instron 3366, Figure25a). The specimens were placed on a flat stainless steel support and crushed by a lead piston moving downward. The piston was chosen with a flat rounded surface slightly bigger than the apex region (Figure25b).

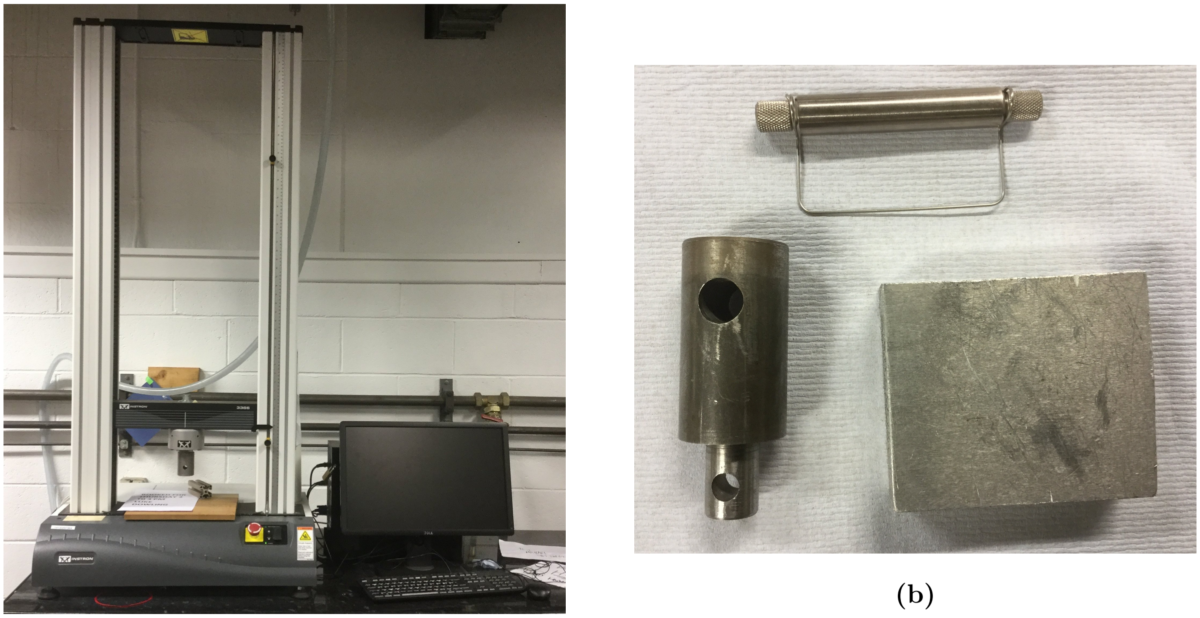

(a) (b)

Figure 25: Compression test equipment: (25a) Instron 3366 compression machine; (25b) piston, support and connecting shaft.

To guarantee quasistatic condition to be respected piston compression rate was set at $1mm/min$, even slower than the one chosen by Cabral in his own tests[39]. The compression was stopped as a load of $200N$ was reached. The maximum allowed load was chosen from the analysis of previous tests, where the first symptoms of damage were observed. Damage was emphasised by the presence of sudden drops in the load-displacement curves, and the first ones appeared over $250N$. Compression rate and maximum load applied could heavily affect the results if not chosen properly. Being able to classify the compression as quasistatic is important to avoid uncertainties due to the crushing procedure. Avoiding damage during the first compression test is essential not to jeopardize shell integrity and affect the output of the impact test.

Before the first compression a grinding machine (Figure17a) was used to remove excessive roughness at the rim. No grinding procedure was adopted in previous attempts, the presence of a very uneven rim caused consistent scatter in the curve behaviour generating unreliable results. Load-displacement curves were plotted after both compressions for each specimen and the difference between the areas underneath the two curves was used as an estimate of the energy actually lost in the cracks generation. The impact energies were then corrected for the factor just evaluated and a the critical energy release rate (G_c) was updated using equation3. The critical stress intensity factor (K_c) was then obtained assuming a Young modulus (E) of $18GPa$ the following equation:

$$K_c = \sqrt{G_c \cdot E} \tag{5}$$

4.4.2 Radial crack

In order to use a computational approach as a validation procedure, similar condition to the ones created experimentally by Taylor[52] were modelled. The initial model adopted was the very same as the one already presented, the only modification made was the introduction of a sharp notch. A sharp notch was designed in the radial direction moving from the rim towards the apex region, and placed precisely upon one of the two symmetry planes, so that the model simplicity is preserved and computational effort kept low. The characteristic length of the notch itself, $6mm$, was chosen accordingly to the ones carved by Taylor in his specimens (Figure26a). In order to analyse the stress distribution in the neighbourhood of $2.5mm$ radius from the crack tip, twelve contour regions were designed. An increasing gap between consecutive contours was implemented, specifying 1.2 as growing factor moving away from the crack front (Figure26b, 26c and 26d).

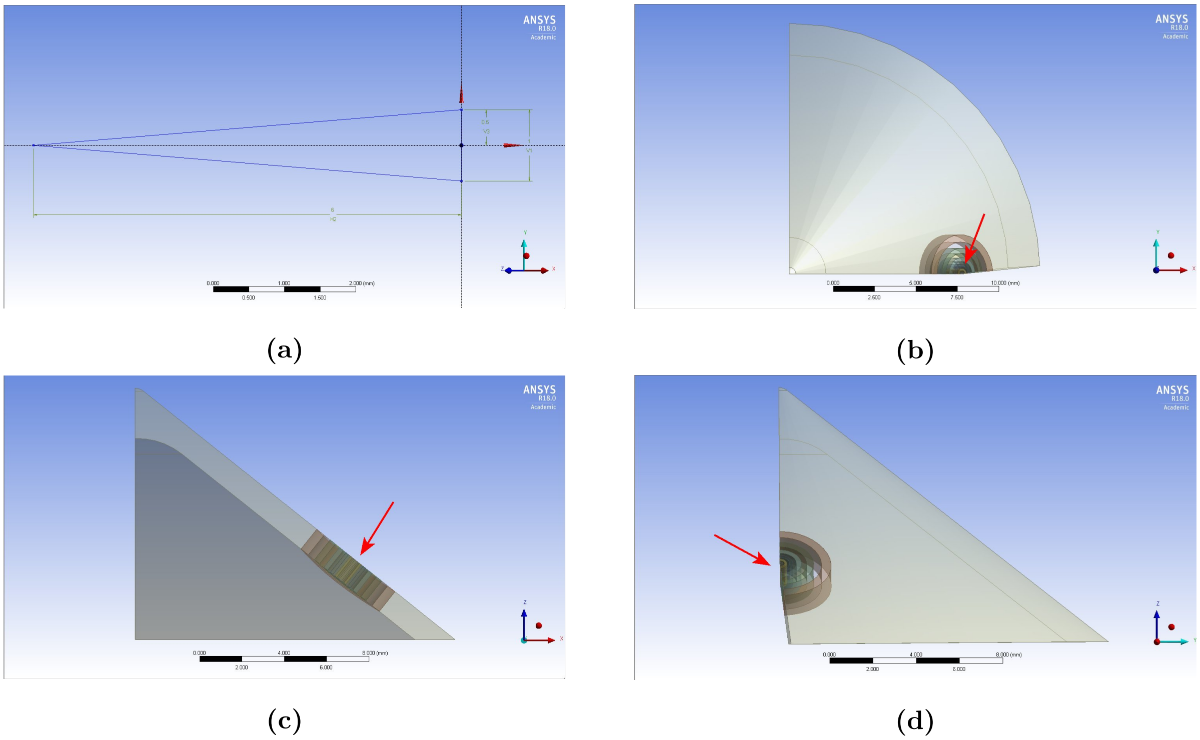

Figure 26: Crack model: (26a) sketch of the sharp crack extruded through the shell thickness; (26b), (26d) and (26c) contour regions surrounding the crack front from different prospectives. The arrows point out the notch tip.

Similarly to what has been done for the dynamic analysis, a tetrahedral mesh was adopted. The only adjustment made involved the area around the notch tip, where hexahedrons were used in order to follow the stress pattern moving away from the crack front (Figure27). Few pyramids could be found around the contour area as transitional element between the two meshes.

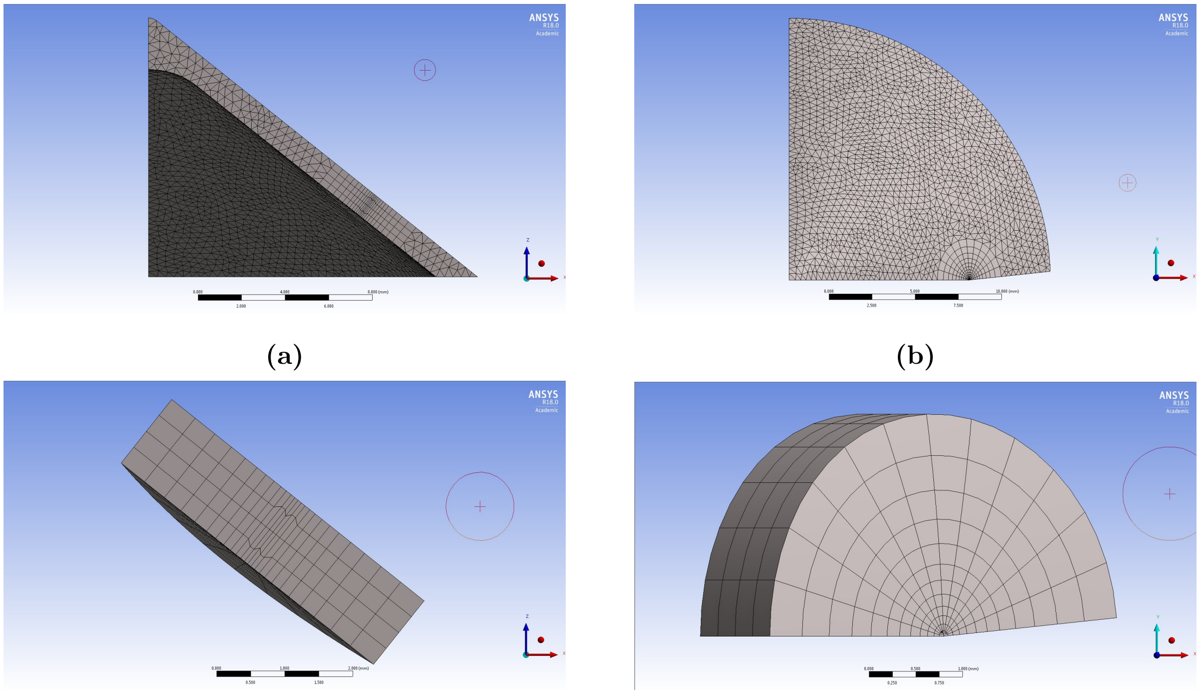

(a) (b) (c) (d)

Figure 27: Notch mesh: (27a), (27a) tetrahedral mesh of the full model; (27c), (27d) hexahedral mesh in the crack region.

The choice of the notch shape was made in order to avoid a transitional behaviour in stress (σ) distribution around the tip, and obtain a reliable value of critical stress intensity factor K_{Ic} as described by equation6. The calculation was performed along seventeen paths having directions from 0° to 180° all around the crack front, focusing the search between 45° to 90°. Similarly nine different depths were studied and the three different modes of crack propagation were compared (opening, in plane shear and out of plane shear).

$$K_{Ic} = \sigma_1 \cdot \sqrt{2\pi r} \tag{6}$$

The K_{Ic} value obtained is considered as critical since the loading condition simulated a vertical compression, of $1000N$. It has been showed already such a value of compressive load causes extensive damage in the structure (Figure24).

As in the previews simulations, some variations in the model parameters were applied to see if and how they would affect the final results, as friction coefficient between shell and support, shell

Poisson coefficient, apex thickness and load application method. What is meant by load application method is that instead of modelling the compression to be transferred to the shell by means of the weight (piston) it was applied directly on a defined portion of the superior surface of the shell. This condition is clearly less representative of what really happens in the experimental situation, it is however useful to see if a FEM model of a concentrated load introduces some unexpected features.

5 Results

5.1 Impact strength

A detailed study on how shells belonging to different groups failed during the impact is not one of the purposes of the present study and no further analysis was carried on. It is clear however that the most common failure mechanism for the abraded impact and the pierced shells is the formation of a hole in the apex or its enlargement, while the abraded ones are more likely to collapse, breaking in several pieces (Figure28).

(a)

(b)

(c)

(d)

Figure 28: Failed specimens after the impact test: (28a) abraded shells; (28b) impacted shells; (28c), (28d) pierced shells.

The numerical results of the impact tests are summarized in table3. Besides the number of specimens tested for each group (N) it is also expressed the number of specimens really involved in the calculation of the critical length (N_{cr}). The great variability in this number is reflected in the average size for of the shells tested; specimens too big are much less likely to fail and to be included in the critical length evaluation. Looking at the critical energies calculated using the equation1 obtained for different groups, a major role is played by the uncertainty terms. The only statistical difference can be seen between repaired and fresh shells: the first ones shows a much better response to the impact, having a value of critical energy more than twice the seconds.

	L_{av} [mm]	$N(N_{cr})$	e_{tot} [mm]	L_{cr} [mm]	E_{cr} [J]
Impated (Recovered)	36.42 (0.87)	34 (6)	0.01	27.87 (1.24)	7.10 (1.55)
Abraded (Recovered)	26.09 (0.51)	25 (15)	0.02	27.50 (0.97)	7.55 (1.33)
Apex hole (Recovered)	31.51 (0.91)	17 (7)	0.02	28.84 (2.27)	6.07 (2.28)
Apex hole (0days)	34.63 (1.60)	21 (6)	0.01	35.48 (1.83)	2.34 (0.59)
Near apex hole (0days)	33.58 (1.78)	20 (11)	0.01	33.96 (3.85)	2.87 (1.53)

Table 3: Impact test results: average size, number of specimens tested (number of specimens useful to evaluate the critical length), critical length and normalized critical energy. Variability is expressed as standard deviation.

Normalized critical energies obtained during this study for impacted and abraded groups are plotted together with the ones at different healing times and compared to the chart containing the preliminary values at two months already available[63]. Additional tests in the impacted groups after 60 days did not generate any appreciable difference with the previous data (Figure29). Abraded shells in comparison show a relative increase in the normalized energy (Figure30).

It is comforting to see that the new value at 60 days is higher than the one at 30 days, even though there is no statistical difference. A meaningful difference can however be noticed if compared with the specimens collected after 10 days. Impact strength after two months is hence significantly improved not only from fresh and beach shells (naturally abraded) ones but from the ones with a short repairing time too, which means that longer repairing time really affect the shell response. Results obtained are compared with a value labelled as control, which is nothing but the normalized critical energy evaluated by Taylor[47] for the in situ shells. In both cases, it seems that the healing process after two months is not complete yet; nothing can however be said for certain due to the wide uncertainties involved.

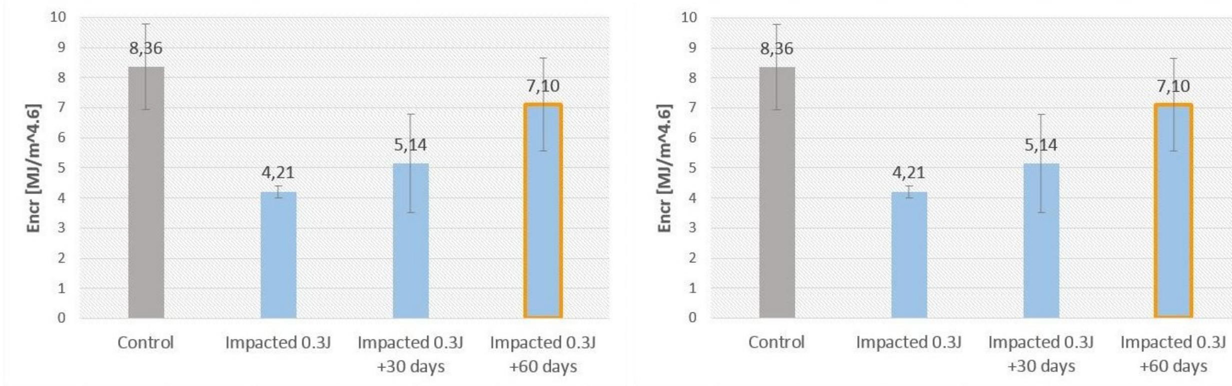

(a) (b)

Figure 29: Impact strength recovery process for impacted limpets at different recovery times: (29a) with the old energy value at 60 days (29b) with the updated energy value at 60 days.

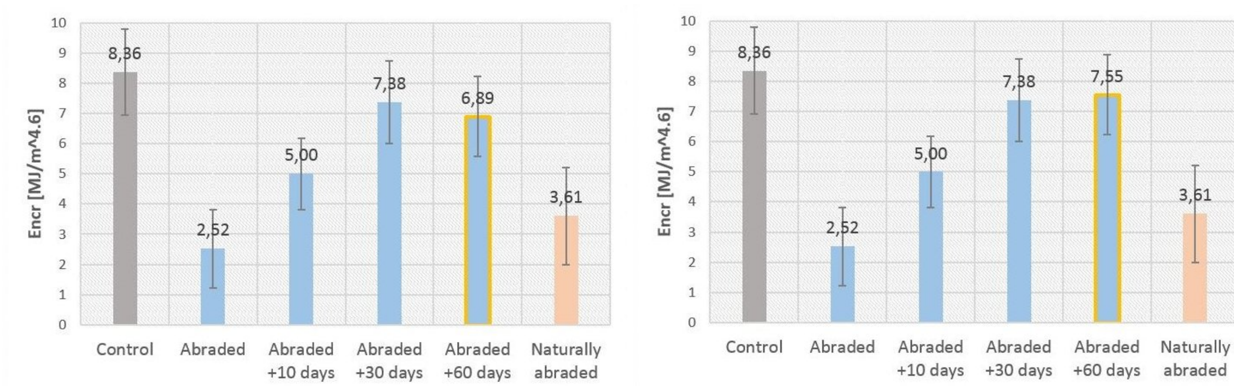

(a) (b)

Figure 30: Impact strength recovery process for abraded limpets at different recovery times: (30a) with the old energy value at 60 days (30b) containing the updated energy value at 60 days.

Pierced shells at the apex show improved mechanical resistance to the impact when left in situ for two months (Figure31). The use of shells which experienced multiple repair times (52, 63 and 74 days) increases the variability of the measurement such that it is hard to tell any meaningful difference with the control group. The shells pierced off-centre showed a value in between the impact strength evaluated for pierced and healthy shells. A meaningful difference with respect to the shells pierced in the apex is however not showed, meaning that small variation in hole location does not significantly affect the mechanical behaviour of the shell. A much larger standard deviation is a proof that the presence of a hole off-centre does not affect the impact strength always in the same way but varies from time to time. Finally, whatever the actual location of the hole is the impact strength appears heavily reduced.

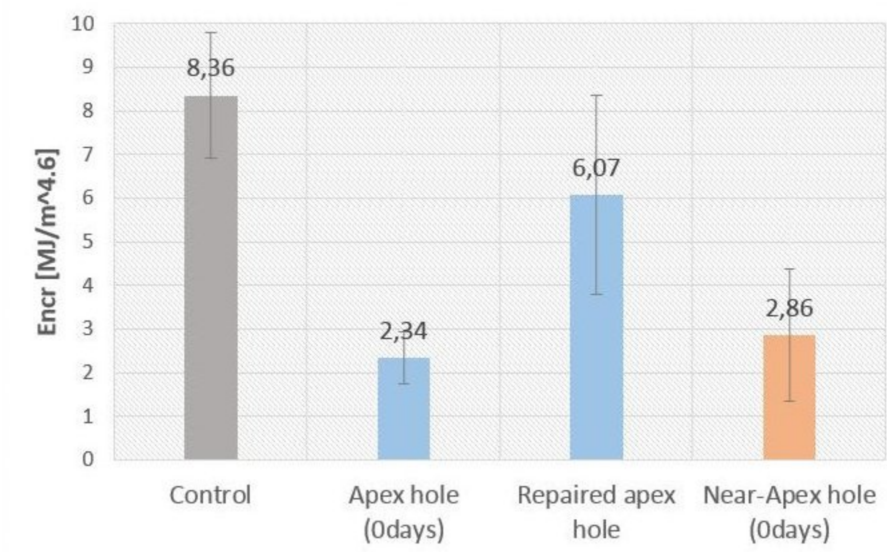

Figure 31: Apex hole effect on shell impact strength: critical normalized energy for fresh shells, off-centre pierced shells and shells collected after 60 days.

Critical energies obtained for pierced shells at zero days (centred hole or not) are compared to the ones obtained for other groups that did not experienced repair (Figure32). Pierced shells show similar mechanical properties to abraded and beach groups. In particular the ones with a centred hole have the lowest critical energy ever measured, proving once more that when the integrity of the apex is compromised the impact strength of the structure falls rapidly. A very effective repairing seems to happen in groups whose mechanical properties heavily drop at 0 days time. Pre-impacted limpets are the only group showing an intermediate behaviour, as the damage created is not as severe as during the abrasion or the piercing mechanisms. Naturally abraded shells have a similar behaviour to the impacted ones, but they are affected by large variability as they include specimens that experienced a wide range of damage and modifications.

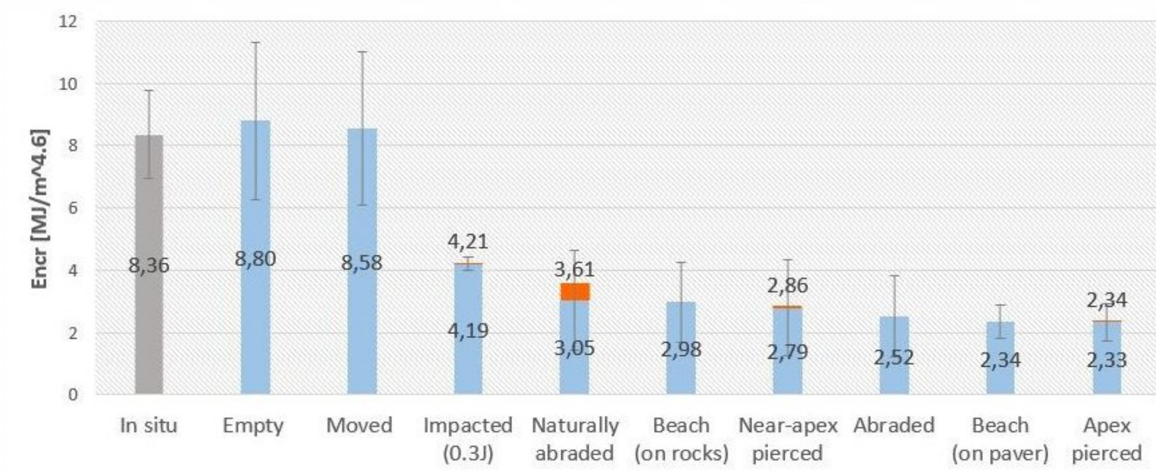

Figure 32: Zero days recovery time Impact strength: Normalized critical energy for different groups; corrections made with MATLAB® algorithm emphasised in orange.

5.2 Fatigue

5.2.1 Consecutive impacts

Normalized energy (E_n) and accumulated normalized ($Accumulated\ E_n$) energy are plotted versus the number of impacts to failure (Figure33). The lines drawn on both charts consider all the points where the total accumulated energy is equal to the control group impact strength 8.36 ($\pm$1.43) $J/m^{4.6}$. The result obtained is the very same as the one obtained by Taylor[47], but this time pre-damaged specimens are plotted.

It can be noticed that some of the specimens fail after only a few cycles as consequence of impressive values of E_n and $Accumulated\ E_n$, compared to the impact strength already evaluated and marked at $N_f = 1$. This phenomenon as well as the high variability in this result is partially due to the high impact energy adopted for the tests, 0.5 ($\pm$0.01) J. Such an energy is very close to the critical value of specimens only a few millimetres bigger than L_{cr}; as consequence most of the shells failed after only a couple impacts having overestimated energy values. It is possible to refer to this problem as an accuracy problem of the procedure. On the other side this problem affects only the smaller specimens but the majority of the tested shells was significantly bigger than L_{cr}, leading to accurate measurements.

Results can be considered as reliable for the purpose of the study, since it is actually the right-hand side of the graphs (low normalized energy and several impacts) that is really meaningful. Once more, specimens impacted with a E_{app} ten times smaller than the critical value require ten strikes or so to reach failure, pointing in the direction of the accumulated damage theory.

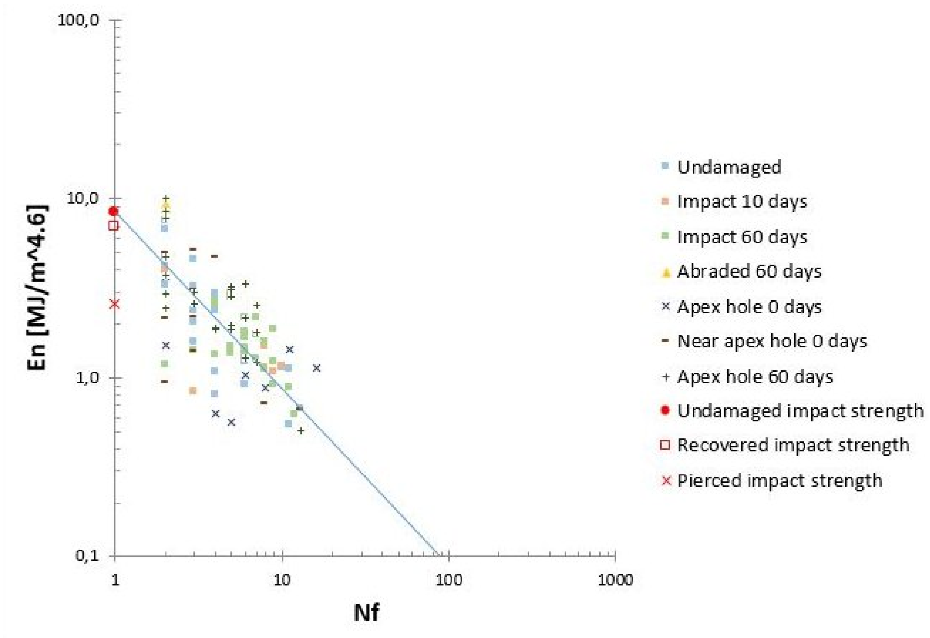

(a)

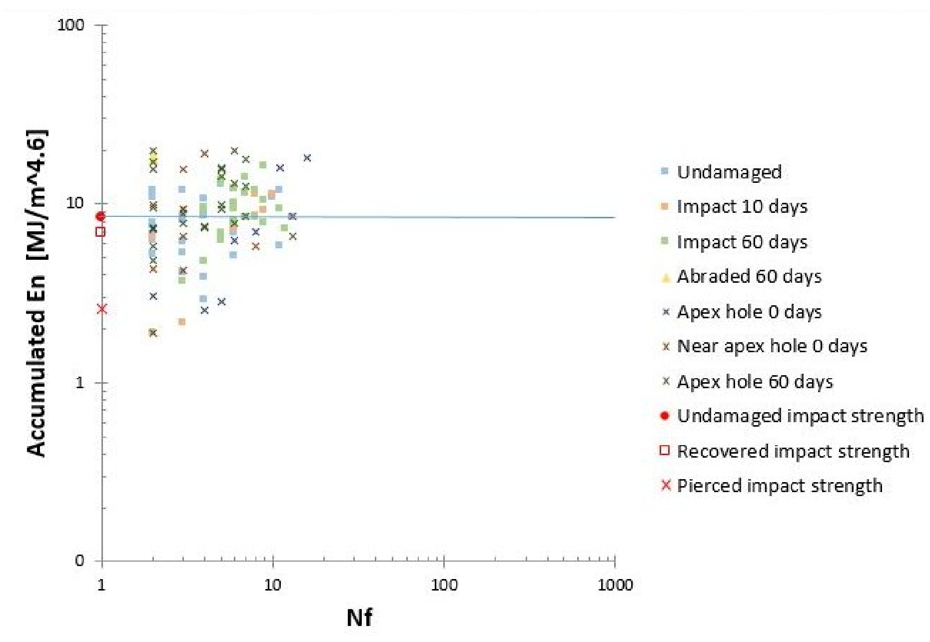

(b)

Figure 33: Consecutive impacts fatigue plots: (33a) normalized energy over the number of strikes to failure (33b) accumulated normalized energy over the number of strikes to failure.

The number of specimens involved in the experiment varies between different groups since different range of sizes were used. The abraded groups average size is considerably smaller than the impact group one for instance (Table3), hence less specimens could be employed for the study.

5.2.2 Cyclical impacts

Whenever an experiment is carried out in an open environment, as in this case, there is always a series of uncontrollable variables that can affect the results. One of these variables, other than human presence and predatory events, certainly is the weather conditions. The presence of ever-changing conditions, even stormy ones, are taken into account by choosing an overstated number of specimens to start with and narrowing the impact site to a single group of rocks gathered together. What was not expected was a very unique meteorological event for the Irish climate like Hurricane Ophelia. Originating from in the Atlantic ocean, Ophelia reached Irish coast on October 16^{th}, causing damages all over Ireland. Even though Dublin county has not been one of the most affected areas, unusually high waves and strong winds have been recorded during the whole day, and the harmful effect of high waves on limpets integrity has already been proved[42].

During the event an unusual number of limpets went missing, especially in the groups impacted at 20%, as shown in table4. The amount of shells lost during the event was even more impressive considering that the hurricane reached Irish shores at the beginning of the work, when the tested specimens had only received a couple of impacts. In the following analysis it was chosen to neglect these shells from the results, because their failure was evidently not related to the impacts applied. It is important however to bear in mind that even the surviving limpets may have been affected by the hurricane, leading to results that could be partially compromised.

	10% (7days)	20% (7days)	20% (14days)
Limpets lost in the hurricane	7.02%	31.48%	38.10%

Table 4: Ophelia hurricane effect on studied specimens: percentage of lost specimens over the total number of limpets tested.

The rest of the shells have been impacted as planned. Quite surprisingly none of the specimens failed during the impact sessions, except for three shells belonging to the 20% energy every 7 days group, which failed after only one or two strikes (Figure34). All the three specimens showed an abnormally soft shell and experienced a massive collapse of the apex.

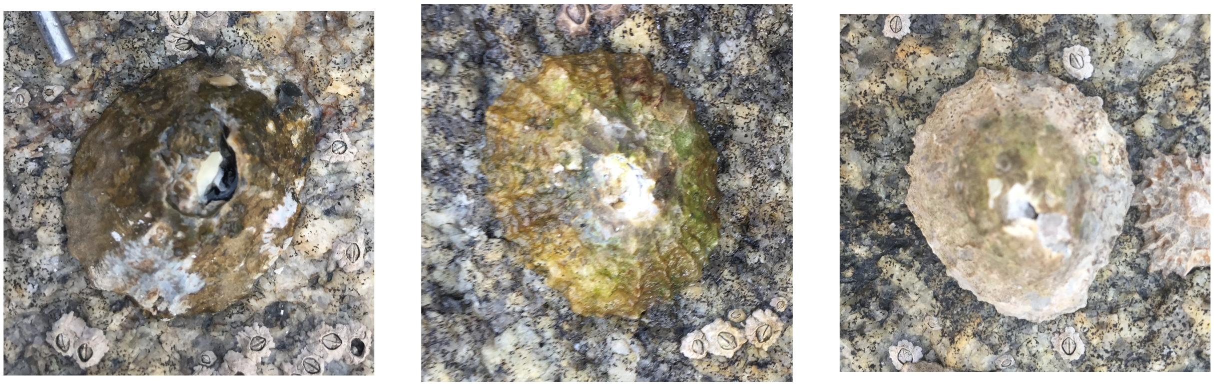

(a) (b) (c)

Figure 34: Early failed limpets: (34a) experienced only 20% of the critical energy; (34b) and (34c) experienced only 40% of the critical energy. All of them were impacted every 7 days at 20% of the critical energy.

The fate of the limpets tested after four months is summarized in table5. Although some of the shells survived the whole experiment, most of them went missing or were found broken (Figure35). The specimens found broken were still hosting the living animal inside and went missing in the following weeks.

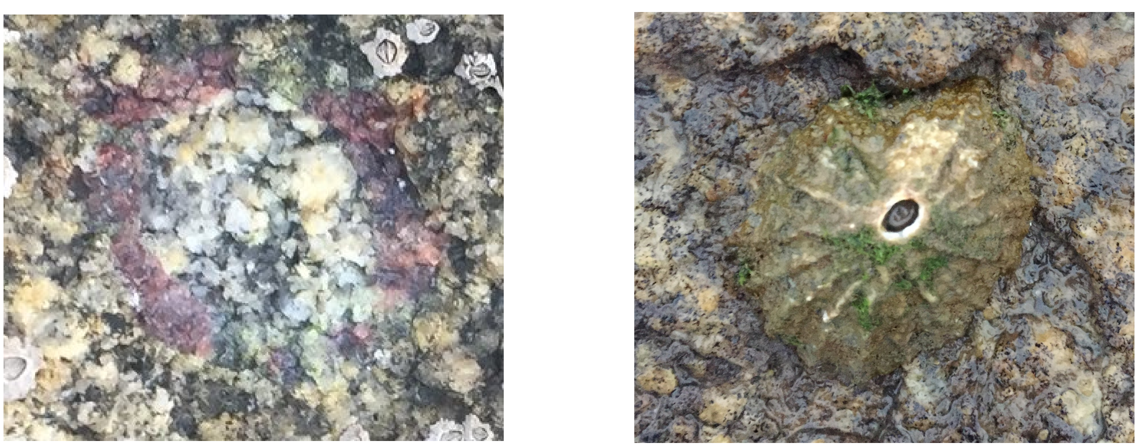

(a) (b)

Figure 35: Limpets fate examples:(35a) example of missing limpet print on the rock;(35b) example of found broken limpet with the living animal inside.

The aim of the study was to see when limpets would start failing, and neither missing nor found broken limpets can be considered in this evaluation because they did not fail during the impact sessions. It is however proved by the behaviour of the control group in table5 that both fates are indirectly caused by the damages suffered during the cyclical impacts. As matter of fact only one over 46 control limpets monitored went missing in four months.

	Accumulated energy	Survived	Missing	Found broken	Failed
10% (7 days)	140%	42.31%	50%	7.68%	0%
20% (14 days)	140%	40.54%	54.05%	5.41%	0%
20% (7 days)	260%	2.56%	82.05%	7.69%	7.69%
Control	-	97.83%	2.17%	0%	0%

Table 5: Cyclical fatigue test outcome: The accumulated energy is written as percentage of the undamaged shells critical energy ($8.36 MJ/m^{4.6}$) obtained by Taylor[47]. Specimens' fates are expressed as percentage of the total number of shells tested.

What seems to happen is that before a limpet fails it reaches a condition where its shell is whole but the cumulated damages inside the structure severely affects the mechanical properties, leading to death under natural conditions (waves, pebbles and predations). Differences can be seen in terms of survival rate between different groups (Figure36). Limpets impacted every 7 days with 20% the critical energy get lost at constant rate during the whole experiment, while the other two have a constant phase before 50% of the E_{cr} followed by a sudden drop and a second knee after the E_{cr} (vertical red line in figure36). It seems like for higher value of subcritical energy the resting period has an effect in the way limpets interact with to the environment. In addition, 50% of the initial limpets were lost when the accumulated energy reached the critical energy, regardless of the pre-damage suffered.

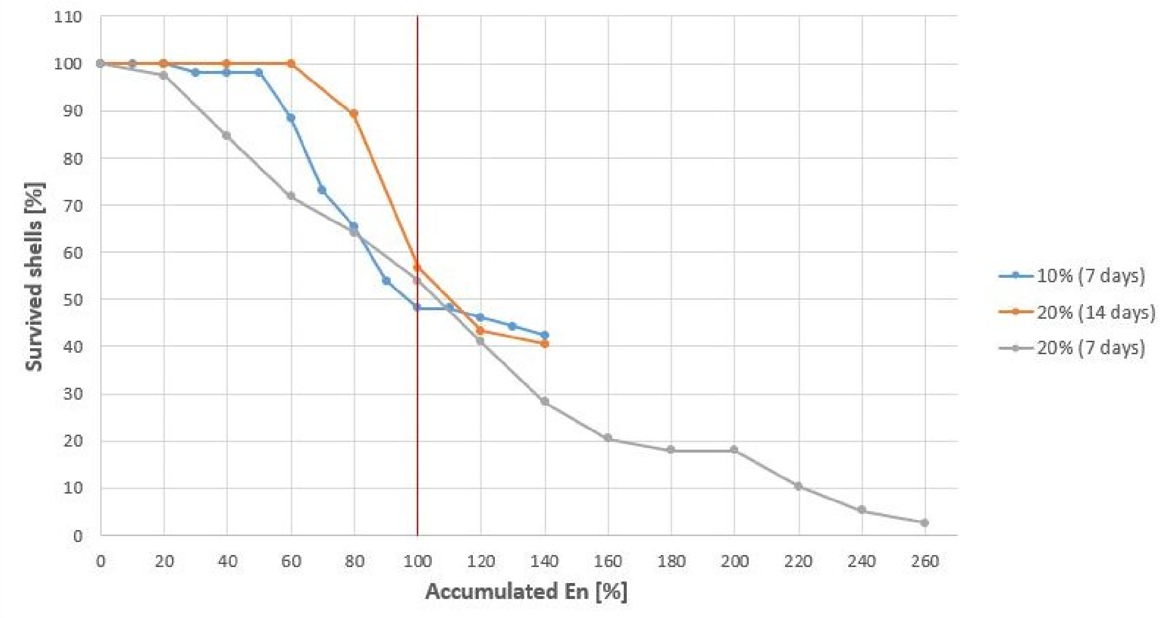

Figure 36: Survival rate: percentage of survived limpets over the accumulated energy already applied. The vertical red line points out the accumulated energy reaching the critical value.

The average size for the three groups is around $35mm$ but differences can be noticed on how it changes over time (Figure37). Bigger size shells seems more susceptible to be lost than the small ones for the groups impacted every $7days$.

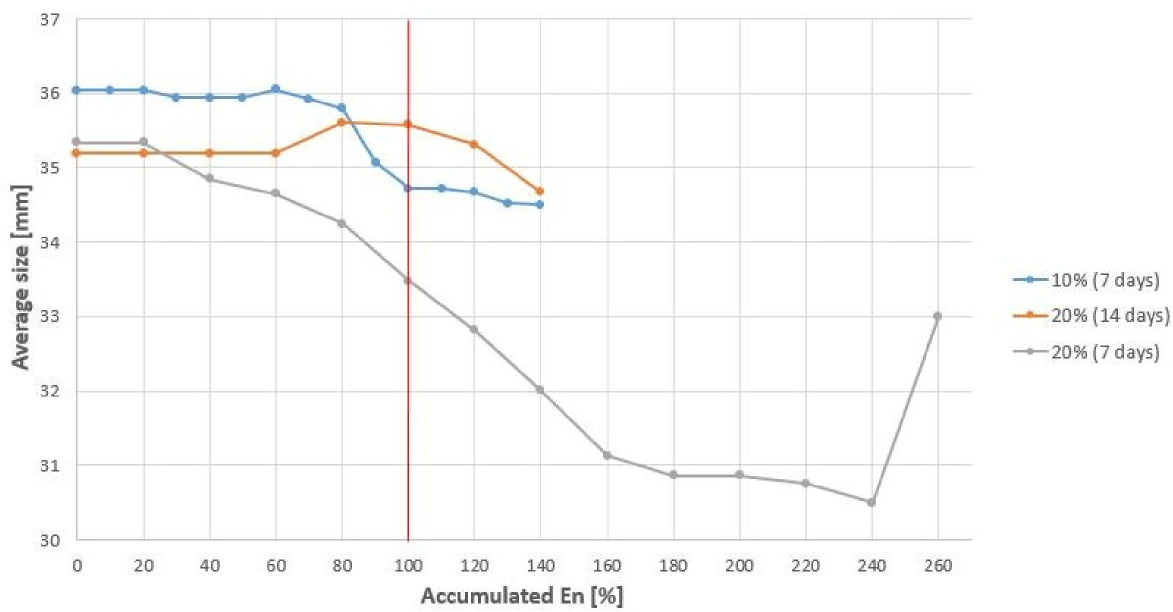

Figure 37: Size variation: survived limpets average size over the accumulated energy already applied. The vertical red line points out the accumulated energy reaching the critical value.

Lack of failure makes impossible to plot a fatigue plot as the one for consecutive impact fatigue analysis. It is however possible to consider E_n and *Accumulated* E_n applied at the end of the study for the three groups and overlap such values with the one already obtained (Figure38). All surviving limpets experienced an accumulated energy well above the critical value, and very similar to the best results obtained for the consecutive impacts, suggesting that repairing mechanisms somehow improve the fatigue properties of limpets shells.

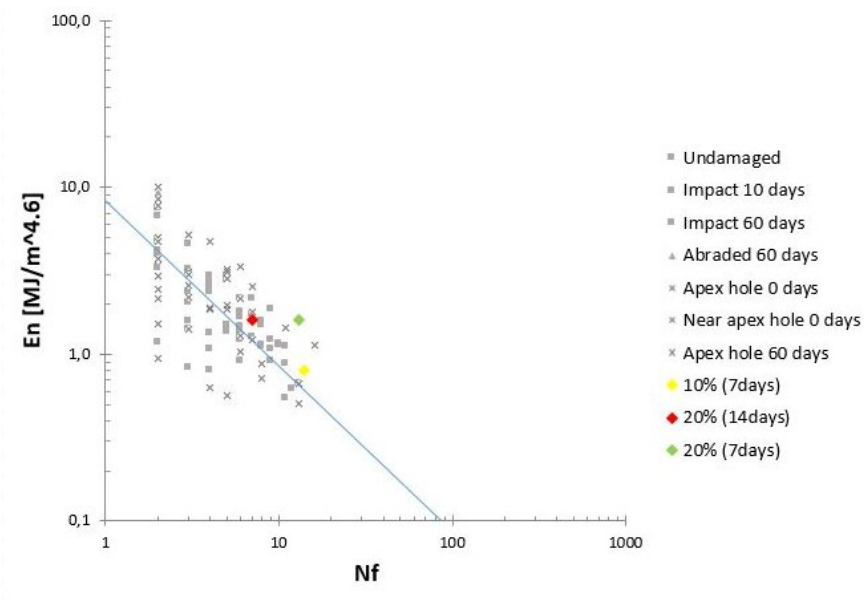

(a)

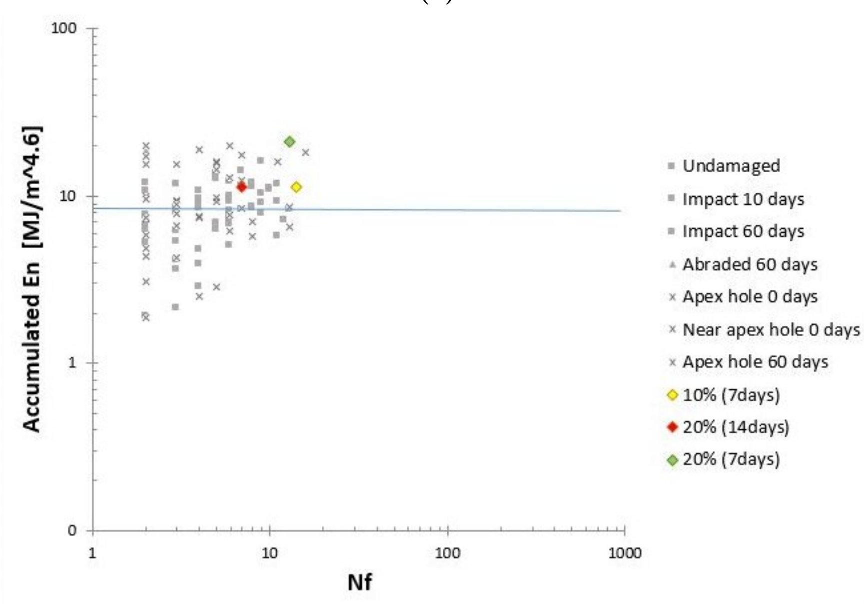

(b)

Figure 38: Cyclical impacts fatigue plots: (38a) normalized energy over the number of strikes to failure (38b) accumulated normalized energy over the number of strikes to failure. The blue lines point out when the impact strength is reached.

Nine specimens were observed at the SEM machine: the only survivor impacted with 20% of the E_{cr} every 7 days and four belonging to each of the other two groups. The damage generated by the cyclical impact is entirely localized in the apex region. Apex upper layer breakdown, spalling process and delamination cracks along the calcite laminar structure are the main phenomena taking place in all the specimens observed. These three phenomena have a macroscopic effect, as they can be noticed without any technological support and no differences can be noted in different groups. Increasing the resting period between following impacts seems to induce less cracks, or the healing process has time to close small cracks. The result is that fewer cracks can be seen in the apex area (Figure39).

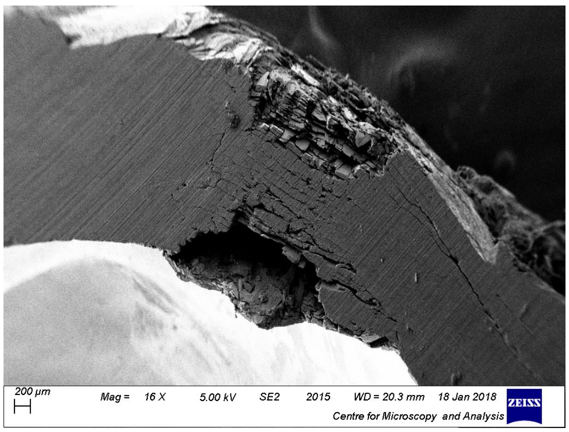

(a)

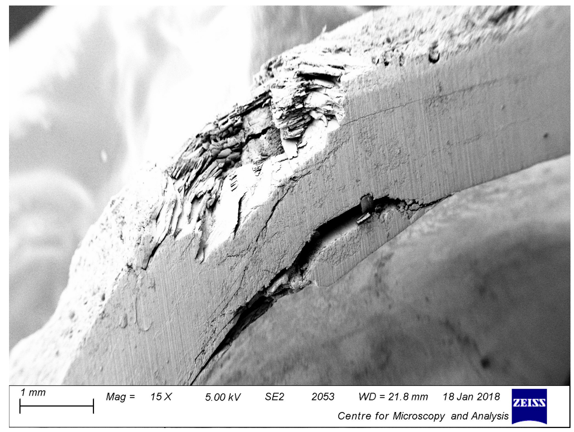

(b)

Figure 39: Cyclical impact results: (39a) specimen impacted at 10% of E_{cr} every 7days; (39b) specimen impacted at 20% of E_{cr} every 14days. Specimens have similar sizes but the second one shows a reduced number of cracks.

Even though none of the observed specimens failed properly during the experiment, the microscopical structure received a considerable amount of damage. As consequence the apex region of some of them collapsed during the cutting process, revealing the cross-lamellar structure underneath (Figure40a, 40b, 40c). These specimens are not useful to see what really happened but shows a characteristic pyramidal shape, larger outside and larger inside, similar to the calcite made area observed by Ortiz et al.[38].

Delamination cracks are concentrated in the central, upper part of the apex and show a very smooth shape. Cracks are hardly longer than a few millimetres and the longest ones often grow from the apex tip towards the front of the shell (Figure40d, 40e, 40f). The few cracks that grows perpendicular to the lamellar structure are much more rough and located preferably in the area where a hole would appear during failure (Figure40g, 40h, 40i).

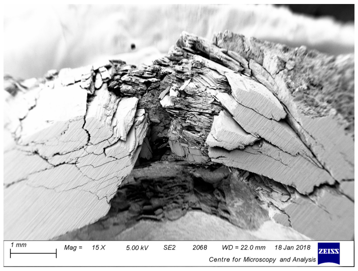

(a)

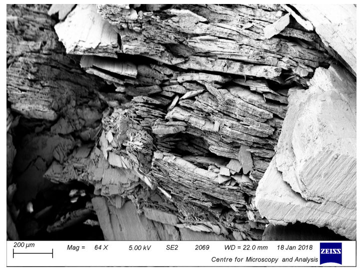

(b)

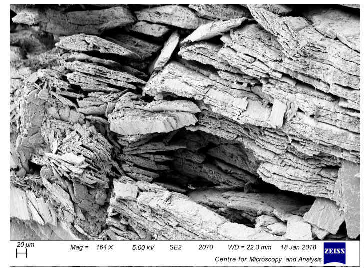

(c)

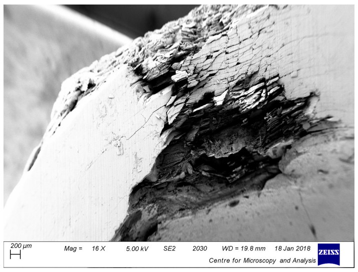

(d)

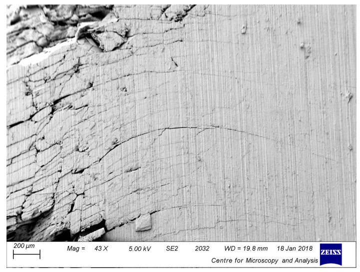

(e)

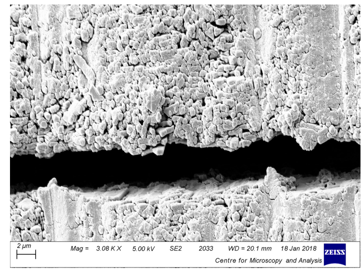

(f)

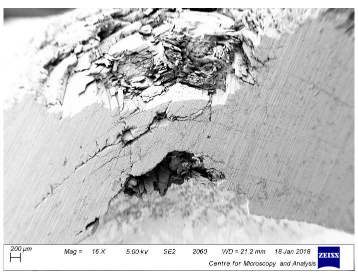

(g)

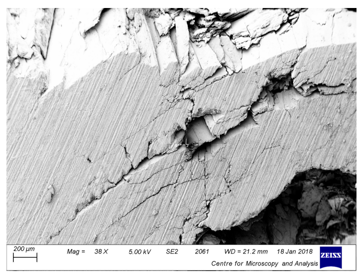

(h)

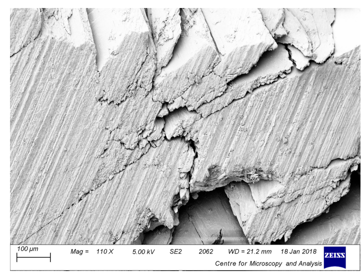

(i)

Figure 40: Damage characterization: (40a), (40b), (40c) collapsed apex detail; (40d), (40e), (40f) delamination crack; (40g), (40h), (40i) vertical crack.

5.3 Computational modelling

5.3.1 Impact simulation

Because of the shell has been modelled as purely elastic, the impact could be approximately associated to a mass-spring with a force applied vertically and directed downwards changing over time. Considering the origin of the reference frame on the support upper surface and positive the upwards direction, weight position, velocity and acceleration vary accordingly to such a model (Figure41).

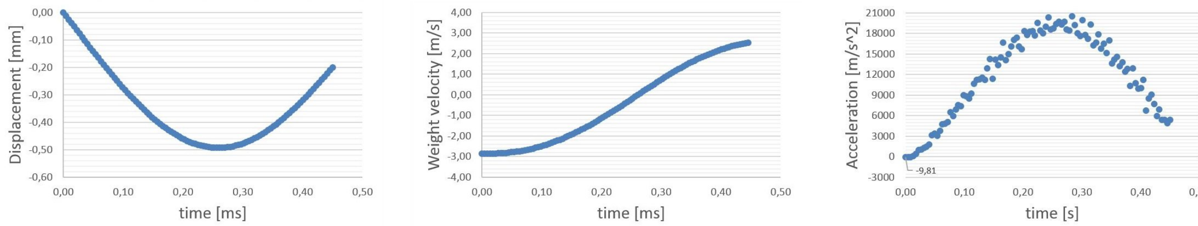

(a) **(b)** **(c)**

Figure 41: State of motion of the falling weight: (41a) vertical displacement, (41b) velocity and (41c) acceleration of the weight during the first $0.4ms$ of the impact.

Initially all the energy of the system is equal to the kinetic energy of the falling weight. As the weight hits the shell, some of the energy is progressively transferred to it until the weight stops and the whole energy is internal energy. In the second phase of the impact the energy is returned to the weight that starts moving upwards until they move apart (Figure42a).

The shell is modelled as purely elastic, however the energy returned is not equal to the initial energy. A major source of dissipation is represented by the frictional contact between the shell and the support. As the weight transfers its energy to the shell, it is squashed and the rim slides along the steel support releasing some of the energy received. Further proof is the fact that the contact energy is almost null when the shell-support contact is considered as fixed (no degree of freedom allowed).

Hourglassing and shear-locking are avoided and no error can be seen in the energy conservation chart (Figure42b) confirming the previous analysis. Since a vertical velocity was assigned to the weight, its momentum is focused on the z axis (vertical direction) increasing in the first phase of the contact and decreasing in the second one (Figure42c).

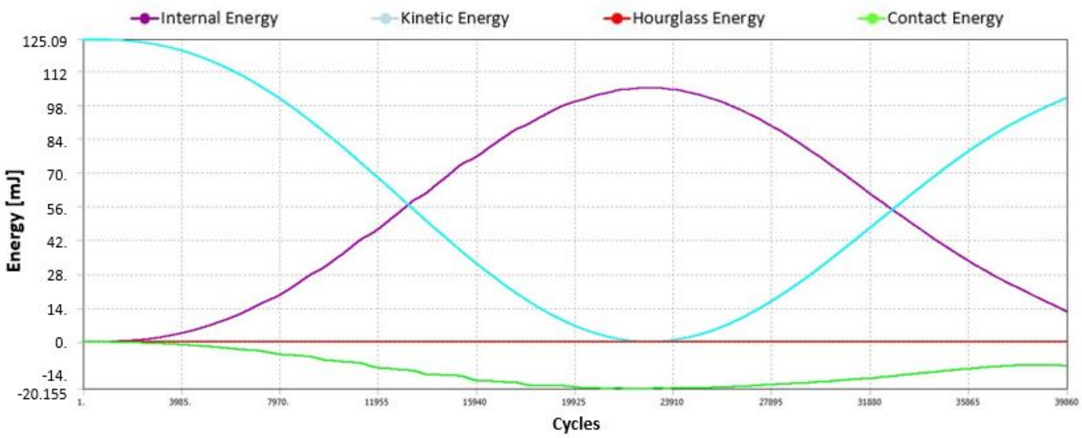

(a)

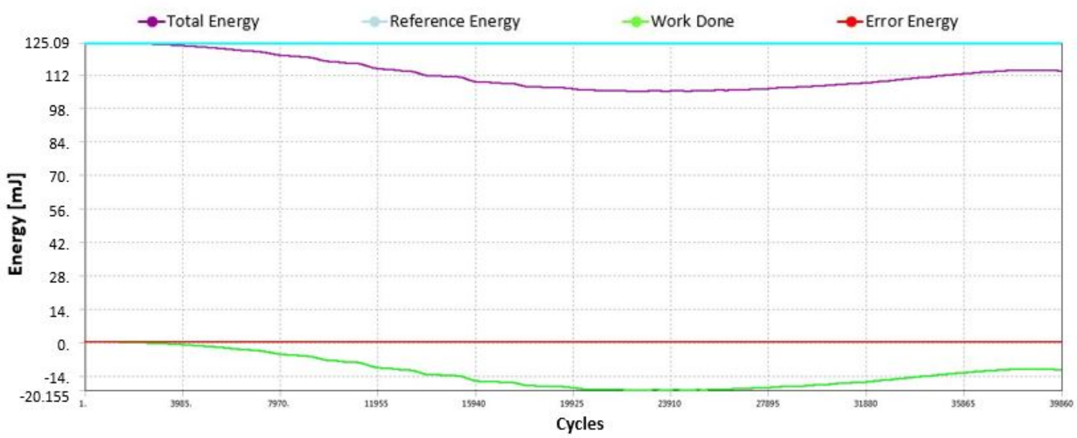

(b)

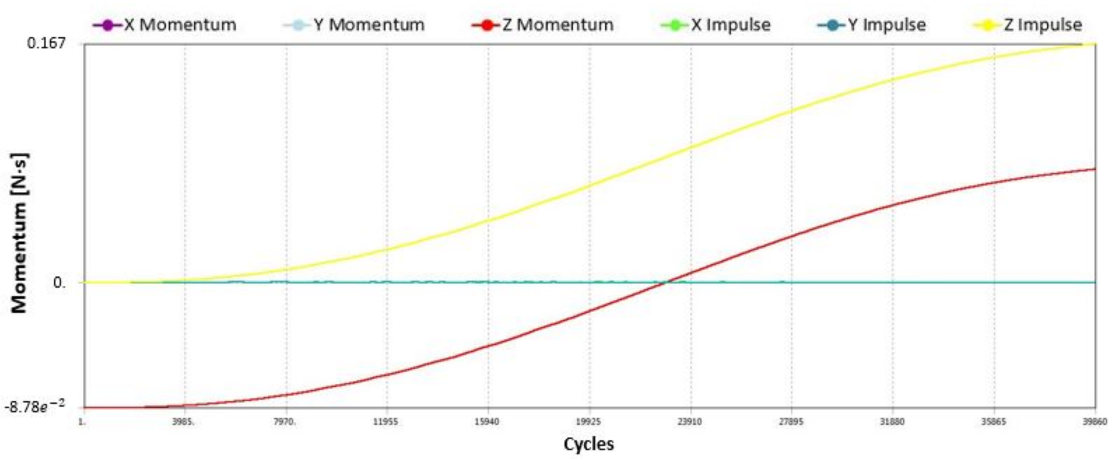

(c)

Figure 42: Impact energy and momentum analysis: (42a) energy transfer, (42b) energy conservation and (42c) impulse applied during first $0.4ms$ of the impact.

In order to understand how the stresses are distributed within the model, maximum principal stress (σ_1) and equivalent stress (Von Mises, σ_{eq}) are studied (Figure43). All the images refer to the maximum shell deformation point or zero weight velocity point, so that the stresses shown are the maximum perceived by the model during the whole simulation.

The weight has a very easy geometry and it is five times stiffer than the shell. As consequence the compression wave quickly propagates through the whole body from the contact region all around (Figure43a). Stresses in the order of thousands of MPa are perceived in proximity of the contact point and are propagated all around. The analysis of the maximum principal stress shows very low values, proving the compressive nature of the stress perceived by the weight (Figure43b).

The support is much less stressed, and the area involved restricted to the one nearby the contact surface (Figure43c). A maximum of $20MPa$ is observed close to the shell inner surface as tensile stress and close to the outer one as compressive one, consistent to the physics of the rim sliding over the surface (Figure43d).

The shell body is mainly stressed both in the apex and in the rim regions. From the σ_{eq} analysis it can be noted how the shock wave really propagates from the contact region and avoiding the inferior part of the apex propagates radially down the structure mainly close to the inner wall (Figure43e). Looking at how σ_1 is distributed it can be noted that even though compression is dominant in the contact zone, impressive tensile stress is experienced both deep in the thickness of the apex and at the rim reaching values in the order of hundreds of MPa (Figure43f).

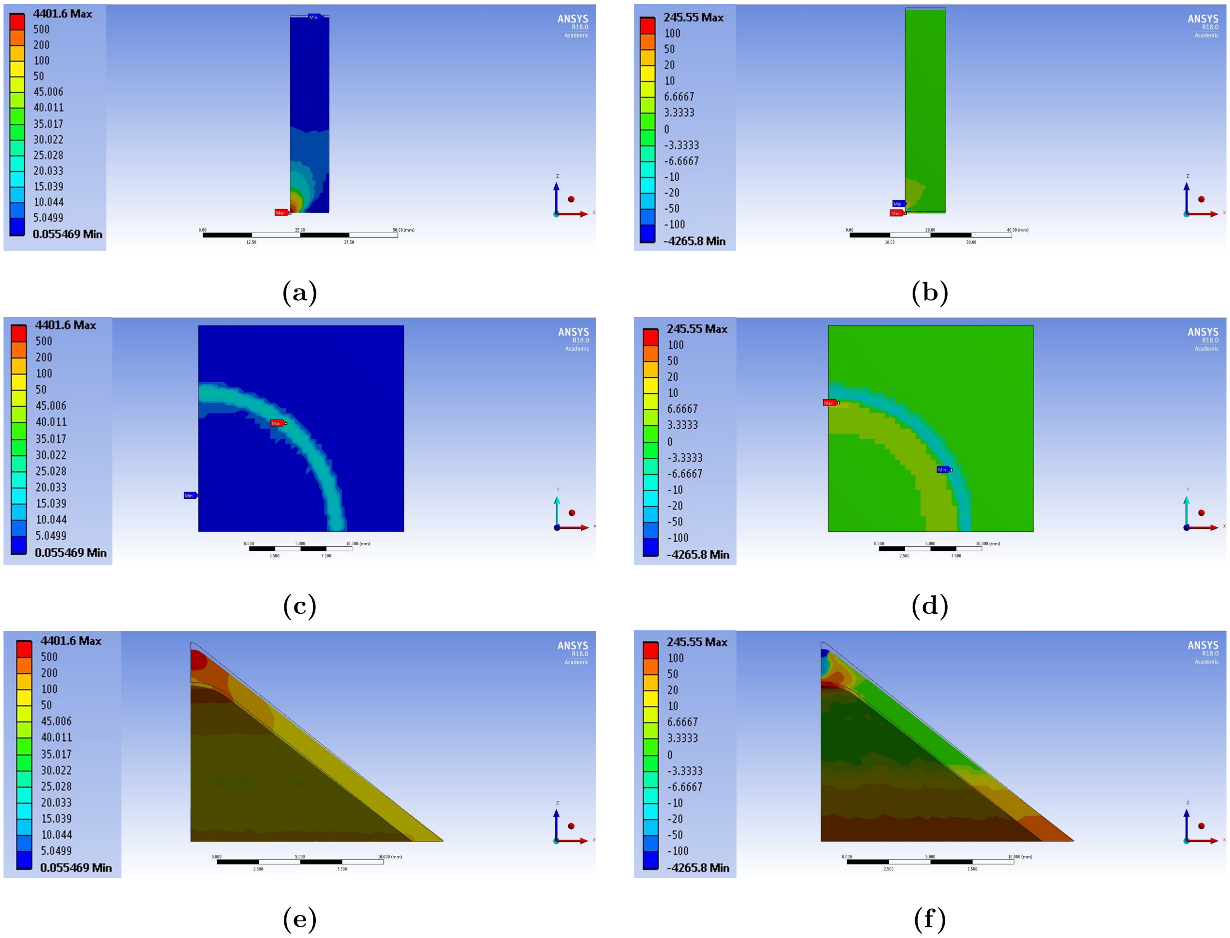

Figure 43: Stress distribution in the model: (43a), (43b) equivalent stress and maximum principal stress in the weight respectively; (43c), (43d) equivalent stress and maximum principal stress in the weight respectively; (43e), (43f) equivalent stress and maximum principal stress in the weight respectively. Stresses are expressed in MPa.

The geometry adopted focuses the stresses within the apex region; it is therefore interesting to further investigate what really happens in that region. As already mentioned, compression and tension are both experienced in this area. The choice of a very refined tetrahedral mesh enables to see how high values of stress are concentrated around the contact point but slip away very quickly. The minimum principal stress vectors directed parallel to the shell walls emphasises how the compression wave really follows the geometry and propagate in the radial direction (Figure44a).

A focused look at the σ_{eq} shows a stress concentration on the inner surface moved approximately one millimetre away from the apex (Figure44b). This detail finds a match in the tested specimens as the spalling phenomena usually involve a restricted area of the internal wall at the apex (Figure40). The presence of considerable compressive status in this region may be related to the reason why spalling does not proceed any further.

Principal stress vectors highlight the compressive status at the apex tip and shows that the traction already observed in the deepest region tilts more and more as we come from the apex until a direction orthogonal to the shell walls (Figure44c). The σ_{eq} information overlaps the one just observed in the vectors but emphasises the region detecting a relevant tensile status (Figure44d). This information is quite interesting if compared with some of the SEM pictures already obtained as it approximately replicates the conical shape of the collapsed apex (Figure40).

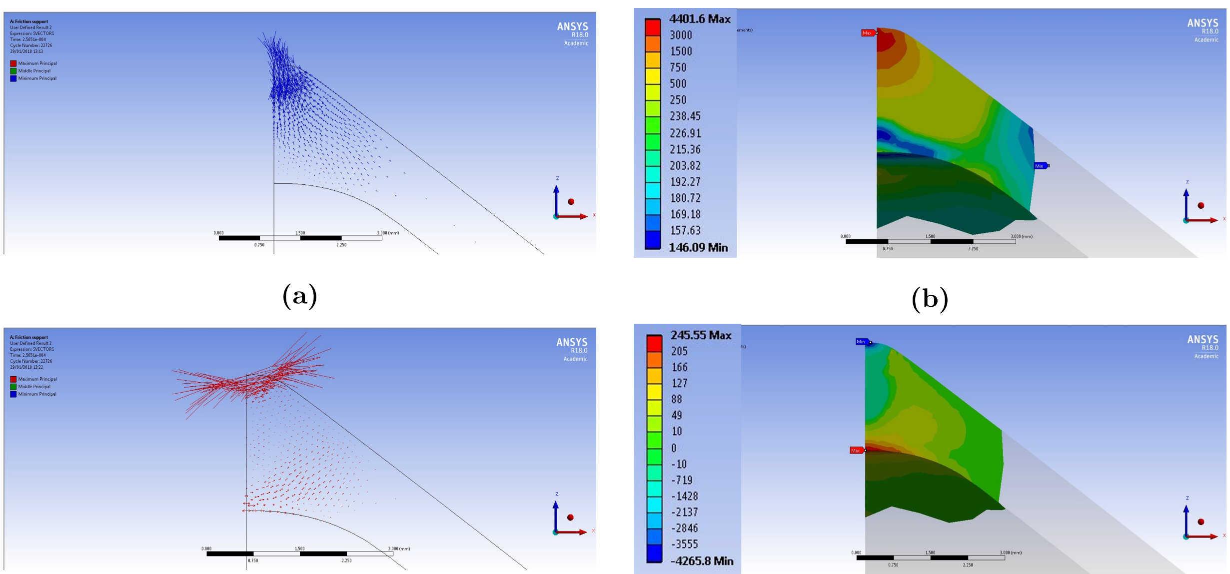

(a) (b)

(c) (d)

Figure 44: Stress concentration and direction in the apex region: (44a) minimum principal stress vectors; (44b) Von Mises equivalent stress in the apex region; (44c) maximum principal stress vectors; (44d) maximum principal stress in the apex region. Stresses are expressed in MPa.

Further attention is given to the stresses in the apex region, as around 90% of the cracks are found in this area. Almost all the cracks observed are due to the delamination process taking place between different layers of the structure; it is therefore of great importance to further investigate if the stresses perceived get along well with it. In detail, shear stresses are analysed finding values on the transversal plane four times higher than the ones on the sagittal one.

For further investigations the xz plane (τ_{xz}) is considered, where z is the vertical direction x the horizontal one (Figure45a). Tilting such a plane around its orthogonal direction by a variable angle, it has been found than the shear stresses get closer and closer to the maximum shear stress (τ_{max}) as the angle approaches 38°, which is the steepness assigned to the shell walls (Figure45b). Even more interesting is the fact that the maximum values are found in the upper half of the apex area where cracks are normally found (Figure40).

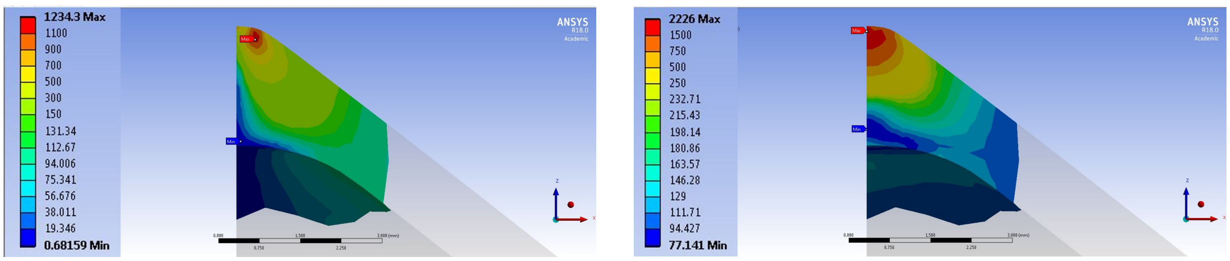

(a) **(b)**

Figure 45: Shear stress on the apex area: (45a) shear stress in the xz plane, where z is the vertical direction and x the horizontal one; (45b) maximum shear stress. Stresses are expressed in MPa.

The comparison of the stress distribution evaluated and the damage observed experimentally provides comforting results; although full match is not found (Figure46).

- Maximum shear stress is evaluated in the upper area, where long delamination cracks can be noticed in the majority of the observed specimens;
- Height stress concentration are noticed at the tip where the pull out of the apex superficial layers takes place in the experiment;
- Considerable tensile stresses are measured in the lower part of the apex region, accordingly to the region where spalling phenomena is observed.

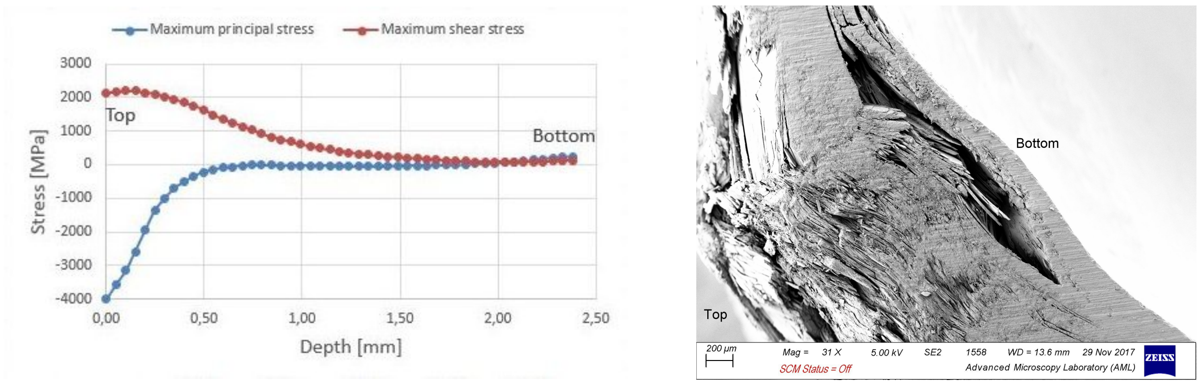

(a) (b)

Figure 46: Validation of the experimental results at the apex: (46a) maximum shear and principal stresses along the vertical direction at the apex; (46b) apex SEM image of a specimen impacted with $0.3J$.

As considerable values of tensile stresses were noticed in the rim region, further analysis were performed. The traction felt in the region happens to be in the circumferential direction (Figure47a). This behaviour fits perfectly with the physics of the impact since when the shell is compressed the rim gets wider. The traction felt at the rim is reduced as we move from the rim towards the apex as predictable from the geometry (Figure47b).

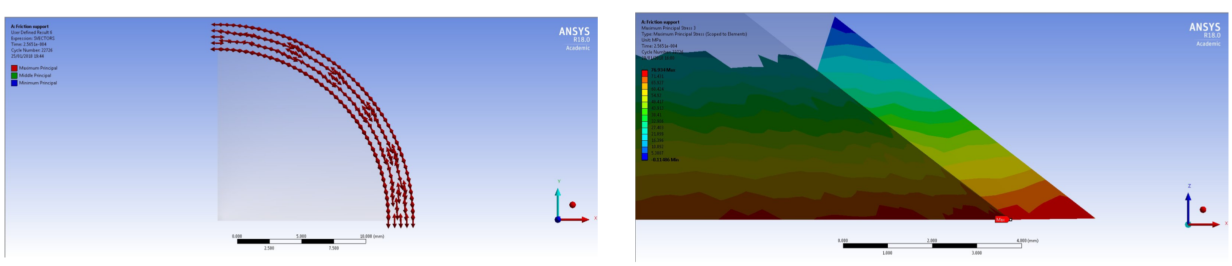

(a) (b)

Figure 47: Stress concentration and direction in the rim region: (47a) maximum principal stress vectors; (47b) maximum principal stress contours.

In order to better investigate how the stresses change along the radial direction, results are extracted from a path that goes from the apex to the rim at mid-depth inside the shell structure (Figure48a). It is chosen far away from both outer and inner surface in order to avoid local stress concentration caused by the geometry of the model. In addition some of the SEM images obtained pointed out that this region at the centre of the apex is the one where delamination cracks are generated.

A compressive stress and a shear stress around $400MPa$ are coherent with the experimental findings. As we move away from the apex the shear stress is decreasing until it is almost null at the rim where delamination cracks are absent[52]. The maximum principal stress is more complicated as it increases until tensile behaviour in the apex neighbourhood (from 1 to $5mm$ around the apex), then it decreases to zero and increases once more at in the last few millimetres from the rim (Figure48b).

It is very interesting to notice how the stress distribution inside the shell model matches with the microscopical structure described by Ortiz et al.[38]. Stress is concentrated in the areas where calcite phase is dominant, while it is much less relevant where there is the aragonite one. Analogous differences can be noticed in the shell thickness, as the areas where stresses are concentrated maximum thickness is typically measured in healthy limpets (Figure20b). It seems therefore that limpets fight stress concentrations with aragonite structure and enhanced thickness.

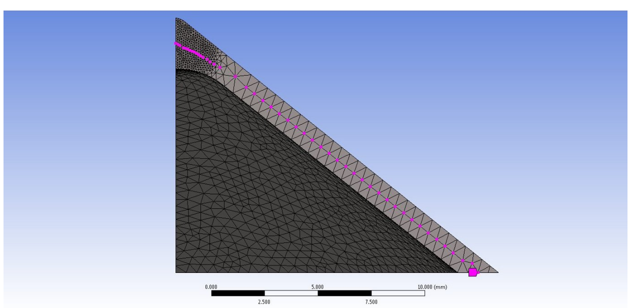

(a)

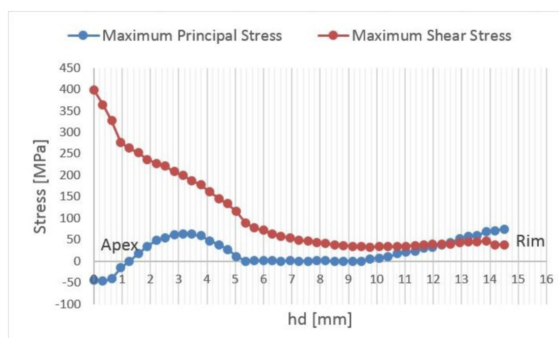

(b)

Figure 48: Stress variation along the radial direction: (48a) nodal path selected to extract stress values along the radial direction; (48b) maximum shear and principal stress along the radial direction, plotted versus the horizontal distance from the apex (hd).

Shell-support contact plays a major role in the stress distribution around the rim. In particular, decreasing the value of friction coefficient the σ_1 increases proportionally (Figure49). No differences are noticed in terms of shear stress. Varying the impact energy simply emphasises or reduces the behaviour already described in the shell (Figure51). No more information is provided. Differences can be noticed in the apex region as its thickness is modified. Having a thicker apex results in a spread stress on a larger area even if the tensile behaviour on the inner surface seems enhanced, maybe to ease the spalling mechanism (Figure50).

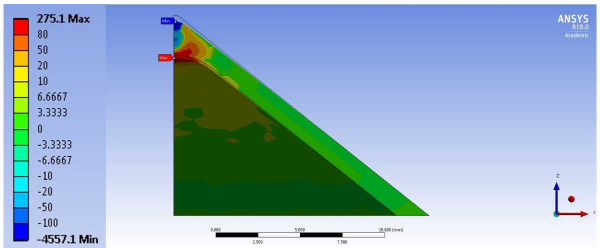

(a)

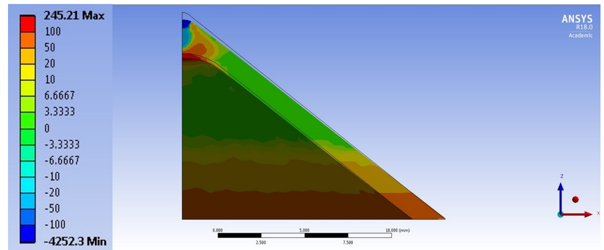

(b)

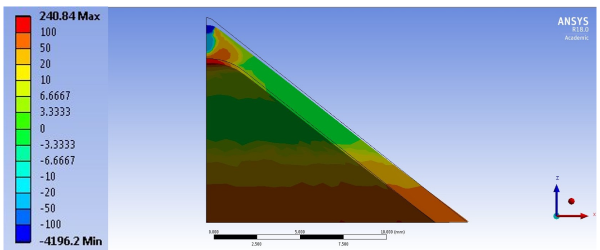

(c)

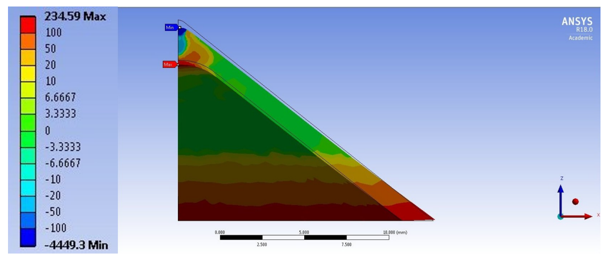

(d)

Figure 49: Friction coefficient effect: maximum principal stress for (49a) ∞, (49b) 0.5, (49c) 0.3 and (49d) 0 friction coefficient between shell and support. Stresses are expressed in MPa.

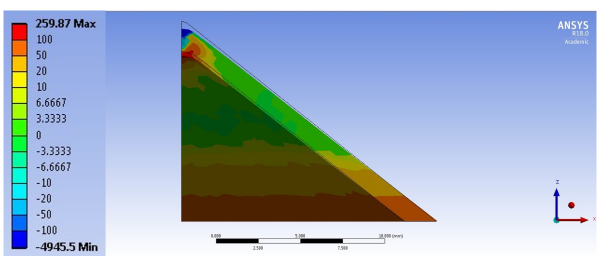

(a)

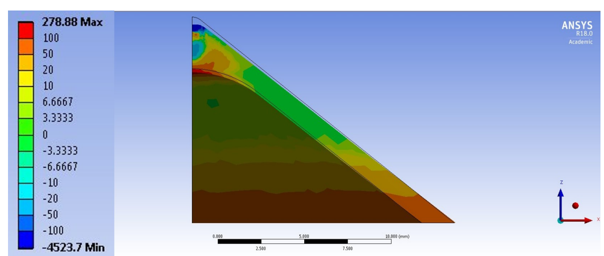

(b)

Figure 50: Apex thickness effect: maximum principal stress for apex (50a) 1.5 and (50b) 2.5 times thicker than the sideways walls. Stresses are expressed in MPa.

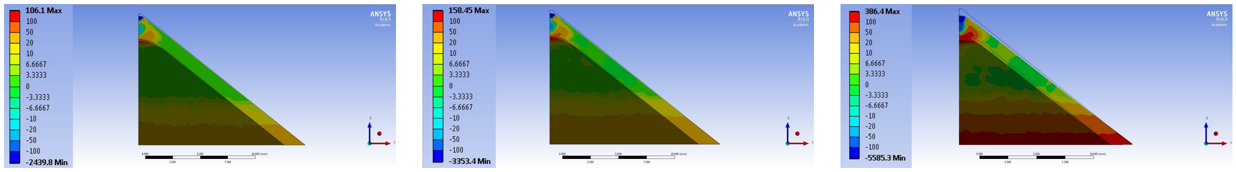

(a) **(b)** **(c)**

Figure 51: Impact energy effect: maximum principal stress for impact energy (51a) 10%, (51b) 20% and (51c) 100% the critical value. Stresses are expressed in MPa.

5.3.2 Compression simulation

A critical element is represented by the weight(piston)-shell contact. Due to the small portion of surface involved in it (Figure52a), the convex shape of the shell and the impressive amount of force applied ($1000N$) penetration becomes a major problem. The use of a refined mesh in the contact region other than a carefully designed relationship between the two bodies generated an acceptable value of penetration, around $0.01mm$ (Figure52b).

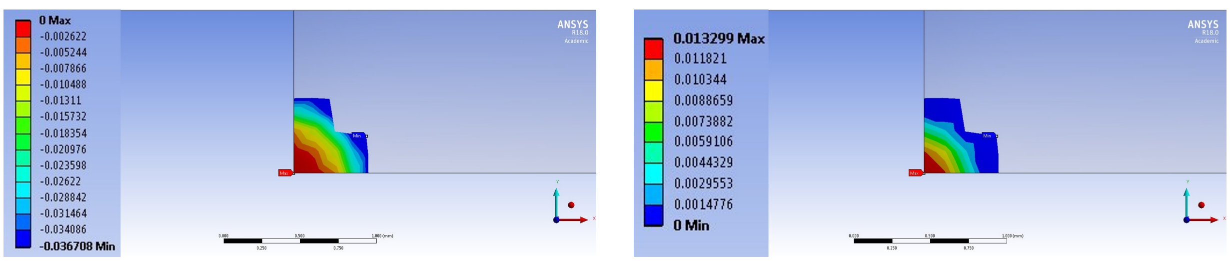

(a) **(b)**

Figure 52: Contact status: (52a) gap between the two bodies in the contact area; (52b) penetration observed between piston and shell. Both gap and penetration are expressed in mm.

A similar physical response to the one described for the impact is expected in compression condition. The shell is crushed under the vertical compressive load applied in the apex, so that the maximum deformation is felt at the apex tip and is around $0.2mm$ (Figure53a). As we move away from the apex region, the vertical deformation component is drastically reduced. The horizontal one directed outwards appears as we approach to the rim instead (Figure53b). As already described, the rim is getting wider under the load applied.

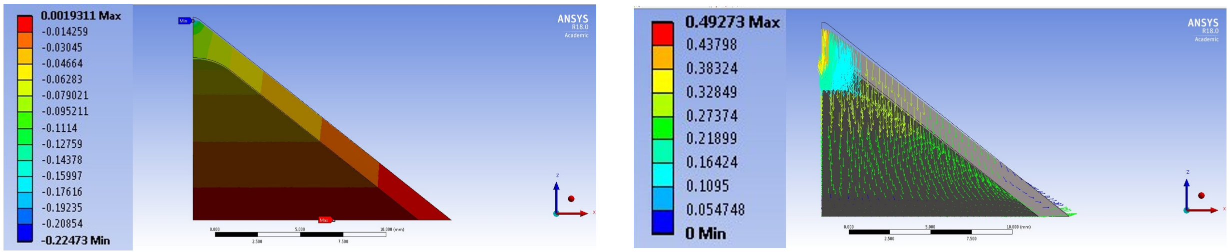

(a) **(b)**

Figure 53: Shell deformation under compression: (53a) vertical deformation contours; (53b) deformation direction inside the shell. Deformations are expressed in mm.

The displacement experienced at the tip of the shell is plotted under the instant load applied for some of the crushed shells (Figure24). The initial and final part of the load-displacement curves obtained experimentally are not considered. Initially the piston is not properly in contact with the shell and no load is transferred to the structure. At the end of the test great variability appears due to the damage accumulation inside the structure. For the purpose of the analysis both parts were deleted and compared with the results obtained modelling the Young modulus as $18GPa$ and $50GPa$. It is shown that $18GPa$ better fits the experimental results (Figure54), proving the accuracy of the information found in literature.

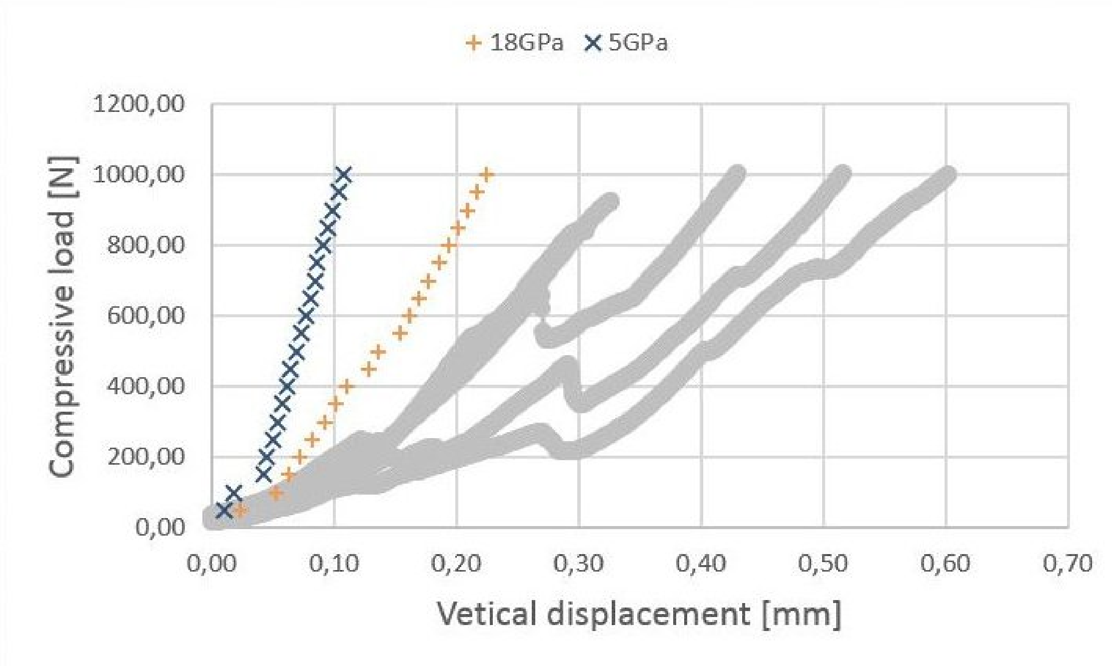

Figure 54: Compression curves comparison: load-displacement values obtained for a Young modulus of $18GPa$ and $50GPa$ are overlaid on the compression test results.

Table6 shows the same comparison in terms of curves slope. Slopes obtained through compression tests for subcritical maximum compressive load, approximately $250N$, are added. These specimens did not experience any damage and the curves appear more linear.

	Test (250N)	Test (1000N)	Model (18GPa)	Model (50GPa)
Load/displacement [N/mm]	2360	2300	4090	6990

Table 6: Compression slope comparison: load-displacement slope obtained experimental using a maximum load of $250N$ and $1000N$ compared to the ones obtained through numerical model for a Young modulus of $18GPa$ and $50GPa$.

The stresses evaluated in the dynamic and static model are different. What is more interesting is to compare qualitatively the stress field in the two situations inside the shell model. σ_{eq} and τ_{max} behaviour do not seem to reveal any difference with respect to the one already evaluated in the impact situation (Figure55c and 55d). The analysis of σ_1 points out some unexpected tensile behaviour around the apex tip, other than a reduced stress close to the internal surface (Figure55a and 55b).

The high values of tensile stress measured at the tip are probably enhanced by the hexahedral mesh that slightly bends under the applied load and that causes the maximum principal stress to increase. The reduced tensile stresses in depth could be a relevant in terms of understanding differences spalling mechanism between dynamic and quasistatic tests. None of these observations however are useful in understanding differences observed experimentally between the compression and the impact test. As matter of fact, limpet shells show a great strength, regardless of the presence of the animal inside, the wetting condition or the experiment surface only when they are impacted.

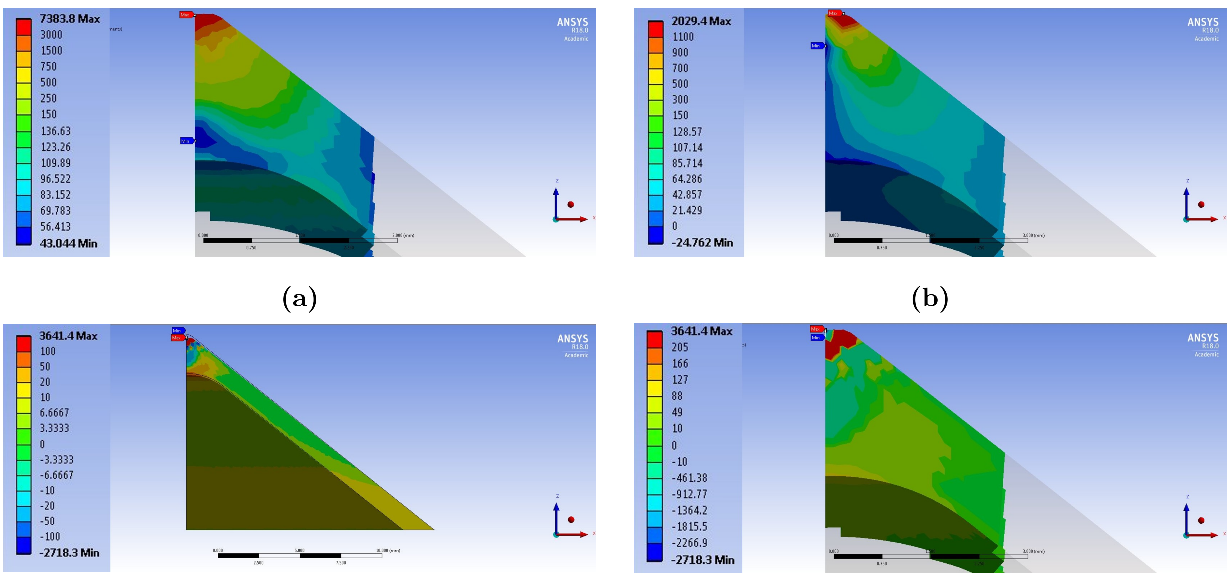

(a) (b)

(c) (d)

Figure 55: Stress distribution inside within the apex: (55a) Von Mises equivalent stress;(55b) shear stress in the xz plane; (55c), (55d) large and close view of the maximum principal stress distribution. Stresses are expressed in MPa.

5.4 Toughness

5.4.1 Delamination crack

Poor quality curves are obtained if the rim is not grounded before being impacted (Figure56a), so that the excessive scatter noticed would most certainly jeopardize the results. The reason for such a behaviour is found to be in the presence of an uneven rim. On the other hand, compression curves obtained after the impact are much smoother and unexpectedly stiffer (Figure56b) as consequence of the rim flattening. For this reason the specimens used for the study are all grounded, obtaining the expected behaviour both before (Figure56c) and after (Figure56d) the impact.

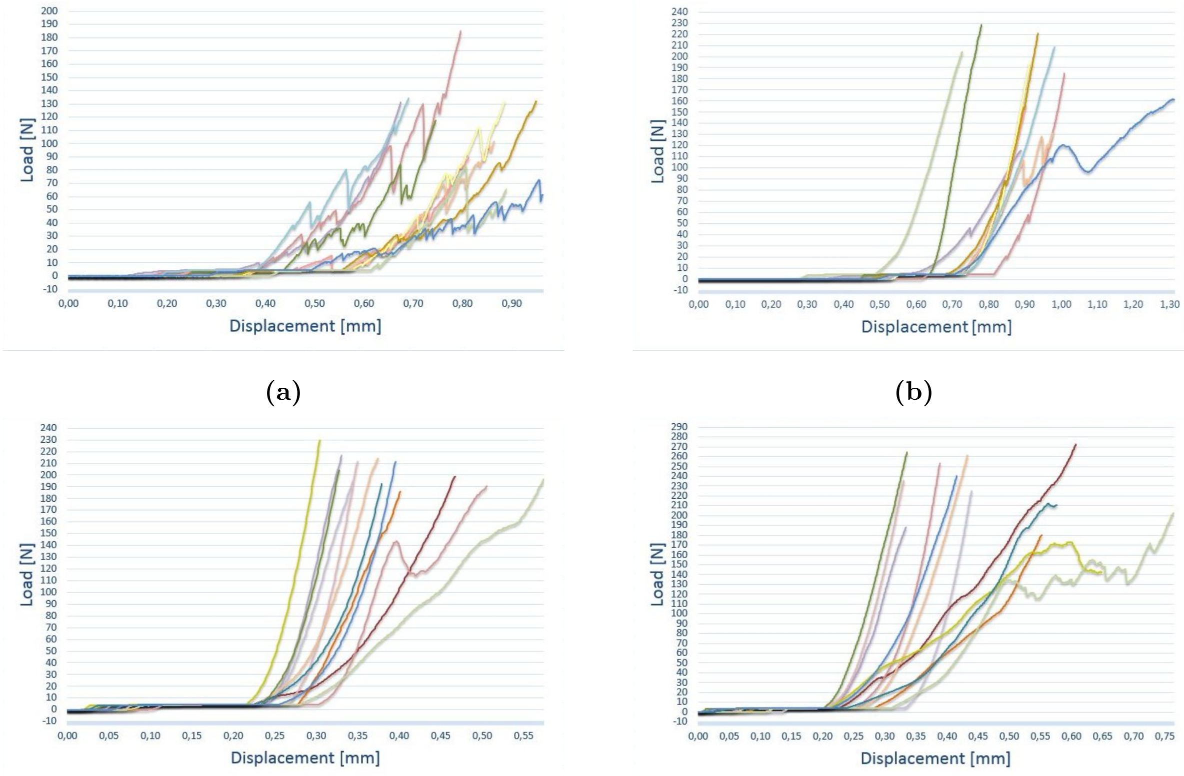

(a) (b)

(c) (d)

Figure 56: Rim grinding effect: (56a), (56b) load-displacement curves before and after the impact for non ground specimens; (56c), (56d) load-displacement curves before and after the impact for the ground specimens.

As for the compression tests that reached the failure point, the initial phase of the compression is removed. Among the tested specimens used nine behaved as expected[49]. Load grows steeper before rather than after the impact (Figure57a), which means that the energy involved in the first compression is higher than the one in the second compression. Two shells behaved the opposite (Figure57b). Finally, one specimen has not been considered for the evaluation as a sudden drop in the load was noticed during the first compression (Figure57c), since it means that some damage was already present in the specimen before the impact test could be performed.

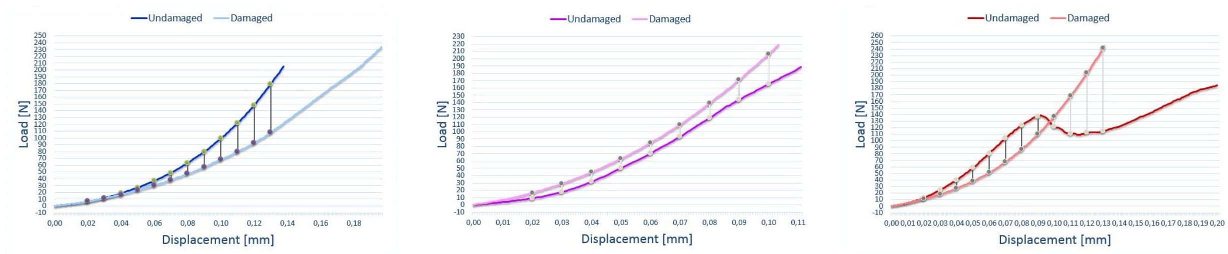

(a) (b) (c)

Figure 57: Compression test observed outcomes: (57a) example of expected behaviour with higher energy involved in the the compression of the undamaged specimen (not impacted yet); (57b) example of unexpected behaviour with higher energy involved in the compression of the damaged specimen (already impacted); (57c) neglected specimen because of a load drop can be seen in the undamaged condition.

Instead of evaluating the energy lost in the impact as the ratio between the areas, the ratio between the curves slope is considered instead. The reason behind this choice lies in the shape of the curves measured and their variability. Since the load does not increase linearly with the displacement, the area ratio changes depending on the displacement considered. In addition, there is a noticeable variability in shells stiffness, so that the time required to reach a certain load is not the same for every shell but subjected to considerable differences. These problems are bypassed using the slope ratio of the best-fit regression lines. In addiction it is noticed that the ratio of the two areas quickly approaches the value obtained slope method as the displacement increases (Figure58).

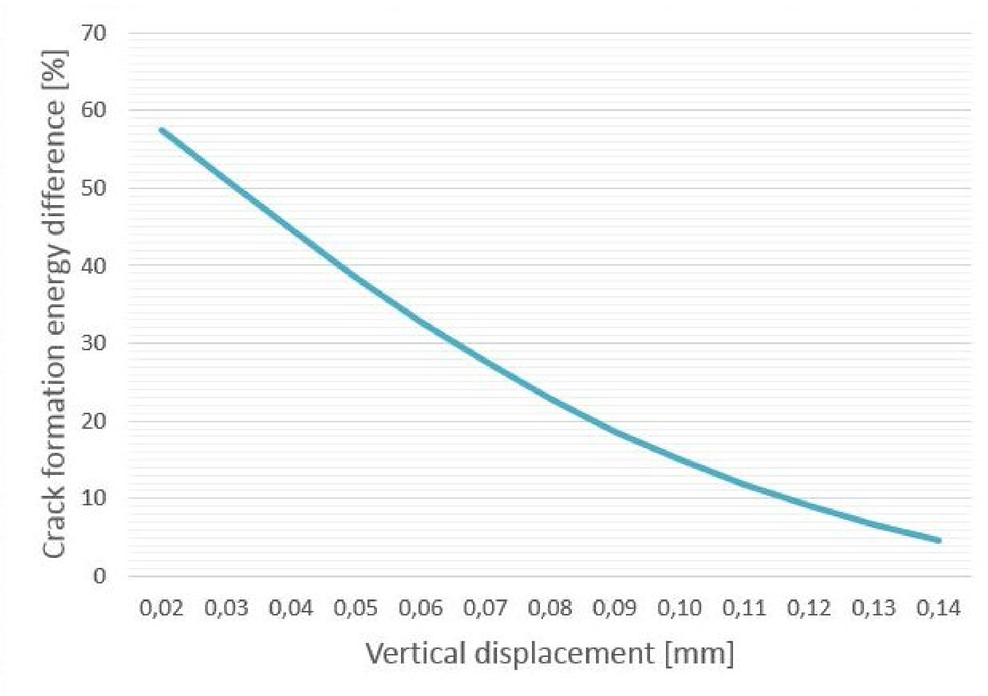

Figure 58: Convergence plot: difference between the measure of the amount of energy involved in crack formation process using the areas approach and the measure using the slopes approach, as the the piston moves downwards crushing the shell. Both the energy measures are expressed as percentage of the total applied energy.

Each of the shells tested[4] give a value of energy loss expressed in percentage over the total applied energy (Figure59). Some variability is found in the results obtained as described previously and no statistical correlation is found between the shell size and the amount of energy stored in the structure during the impact. The average of the results obtained for the single specimens gives a final value of 27%.

[4] All except for the one showing a sudden fall in the load.

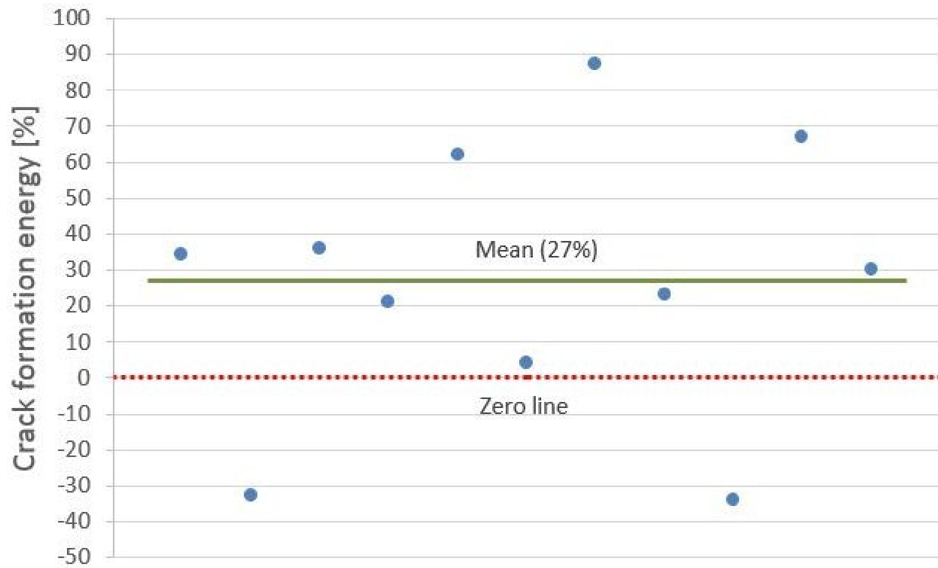

Figure 59: Energy stored in the crack formation for each specimen: results obtained for the tested shells. In green is highlighted the mean value of approximately 27%, in red the zero line points out two negative values, which are nothing but the specimens showing unexpected behaviour.

The mean value found as described is used to update the G_c assessed previously. In detail, the percentage of the E_{app} in the crack formation process is evaluated and such a value is used obtain G_c with equation3). Table7 shows the mid step as well as the final result of the delamination toughness evaluation procedure.

Energy applied (10%) $[J]$	0.25
Energy applied (20%) $[J]$	0.35
Energy involved in crack generation (10%) $[J]$	0.07
Energy involved in crack generation (20%) $[J]$	0.13
Crack area (10%) $[mm^2]$	630.11
Crack area (20%) $[mm^2]$	1096.17
Critical strain energy release rate (G_c) $[J/m^2]$	146.66
Critical stress intensity factor (K_c) $[MPa\sqrt{m}]$	1.60

Table 7: Critical stress intensity factor evaluation: relevant steps in the the fracture toughness evaluation for the delamination analysis.

5.4.2 Radial crack

The introduction of a sharp notch in the model modifies considerably the stress distribution in the neighbourhood (Figure60). The σ_{eq} shows a peak of stress around the notch tip, while the σ_1 point out that it is a tensile stress. Having a look at the stress intensity (difference between σ_1 and σ_3) an analogue response to the σ_{eq} one is obtained. This last information is indicative of a very directional stress in the crack front.

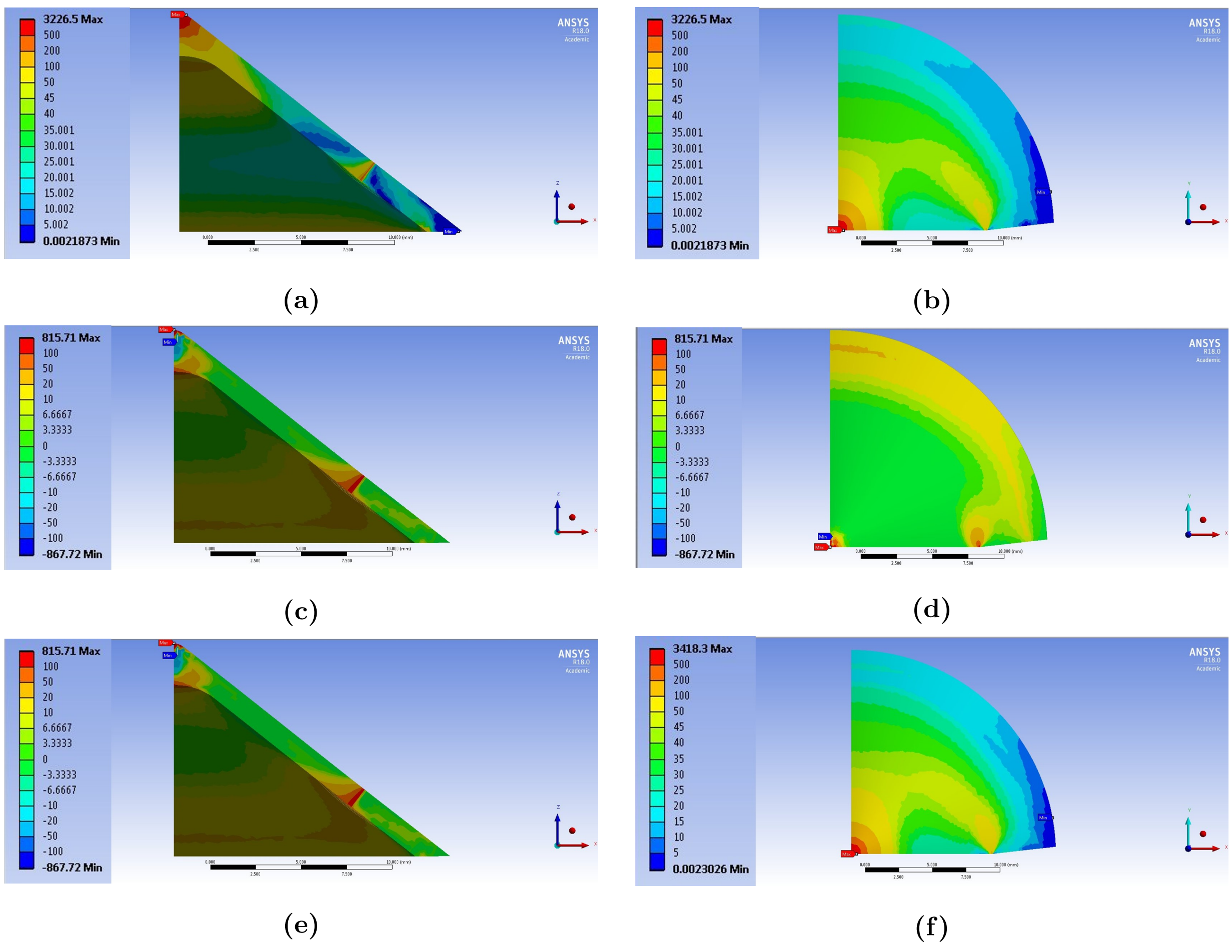

Figure 60: Stress distribution in the full model: (60a), (60b) Von Mises equivalent stress; (60c), (60d) Maximum principal stress; (60e), (60f) Stress intensity, difference between maximum and minimum principal stress. Stresses are expressed in MPa.

Moving closer to the area of interest it can be observed how stresses decrease as we move away from the crack tip, where a peak of almost $500 MPa$ is reached. The rate at which stresses decrease gets higher and higher as we move in depth (Figure61a); on the other hand it shows a maximum approximately in circumferential direction (Figure61b). Giving a further look at σ_1 vectors it seems clear that the notch is opening under the compressive load (Figure61c) and that the same effect is felt in the notch neighbourhood (Figure61d).

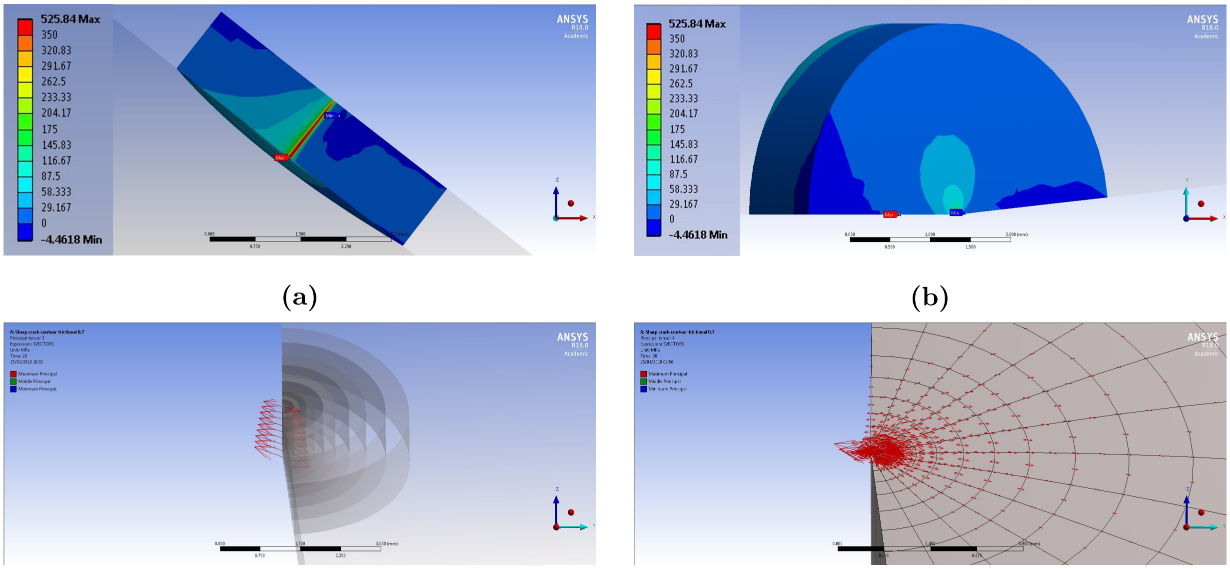

(a) **(b)** **(c)** **(d)**

Figure 61: Maximum principal stress in the crack area: (61a), (61b) contour description of the area; (61c), (61d) direction of the stresses at the tip. Stresses are expressed in MPa.

As already noted, stress propagation from the notch tip appears very directional. Stress concentration in one direction suggests that a crack is encouraged to grow from the notch tip in that direction rather than in any other. K_{Ic} evaluation for angles between 0° and 180° from the radial direction of the notch shows a defined pattern. K_{Ic} evaluated increases as the angle increases until a maximum is reached around 73° (Figure62), before decreasing again.

Changing the shell-support friction coefficient and repeating the same procedure, the same behaviour is observed simply shifted towards higher values of K_{Ic} as the friction is reduced. The maximum allowable value is clearly obtained when the contact is modelled as frictionless. A frictionless condition is not realistic; friction coefficient of 0.3 or 0.5 could be more reliable instead. For these value of friction K_{Ic} obtained is around $6MPa\sqrt{m}$ which are physically acceptable values but not coherent with the ones already obtained and certainly not coherent with the real material behaviour.

Magnitude aside, the crack preferential growth direction does find a match in the experimental results. Cracks running almost circumferentially are often observed during compression tests of shells with a notch caved at the rim[52]. This means that the approximated geometry of the model is enough to justify the fracture behaviour of the structure.

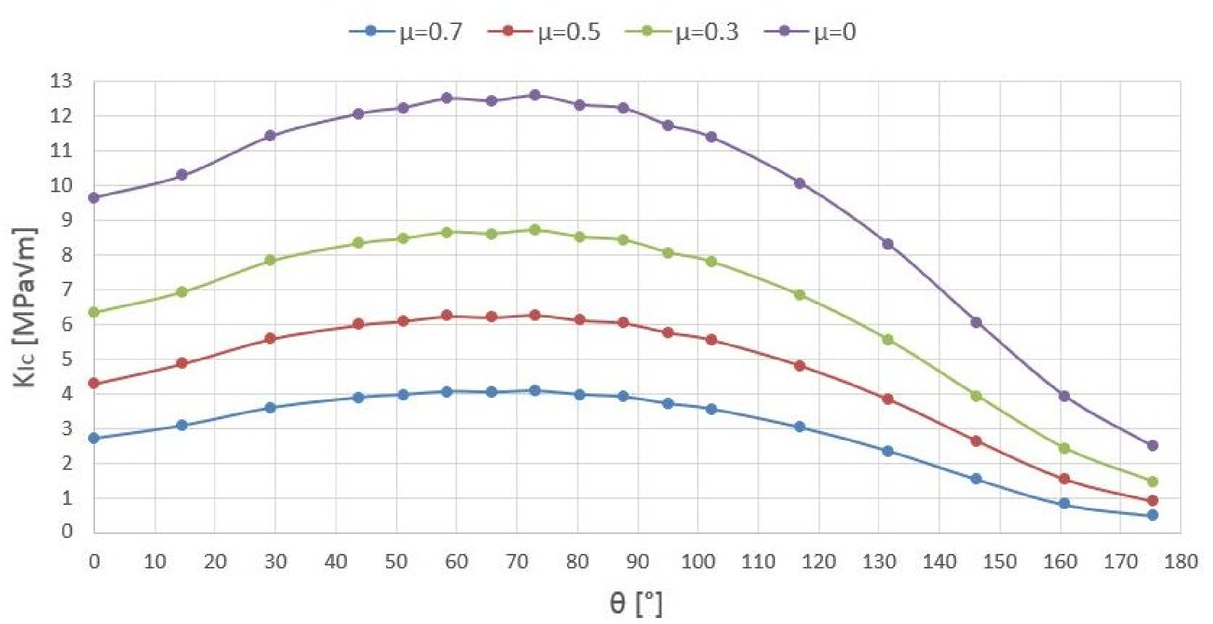

Figure 62: Crack propagation direction: stress intensity factor evaluated between 0° and 180° (θ) around the notch tip, and considering friction coefficient of 0, 0.3, 0.5 and 0.7.

The stress pattern obtained for 73° at half depth in the shell wall, is plotted (Figure63). Great adherence is found with the behaviour described by equation6 showing that the approximation used to assess K_{Ic} is extremely accurate.

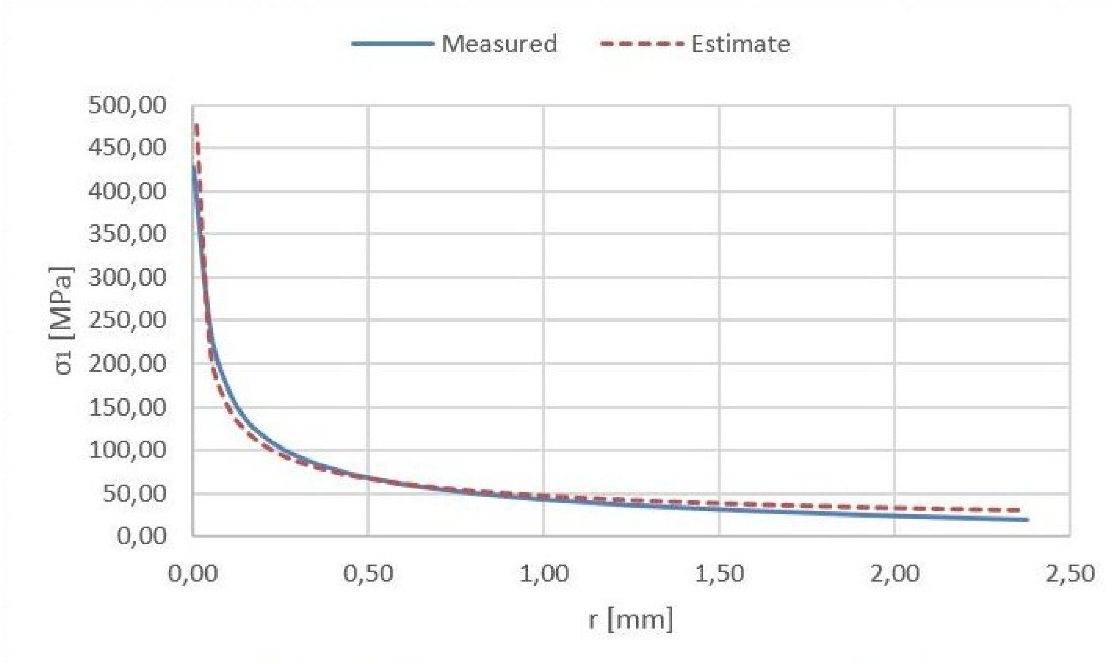

Figure 63: Stress distribution approximation: Maximum principal stress pattern moving away of the notch tip at 73° compared to the approximation made using equation6. Where r is the distance from the notch tip.

Since the stress distribution is not constant moving through the shell thickness, evaluating the K_{Ic} for different depths gives a complete view of how it changes. In this situation the variation is approximately linear (Figure64), proving that the value obtained at mid-depth actually gives a good approximation of the structure behaviour in a given direction.

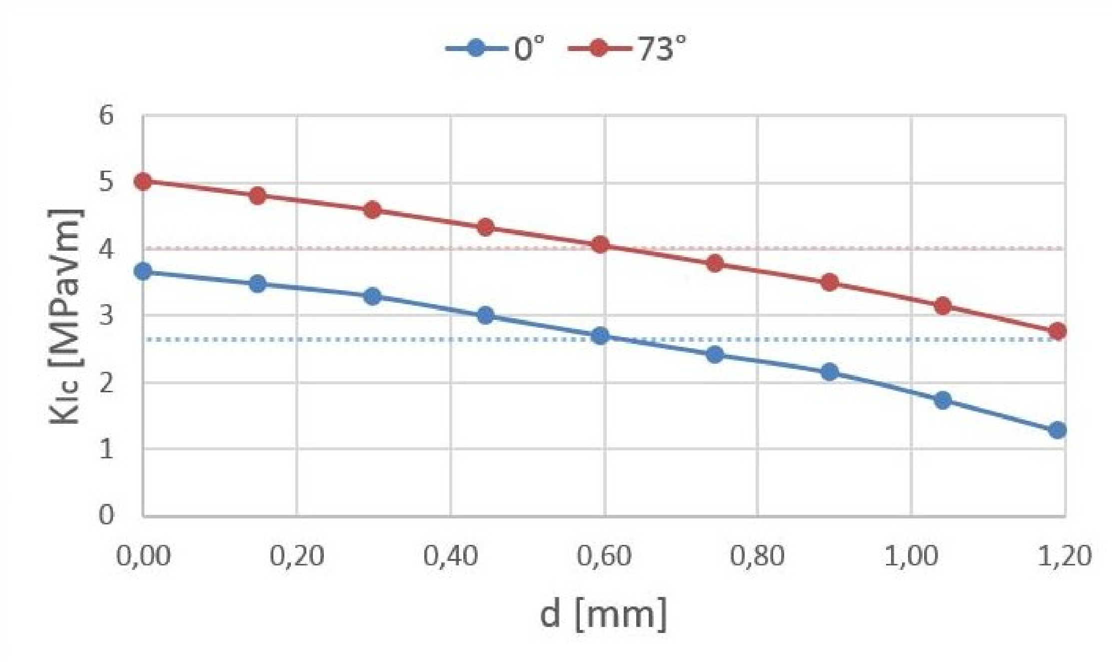

Figure 64: Stress distribution in depth: Stress intensity factor evaluated for different depth (d) in the shell walls at 0° and 73° from the crack direction. Dashed lines represent the average of the stress intensity factors evaluated along the thickness.

Findings change completely if the contact with the support is modelled as fixed (Figure65). Stress concentration around the crack is drastically reduced; the maximum principal stress at the crack front is in the order of few MPa, instead of hundreds. Only $0.2mm$ away from the notch tip the behaviour is dominated by the stresses coming from the apex and the rim. This situation turns out to be much more sensible to Young modulus (E) and Poisson ratio (ν) values. E affects only quantitatively the stress perceived at the crack tip, while ν induces a compression condition at the tip of the shell (Figure65c). The opening mechanism showed previously is restricted to the lower part of the notch tip, overruled by a general compressive status.

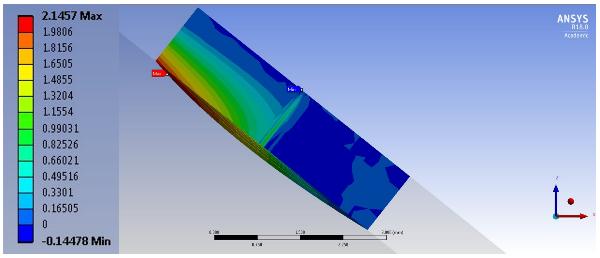

(a)

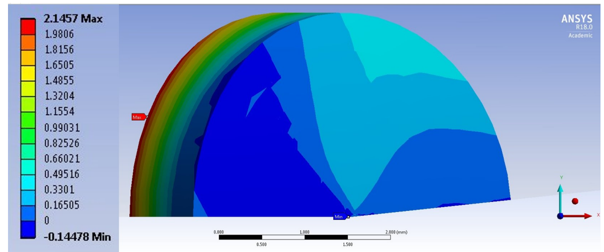

(b)

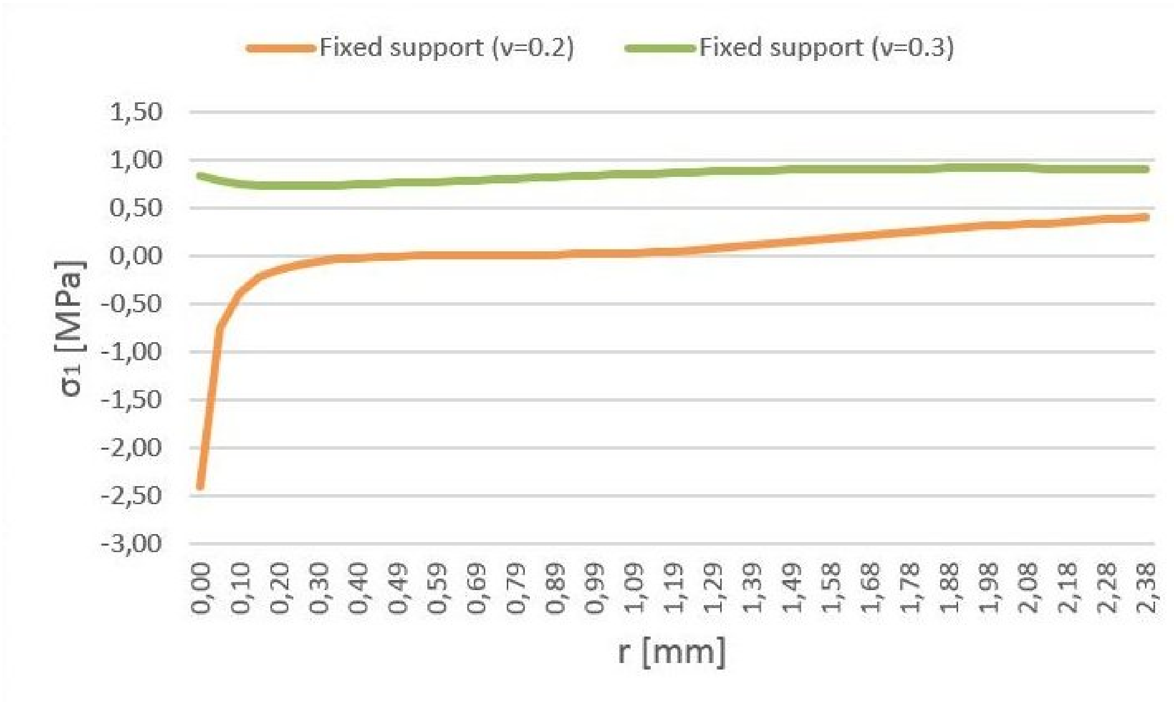

(c)

Figure 65: Maximum principal stress at the crack tip, modelling the shell fixed to the support: (65a), (65b) contour description of the stress condition; (65c) Poisson ratio effect on the stress distribution, values of 0.2 and 0.3 are plotted. Where r is the distance from the notch tip. Stresses are expressed in MPa.

Either increase or decrease for the apex thickness generated slightly higher stress intensity factor. On the other hand, the application of a distributed load does not affect at all the K_{Ic} evaluated in the original situation (Figure66). Finally, a change in the apex geometry or in the application area do not meaningfully affect what is happening around the notch, such that similar values of K_{Ic} are evaluated and the maximum is found to be always in the same direction (around 73° from the notch direction).

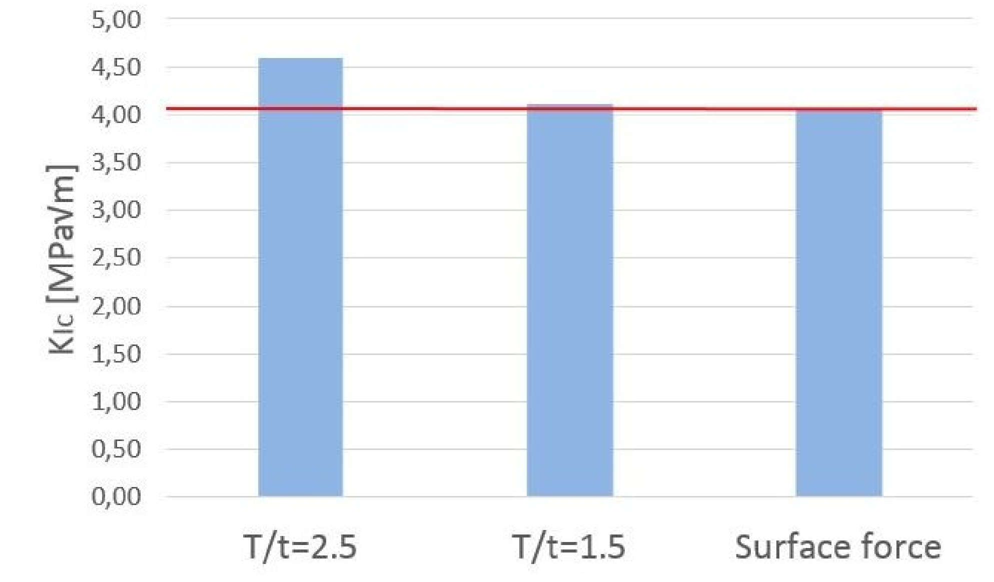

Figure 66: Apex thickness and load application effect on shell toughness: stress intensity factor obtained at 73° for thickness ratio (T/t, where T is the thickness of the apex and t is the one of the sideways walls) of 2.5 and 1.5 and for distributed load. The red line is the value obtained in standard condition.

The evaluation of K_I, K_{II} and K_{III} revealed that in plane shear and out of plane shear are negligible with respect to the opening mechanism which is extremely similar to the one obtained at 0 for the maximum principal stress shown in Table8). These results are not surprising, they simply prove quantitatively that, as the shell is compressed, the notch tends to open wide and that the use of the maximum principal stress for the fracture toughness evaluation is reasonable.

$K\ (\sigma_1)\ [MPa\sqrt{m}]$	$K_I\ [MPa\sqrt{m}]$	$K_{II}\ [MPa\sqrt{m}]$	$K_{III}\ [MPa\sqrt{m}]$
2.71	2.48	0.21	0.0001

Table 8: Stress intensity factor for the three modes compared to the one obtained using the maximum principal stress.

6 Discussion

6.1 Impact strength

The metabolic processes that are taking place inside the damaged limpets were not studied during the tests; the expected thickening of the apex is not proved due to difficulties in performing accurate measurements. There is therefore no direct proof that repairing is actually taking place inside the limpets. Nevertheless, impact tests findings shows clear evidence that the mechanical response is improving over time and approaching the original value after two months. A similar or longer period was expected to be seen as previous studies already showed macroscopical proof that drilled specimens were able to mend the damage in a similar time[45], [46].

The impact strength estimate increase over time for all the tested groups (abraded, impacted and pierced) similarly approaching, never reaching it though, the control value ($8.06 MJ/m^{4.6}$) which is the one found for empty shells tested by Taylor[47]. The main result is however that no statistical difference can be observed between the values obtained after two months and the control one. It does not only mean that the repair is actually happening, but also that after two months these animals have the same chances to survive an impact with a moving pebble as one of the undamaged limpets living in the surrounding shore. Pierced shells after two months shows a sensibly smaller impact strength estimate than the other two groups (6.07 against 7.05 and 7.55 $MJ/m^{4.6}$) and is characterized by a wider uncertainty. Once again, it is a comforting result since not all the specimens belonging to the pierced group had the same time to repair themselves as for the other two groups.

Differences can be noticed in how impact strength repairing happens between abraded and impacted shells. Abraded shells lose the sacrificial role played by the apex[47] showing a sudden drop in the mechanical response; something that does not happens in impacted shells, that maintains a better strength after the first impact. This behaviour was already noted; what was not noted is that abraded shells go through an impressive improvement after only $10 days$, and that after two months they show better performance than any other group.

It must be noted however that in both groups the repairing process seems designed to restore the initial abilities and not to improve them. Other natural structures however, when damaged are used to heal themselves enhancing their ability to resist to future damage as for the insect cuticle[23].

It is clear comparing the numerical results that both abraded and impacted shells keep improving their mechanical behaviour but at much lower speed than in the first month. The evidence of such a behaviour is found comparing performances at different resting periods. Meaningful difference is indeed observed comparing the results at $60days$ with the ones at 0 or $10days$ but not the ones at $30days$, as consequence of the reduced repairing rate after the first month.

Abrasion and piercing do affect shell strength in an analogous fashion. In both cases a considerable drop is seen immediately after the damage and in both cases almost full recovery is reached after two months. Comparing the results obtained at zero days it seems clear that removal of material from the apex region by abrasion or drill reduces the impact strength by approximately one quarter. As soon as the damage is moved sideways from the apex shell performances are not as bad. Such a behaviour is easily predicted since the impact happens exactly in that area. The amount of scatter recorded for shells pierced off-center is caused by the combination of several factors: the wide size range, the not repeatable hole size, the variable distance from the centre and even the hole location with respect to the asymmetric geometry of the shell. Nevertheless the impact strength is reduced to one third for this group, which means that the inaccurate location of the hole for the shell pierced in situ and then repaired should not significantly affect the results.

6.2 Fatigue

The aim of the work was simply to increase the fatigue data including piercing limpets and the presence of a repairing mechanism. Results do confirm the poor fatigue performance noticed by Taylor[47]. Even though it was not the main purpose of the work, differences can be noticed between the behaviour of pierced and impacted shells. Fatigue performances are not enhanced by the repair mechanism; on the other hand they are considerably affected by the type of pre-damage applied. The presence of a hole, especially when it is off-center generates unexpected behaviour either in positive and negative direction.

The great variability observed is consequence of the impact energy adopted. The use of $0.5J$ as fixed value for all shell size, inevitably generated inaccurate results for the shells slightly larger than the critical length. These shells failed easily after two impacts generating a relevant peak in the fatigue plots. This is a relevant limitation for the study, not enough however to affect the result of the tests. As matter of fact the most important results are the ones obtained for bigger shells since they are the ones that require a higher of Nf for a fixed energy applied, which narrows the meaningfull data to right hand side of the fatigue plot. Once again, Nf increases proportionally to the E_n without finding a knee for low values of energy like some materials (steel, bone, glass)[49], [22].

It is not even surprising that pierced shells with badly reduced impact strenth show a better fatigue behaviour than the impacted and the healthy ones. The accumulated energy is indeed way higher than its impact strength and more similar to the one of the control group, especially as the number of impacts increases. An analogous behaviour has already been noticed by Taylor[47] for shells collected on the beach. These specimens after being separated from the animal have to face extensive damage in the apex region as consequence of sand blasting, resulting in a very similar behaviour to the abraded one. This comparison is very meaningful because it proves once again that the presence of a hole in the apex region does not only affect the specimen response to a single impact like the abrasion phenomena does, but also its response to consecutive subcritical impacts.

Shells impacted cyclically present much more controversial results. The main compromising issues are the hurricane Ophelia nefarious effects and the indirect failing mechanism occurring before a real failure. The hurricane damages are not easy to calculate: some of the limpets tested went simply missing within a week and it is not clear how the future behaviour of the survived specimens is altered by it. Missing and found broken specimens may not be able to withstand further impacts as consequence of the heavy damages caused by Ophelia. There is no practical evidence that the two phenomena are related, it is however not possible to exclude a scenario where none of the results obtained for this study is reliable. However possible, it is more probable that indirect failure observed in many limpets is not only a hurricane implication. This phenomenon would more likely have happened with or without Ophelia, since the same damaged condition would have been reached even without it, only a few weeks later.

By comparison with the control group, it is proven without a shadow of a doubt that the disappearing phenomena is a consequence of the impact sessions. Only one of 46 shells monitored during the four months but never impacted went indeed missing, even though they were very close to the tested limpets and belonged to several different rocks. The most likely explanation is that as the limpets overcome a certain amount of structural damage, without being able to repair themselves properly, predation and wave caused impacts become a way bigger danger, compromising their safety. From a certain point of view, even the missing phenomena states the specimen failure since these limpets are clearly not able to survive in their own environment any longer. It is not the outcome we were interested though, since the aim of the study was to obtain useful information on their impact failure. The enhanced missing mechanism right before reaching the critical energy is not a reliable information, since it is not known how far these limpets really are from their fatigue failure point.

The use of a longer interval between following impacts seems to postpone the start of the missing phenomena and to avoid larger shells dying prematurely. Such differences are reduced as the test proceed. On the other hand, the combination of a shorter recovery time and higher energy emphasises the average size decrease over time as well as the indiscriminately loss of shells during the whole study. It seems like for higher energy and shorter time, the animals are not able to slow down the damage accumulation, especially the ones larger than $40mm$.

Consistent amount of damage is observed within the specimens tested, so that some of the survivors brought to the lab to be examined collapsed during the preparation step. Nevertheless it is clear from the SEM analysis how the damage proceeds in terms of preferential regions and directions. Delamination cracks are highly concentrated in the central-upper part of the apex; the longest and more visible one is very often observed to be starting from the outermost region of the apex and grows towards the shell front for instance. Spalling phenomenon systematically takes place in all the specimens tested, no matter what energy or time interval are used. The presence of a portion of internal layers that is not completely detached from the rest of the structure allowed to see that these portions fall off entirely, without experiencing delamination.

6.3 Computational modelling

Compression status dominates the shell structure throughout the whole simulation as expected. Experimental findings showed extensive damage to happen strictly in the contact region, where approximately 75% of the total number of cracks observed with the optical microscope are in the apex neighbourhood[52]. This behaviour is confirmed by simulation results since the shock wave generated from the contact region propagates at very slow rate towards the surrounding area, causing stress concentration in the apex region of the model. The sacrificial role of the apex suggested by Taylor[47] matches with the results obtained, since a combination of concentrated load and slow stress propagation is generated in the approximated model. The slow propagation is a not only due to the geometry: a relevant role is played by the material stiffness ($18GPa$)[51] relatively small compared to the nacre ($90GPa$)[28] and the stainless steel one ($200GPa$).

It is relevant to point out the preferential propagation direction of the shock wave. The vertical load applied is almost instantaneously redirected in the radial direction and travels along the structure until it reaches the support (at least a small portion of it). Even though the material is considered as homogeneous and its anisotropy is not modelled, it is clear that the radial direction is the preferential direction for the shock wave to propagate. Looking at the apex region right below the impact area, very low compressive stress is observed. The compressive wave does not move straight vertically but reaches the inner surface at short distance from the apex, where a compressive peak can be seen. From this point on it better propagates along the inside surface than the outside one.

A tensile stress is perceived in the lowest section of the apex region. This behaviour perfectly matches with results obtained during impact tests, in which spalling takes place. This phenomenon is characterized by thin layers of material that fall off the inside surface of the structure. Material detachment is however used to happen in a confined area around the apex, very similar indeed to the one where enhanced tension is observed in maximum principal stress analysis. The meeting point of the compression wave propagating from the contact region and the tensile one rising from the internal surface may be at the origin of the spalling process.

Crack distribution observed in the cross section finds its equivalent in the shear stress analysis performed computationally. Impressive levels of shear orthogonal to the surface normal direction are found directly below the contact region. Impact does not only generate vertical compression in the apex upper area, but horizontal delamination between the calcite layers too. Maximum shear is experienced orthogonal to the vertical direction in the central region of the apex, then it tilts aligning with the shell walls as we move upwards, reaching a global maximum near the top. Once again, these results fit the experimental observations since the majority of the cracks are found to be horizontal in the central area, while the longer ones are found closer to the upper surface and grow within the shell in the radial direction. The lack of delamination in the lower apex region cracks observed in the SEM analysis similarly matches with the shear stress minimum found computationally. For a complete description a few cracks are observed to run close to the internal surface near the apex in some specimens; it must be noticed however that in all these cases a massive fall off is experienced, causing consistent modifications in the local stress field.

The presence of a much more complex structure than the one modelled makes it hard to understand if the stress distribution observed in the model really takes place in the specimen tested. It is hard to tell for instance whether the tensile stress generated in the area nearby the apex really happen or not. It is even more complicated to tell if it has any contribution in the generation of the conical shape of the collapsed region during failure.

Approximations in terms of base ellipticity and eccentricity[58] imply that the shock wave generated propagates uniformly in all directions, preventing the model to predict the preferential damage observed in SEM images. Experimental findings observed preferential delamination that the model is not able to predict due to the approximations made. The geometry asymmetry may have a relevant role establishing differences in stress distribution during impact and during compression. The presence of a very rough outer surface is not replicated at all in the model but loads are obviously applied on the outer surface, as it is in natural impacts. The fact that the uneven topology is not replicated on the inner surface, very smooth indeed, could be a hint that surface roughness may be relevant for an accurate description of the shell mechanical response.

The least stressed region of the whole structure is found to be at midway distance between apex and rim. Such a behaviour is extremely relevant if compared to internal structure of Patella vulgata shell and its thickness variability. Aragonite structure and thin walls occur in this very location[38], suggesting that the computational solution does not only fits with experimental results but even with micro and macroscopic heterogeneity of the structure. In the outermost area (rim) the stress increases again as consequence of the frictional contact with the support underneath. The choice of a lower friction coefficient proved to increase considerably the tension sensed at the rim. This effect is due to the fact that the vertical deformation felt in the apex region gets reoriented horizontally at the rim so that sliding is a major factor in the contact between shell and the support.

Modifications in the contact area or in the impact energy affect the stress entity perceived within the apical region, but they do not modify the overall behaviour of the structure.

No meaningful changes are observed comparing static and dynamic behaviour, showing that the shell reacts very similarly in the two situations. Some interesting features are observed in the apex area, including a tensile peak close to the contact area and a reduced stress condition on the inner surface of the apex. The first issue is probably a faulty behaviour caused by the elements adopted for this simulation together with the presence of a concentrated load. The second one is actually more interesting: tensile stress in the lower region of the apex has been related to the presence of spalling phenomena, so that its reduction could stand for a lower effect in static situation. Finally, no macroscopic difference is observed in the shell response as the dynamic terms are neglected, do not providing a valuable match with the experimental results that showed enhanced behaviour in the dynamic condition[47].

On the other hand, the compression simulation using the E measured by Currey[51] fairly approximates the behaviour observed during the crushing tests. A higher value of E typical for other Gastropoda species is definitely overstiffing the solution. The purpose of the study was to check if the value obtained from literature would be able to describe properly the behaviour of the structure, especially in quasistatic condition. The value obtained by Currey was measured on rectangular wet specimens of the shell subjected to a bending test. Different properties are however observed under compression in previous works testing wet and dry shells[58], [30], although the amount of organic component within the structure is very limited (around 1%) . Testing a full specimen instead of a small sample of it is also a relevant factor that could not have been underestimated.

6.4 Toughness

The evaluation of the correction factor for the crack generating energy led to a reasonable value of 27%, around one third of the impact energy. A large amount of scatter in the solution is observed since two specimens behaved at the opposite of the expectations, providing backfiring results. The source of variability should be found in the procedure followed, since accurate instruments and repeatable measurements are adopted. The problem is mostly related to the inherent differences of the tested specimens. Size, shape, previous damage, grinding procedure as well as the application of a single low subcritical energy impact could have unpredictable effects on the shell response. Nevertheless, the estimate obtained by the tested shells is reliable enough to be compared with the one found in circumferential durection by Taylor[52] and in other materials as nacre[27],[33].

The procedure adopted is most certainly the best one in terms of physical description of the phenomena. As matter of fact it is the curve slope that contains the information about the amount of energy involved during the compression, since the area measurement is heavily affected by the variability produced by the contact areas as well as the initial position of the piston. The fact that no trend can be observed in the results obtained for different shells as the size increase does not mean that the shell size does not affect the amount of energy involved in the crack formation but simply that it is not the only factor.

The corrective term obtained produces a value of toughness of $1.62MPa\sqrt{m}$. Against initial expectations the value obtained is higher than the one obtained in the circumferential direction ($0.98MPa\sqrt{m}$), yet not impossible. Delamination represent the main failure mechanism and produces cracks that show a much smoother behaviour than the ones generated through thickness in circumferential direction. It was therefore assumed that a lower energy would be is involved in the delamination process, contrary to what is observed numerically. The difference is however quite narrow considering that two completely different methods are applied to evaluate it. If compared to values obtained for other materials however it does not seems unreasonable. Nacre shows a K_{Ic} way higher $4.3MPa\sqrt{m}$. Although such a difference is much reduced comparing the G_{Ic}, $146J/m^2$ versus $264J/m^2$ of the nacre[27], it seems still a reasonable value.

The FEM analysis produced the expected behaviour in the notch region. As the shell is compressed against the support, the rim diameter is expanding. Since the notch is designed to start from the rim, tensile stresses pulling it on both sides are observed. As consequence, the crack is destined to propagate by opening mechanism (Mode I). The presence of a sharp tip increases even more the stress concentration at the notch front ($500MPa$), allowing a more precise measure of the toughness. The value K_{Ic} evaluated ($4.06MPa\sqrt{m}$) is certainly excessive, although it suits very well the numerical results and a higher value than the ones obtained in the circumferential direction was expected . As matter of fact this value is very similar to the one evaluated for the nacre, which is a world wide famous material for its enhanced toughness. The result is even worse if we express it in terms of G_{Ic}, since it relies on the material Young modulus, and Patella vulgata is approximately four times softer than nacre.

The friction coefficient modelled for the contact with the support plays a major role on the results obtained; in short, the lower the friction coefficient the higher the toughness measured. The results described earlier are obtained for a friction coefficient of 0.7 which is an overestimation of the real friction, which means that the real toughness would be even higher. Professor Taylor[52] estimated the friction coefficient to be around 0.44 obtaining a toughness value of $5.65 MPa\sqrt{m}$ using linear regression.

In conclusion, the procedure followed using the computational model does not give reliable quantitative results. One of the reasons why it happens shall be found in the several simplifications used. The assumptions of a homogeneous structure and an even outer surface may have a major effect in producing misleading results. Various numerical approaches involving contour integration are already implemented inside numeric solver. Results obtained generally investigating the notch neighbourhood are however clear enough to make further complex analysis pointless if the implemented model is maintained unchanged.

A very low value of toughness would be assessed considering the shell as fixed to the support. This situation does not reflect the experimental impact condition but is much more similar to the in situ one, where various mechanisms (biological and mechanical) work together to keep the animal attached on the rock. In this situation the rim does not deform, reducing massively reducing the opening mechanism described earlier, so that compression is observed shortly ahead of the notch tip. Such a condition happens to be much more sensible to the variation of other parameters like Young modulus and the Poisson ratio. A ν of 0.3 appears even less prone to let the crack advance any further. It is no wonder that none of the specimens tested in situ failed with a crack born from a defect in the rim.

On one side it is undeniable that the numerical outcome is misleading, on the other a quantitative approach lead to sufficiently accurate results. The stress distribution described by the model solution around the notch tip is nicely described by the model and finds a match in the experimental findings. The crack propagation direction in the model appears to be inclined of 73° respect to radial direction against the 63° measured experimentally by Tayor[52]. As matter of fact compression tests of shells with a sharp notch at the rim, equivalent to the one modelled computationally, showed a crack propagating almost circumferentially in the shell structure. Minor or null variations in the toughness measures are observed as changes are applied to either the apex geometry or the load application surface. This behaviour is once more comforting since crack propagation does not depends on far field stress, but simply on the local geometry and material properties assigned to the body.

7 Conclusions and future works

7.1 Impact strength

After two months no significant difference can be noticed between the control group and the pre-damaged specimens, regardless of the type of damage initially provided. Nevertheless, the impact strength found still does not match with the undamaged shells one. A meaningful improvement of the impact strength compared to zero days is observed in all groups. The repair speed observed in the first month changes accordingly to the type of pre-damage performed. For longer repair times the impact strength approaches the control group one with speed that decreases more and more.

Hole generation in the apex region critically affects the impact strength of the specimens. Similar behaviour is found only in abraded specimens, either artificially using a file or naturally by the sand. Hole location is proved to be meaningful for the impact behaviour but not repeatable. Off-center holes do increase the strength of the shells; the way it happens is however affected by great variability due to the qualitative nature of the piercing procedure.

A complete overview is obtained on how limpet shells respond to impact from a mechanical point of view. A full understanding on how the repairing process happens was not the purpose for the present work. Further studies could however be performed in the future to analyse the biochemical reactions and the structural changes that operates within the structure at different repairing times and compare them with the increasing impact strength.

7.2 Fatigue

The poor fatigue performances observed in limpet shells do not improve in repaired specimens. Pierced shells have comparable behaviour to the ones collected on the beach. The critical accumulated energy is well above their impact strength and further increases together with the number of impact to failure, approaching the impact strength for the healthy shells. The use of fixed impact energy does affect only the accuracy and reliability of failures happening within a few impacts. Larger size specimens do fail after several strikes giving a reliable failure energy.

A clear answer can not be given to the limpet fatigue performances during cyclical impacts. No specimens failed during the impact sessions and the accumulated energy reached at the end of the experiments overcame the critical value, suggesting enhanced fatigue behaviour. The impressive amount of missing and found broken specimens as the accumulated energy approaches the critical value makes the output unclear. The combination of a very short recovery time and a high impact energy shows a better behaviour for small limpets and spreads the beneficial effect of the healing process (if there is any) during the whole test. Longer repairing time delays the point where shells start to go missing and reduces the amount of delamination experienced by the specimens.

The main limitations of the present study is represented by the choice of working on an open system. The natural environment introduces too much variability to be able to obtain consistent and incontrovertible results. Impacting living organisms on a more controlled environment could avoid this problems. On the other hand, further modifications in the applied energy as well as in the repairing time would not affect the results.

7.3 Computational modelling

Shell geometry is shown to have a vital importance in the definition of damage and consecutive failure mechanisms. Apex sacrificial role, spalling phenomena, delamination cracks and apex collapse are all reflected in the stress distribution obtained thanks to the simplified model. Material microstructure and shell irregular shape matches the stress field measured in the model as well. Aragonite and calcite arrangement on one hand and a variable thickness on the other play the main role in order to meet the mechanical requirements. A thicker apex implies a stress and strain distribution over a larger area, reducing stress concentration and eventually enhancing mechanical strength. The friction coefficient plays a major role in the describing the rim region behaviour. Differences observed between the static and the dynamic simulations are not enough to describe the different experimental behaviours. The adopted value of Young modulus matches the experimental behaviour.

For even better solutions, capable of describing quantitatively the dynamic and the compressive response, it would be interesting to remove some of the approximations adopted. One option would be to retrieve a specimen specific geometry using micro CT technique and to perform new simulations using the same set up already described. One more step could be to realize a ceramic shell (modelled trough CAD or obtained from Micro CT) using a 3D printing technique, and impact it as usual. This procedure would allow to investigate the shape contribution on shell mechanical performances separately from the effect introduced by its microstructure. Detailed studies could be performed on the apex area to further investigate the spalling process and compare the results with experimental findings obtained through high frame rate cameras and advanced microscopy techniques.

7.4 Toughness

Only 27% of the applied energy is found to be involved in crack formation, meaning that two thirds of the applied energy is transferred to the support. A G_{Ic} of $146J/m^2$ and a K_{Ic} of $1.6MPa\sqrt{m}$ are evaluate to describe the delamination toughness of the material. These values are reliable if compared to the ones found for well established materials like nacre.

In the radial direction the computational approach lead to a K_{Ic} of $4.06MPa\sqrt{m}$. Although it is not unreasonable it is a very impractical value considering that a Young modulus of $18GPa$ would lead to a G_{Ic} of $925.75J/m^2$ which is far too big considering the experimental observations and the values known for established materials. Although the numerical evaluation is not acceptable, a height toughness value in radial direction was expected. Finally, the overall behaviour is comparable to the one observed experimentally, finding a good match especially in the crack propagation direction.

Several approximations were adopted when modelling shell geometry. These approximations are probably the main source of inaccuracy for the numerical results obtained. Once more a possible solution could be to use Micro CT technique to obtain a much more realistic geometry for the SEM simulations. Although shells are made of very brittle material (especially when dried), the characterization of the damping behaviour could affect the results too. Further study of the shells damping ability could represent another future development.

8 Acknowledgements

First of all I want to thank professor Cristina Bignardi for the amazing opportunity she offered me. I owe a great thank you to professor David Taylor from Trinity College of Dublin, not only for the opportunity given, but also for his countless advices and his crucial assistance, especially when my work seemed to have reached a dead end. Thank you to Maeve O'Neall for the fundamental help during the whole work and for the enthusiasm, the energy, the pragmatism and the expertise that she showed every single day. Finally I would like to thank Clodagh Dooley of the Advanced Microscopy Laboratory, as well as Peter O'Reilly, Michael Reilly and all the workshop of the Parsons Building for their help.

Personal thanks:

- To my family, for their endless support, and to physics that avoid apples to fall to far away from their tree;
- To my "Friends", that are always here on my side, no matter for how long I do not text them or how many Saturday night I do not show up;
- To my university comrades, for sharing with me moments of hard engineering student life as well as the ones of stress relief;
- To all my BESTie friends all over Europe, for the unique experiences we shared;
- To my new Irish friends, that shared the last part of my studying career escorting me during my green mile;
- To all my room mates, both in Italy and in Ireland, for the time we spent studying, playing, singing, arguing, drinking, discussing, joking but most of all sharing a piece of our lives.

I would like to end up with few honourable mentions:

- To my parents, for all the looks of disapproval, soft smirks, playful pushes, troubled expressions, tired snorts and light scratches that literally made my days. My gratitude goes beyond all the words in the universe, I though prefer to rely on my beloved sound of silence, that is able to carry every message since it knows no limits or bottom;
- To Damiano, for all the embarrassing hugs and the proud looks that cheered me up and that made me question the "The Big Brother Theory";
- To my grandparents, for being always on my side to comfort me and to guide me every step I take, regardless of the fact that they are still in this world or in the next one;
- To Sofia, who grabbed my message in the bottle and shows me every single day what lives on the dark side of the moon making me richer, making be better;
- To Gabriele, a day may come when I will get tired of this man when I will forsake him and break all bounds, but it is not this day, this day I thank him as a friend, as a room mate, as a brother;
- To Paola, there are people you find and people you choose, she is both to me, so thank you for never giving up on me and for her constant presence;
- To Sebo and Leo, everyone is able to laugh when things are going well, few people though are able to laugh even when there is nothing to laugh for; so thank you for sharing great moments with me and for fighting for our personal "One Piece".

Although I have high hopes, I might break bad, either way I want to live a life as an archer aiming high to reach my goals.

References

[1] **BAR-COHEN, Yoseph**. Biomimetics — using nature to inspire human innovation. *Bioinspiration & Biomimetics*, March 2006, vol. 1, i. 1, p. 1-12.

[2] **HWANG, Jangsun, et al**. Biomimetics: forecasting the future of science, engineering, and medicine. *International Journal of Nanomedicine*, September 2015, vol. 10, i. 1, p. 5701-5713.

[3] **HARKNESS, Jon M**. In appreciation. A lifetime of connections: Otto Herbert Schmitt, 1913-1998. *Physics in Perspective*, December 2002, vol. 4, i. 4, p. 456-490.

[4] **RIPLEY, Renee L.; BHUSHAN, Bharat**. Bioarchitecture: bioinspired art and architecture — a perspective. *Philosophical Transactions of the Royal Society of London A: Mathematical, Physical and Engineering Sciences*, June 2016, vol. 374, i. 2073, p. 20160192.

[5] **KIM, Zae-Geun**. An outline of Korean shipbuilding history. *Korea Journal*, October 1989, vol. 29, i.10, p. 4-17.

[6] **LEPORA, Nathan F.; VERSCHURE, Paul; PRESCOTT, Tony J**. The state of the art in biomimetics. *Bioinspiration & Biomimetics*, March 2013, vol. 8, i. 1, p. 013001.

[7] **GAO, Huajian, et al**. Mechanics of hierarchical adhesion structures of geckos. *Mechanics of Materials*, February-March 2005, vol. 37, i. 2-3, p. 275-285.

[8] **RAUT, Hemant Kumar, et al**. Gecko-inspired dry adhesive based on micronanoscale hierarchical arrays for application in climbing devices. *ACS Applied Materials & Interfaces*, December 2017, vol. 10, i. 1, p. 1288-1296.

[9] **KWAK, Moon Kyu; JEONG, Hoon E.; SUH, Kahp Y**. Rational design and enhanced biocompatibility of a dry adhesive medical skin patch. *Advanced Materials*, July 2011, vol. 23, i. 34, p. 3949-3953.

[10] **OEFFNER, Johannes; LAUDER, George V**. The hydrodynamic function of shark skin and two biomimetic applications. *Journal of Experimental Biology*, February 2012, vol. 215, i. 5, p. 785-795.

[11] **MARTIN, Samuel; BHUSHAN, Bharat**. Modeling and optimization of shark-inspired riblet geometries for low drag applications. *Journal of Colloid and Interface Science*, July 2016, vol. 474, p. 206-215.

[12] **GAO, Lichao; MCCARTHY, Thomas J**. The lotus effect explained: two reasons why two length scales of topography are important. *Langmuir*, March 2006, vol.22, i. 7, p. 2966-2967.

[13] **PATANKAR, Neelesh A**. Mimicking the lotus effect: influence of double roughness structures and slender pillars. *Langmuir*, August 2004, vol. 20, i. 19, p. 8209-8213.

[14] **WAHL, Daniel**, *Designing regenerative cultures*, Axminster, UK: Triarchy Press, 2016. ISBN 978-1-909470-77-4.

[15] **Biomimicry.sciencerays.com**. Science Copies Natures Secrets. [online]. 2018. [Accessed 2 March 2018]. Available from: `http://biomimicry.sciencerays.com/`.

[16] **BAO, Min, et al**. Electrospun biomimetic fibrous scaffold from shape memory polymer of PDLLA-co-TMC for bone tissue engineering. *ACS Applied Materials* & *Interfaces*, January 2014, vol.6, i. 4, p. 2611-2621.

[17] **IZUMI, Hayato, et al**. Realistic imitation of mosquito's proboscis: electrochemically etched sharp and jagged needles and their cooperative inserting motion. *Sensors and Actuators A: Physical*, January 2011, vol. 165, i. 1, p. 115-123.

[18] **MEYERS, Marc A., et al**. Biological materials: structure and mechanical properties. *Progress in Materials Science*, January 2008, vol. 53, i. 1, p. 1-206.

[19] **JONES, Robert M.**, *Mechanics of composite materials*, $2^n d$ edition, Philadelphia, PA: Taylor & Francis, 1999. ISBN 1-56032-712-X.

[20] **BHUSHAN, Bharat**. Biomimetics: lessons from nature — an overview. *Philosophical Transactions of the Royal Society of London A: Mathematical, Physical and Engineering Sciences*, March 2009, vol. 367, i. 1893, p. 1445-1486.

[21] **DOOLEY, Clodagh; TAYLOR, David**. Selfhealing materials: what can nature teach us? *Fatigue* & *Fracture of Engineering Materials* & *Structures*, February 2017, vol. 40, i. 5, p. 655-669.

[22] **OBRIEN, Fergal J.; TAYLOR, David; LEE, T. Clive**. Microcrack accumulation at different intervals during fatigue testing of compact bone. *Journal of Biomechanics*, July 2003, vol. 36, i. 7, p. 973-980.

[23] **PARLE, Eoin; DIRKS, Jan-Henning; TAYLOR, David**. Bridging the gap: wound healing in insects restores mechanical strength by targeted cuticle deposition. *Journal of The Royal Society Interface*, April 2016, vol. 13, i. 117, p. 20150984.

[24] **DIRKS, Jan-Henning; TAYLOR, David**. Fracture toughness of locust cuticle. *Journal of Experimental Biology*, April 2012, vol. 215, i. 9, p. 1502-1508.

[25] **TAYLOR, David**. Fracture Mechanics: Inspirations from Nature. *Frattura ed Integrit Strutturale*, September 2014, vol. 30, p. 1-6.

[26] **CURREY, John D.; TAYLOR, John D**. The mechanical behaviour of some molluscan hard tissues. *Journal of Zoology*, July 1974, vol. 173, n. i, p. 395-406.

[27] **JACKSON, A. P.; VINCENT, Julian F. V.; TURNER, R. M**. The mechanical design of nacre. *Proceedings of the Royal Society B: Biological Sciences*, September 1988, vol. 234, i. 1277, p. 415-440.

[28] **BARTHELAT, Francois, et al**. On the mechanics of mother-of-pearl: a key feature in the material hierarchical structure. *Journal of the Mechanics and Physics of Solids*, February 2007, vol. 55, i. 2, p. 306-337.

[29] **LI, Xiao. W., et al**. Mechanical properties of crossed-lamellar structures in biological shells: A review. *Journal of the Mechanical Behaviour of Biomedical Materials*, October 2017, vol. 74, p. 54-71.

[30] **NEVES, Nuno M.; MANO, Joao F**. Structure/mechanical behavior relationships in crossed-lamellar sea shells. *Materials Science and Engineering C*, April 2005, vol. 25, i. 2, p. 113-118.

[31] **TAYLOR, David, et al**. The fracture toughness of eggshell. *Acta biomaterialia*, June 2016, vol. 37, p. 21-27.

[32] **CURREY, John D., et al**. Mechanical properties of nacre and highly mineralized bone. *Proceedings of the Royal Society of London B: Biological Sciences*, January 2001, vol. 268, i. 1462, p. 107-111.

[33] **BARTHELAT, Francois; RIM, Jee E.; ESPINOSA, Horacio D.**, *Applied Scanning Probe Methods XIII*, Edited by Bhushan B. and Fuchs H., Springer, Berlin, Heidelberg, DE:

2009, chapter 19, A review on the structure and mechanical properties of mollusc perspectives on synthetic biomimetic materials, p. 17-44. ISBN 978-3-540-85048-9.

[34] **ZHANG, Heng, et al**. Preparation of nacre-like composites by reactive infiltration of a magnesium alloy into porous silicon carbide derived from ice template. *Materials Letters*, November 2016, vol. 183, p. 299-302.

[35] **CHEN, Li, et al**. Bioinspired micro-composite structure. *Journal of Materials Research*, January 2007, vol. 22, i. 1, p. 124-131.

[36] **SCHNEIDER, Michael S**. *A beginner's guide to constructing the universe the mathematical archetypes of nature, art, and science*. Edited by Harper Perennial, $1^{s}tedition$, New York, NY: Harper Collins, 1994. ISBN 0-06-016939-7.

[37] **FITZER, Susan C., et al**. Ocean acidification alters the material properties of Mytilus edulis shells. *Journal of the Royal Society Interface*, December 2014, vol. 12, i. 103, p. 20141227.

[38] **ORTIZ, Jos E., et al**. Protein diagenesis in Patella shells: implications for amino acid racemisation dating. *Quaternary Geochronology*, April 2015, vol. 27, p. 105-118.

[39] **CABRAL, Joao P.; NATAL-JORGE, R. M.**. Compressibility and shell failure in the European Atlantic Patella limpets. *Marine Biology*, January 2007, vol. 150, i. 4, p. 585-597.

[40] **BLUNDON, Jay A.; VERMEIJ, Geerat J**. Effect of shell repair on shell strength in the gastropod Littorina irrorata. *Marine Biology*, September 1983, vol. 76, i. 1, p. 41-45.

[41] **DENNY, Mark W**. Limits to optimization: fluid dynamics, adhesive strength and the evolution of shape in limpet shells. *Journal of Experimental Biology*, September 2000, vol. 203, i. 17, p. 2603-2622.

[42] **SHANKS, Alan L.; WRIGHT, William G.**. Adding teeth to wave action: the destructive effects of wave-borne rocks on intertidal organisms. *Oecologia*, June 1986, vol. 69, i. 3, p. 420-428.

[43] **HARPER, Elizabeth M., et al**. Iceberg scour and shell damage in the Antarctic bivalve Laternula elliptica. *PLoS One*, September 2012, vol. 7, i. 9, p. e46341.

[44] **CADE, Gerhard C**. Shell damage and shell repair in the Antarctic limpet Nacella concinna from King George Island. *Journal of Sea Research*, March 1999, vol. 41, i. 1-2, p. 149-161.

[45] **FLEURY, Christian, et al**. Shell repair process in the green ormer Haliotis tuberculata: A histological and microstructural study. *Tissue and Cell*, June 2008, vol. 40, i. 3, p. 207-218.

[46] **SLEIGHT, Victoria A., et al**. Transcriptomic response to shell damage in the Antarctic clam, Laternula elliptica: time scales and spatial localisation. *Marine Genomics*, April 2015, vol. 20, p. 45-55.

[47] **TAYLOR, David**. Impact damage and repair in shells of the limpet Patella vulgata. *Journal of Experimental Biology*, December 2016, vol. 219, i. 24, p. 3927-3935.

[48] **SCHRAUWEN, Bernard; PEIJS, Ton**. Influence of matrix ductility and fibre architecture on the repeated impact response of glass-fibre-reinforced laminated composites. *Applied Composite Materials*, November 2002, vol. 9, i. 6, p. 331-352.

[49] **AZOUAOUI, Krimo; AZARI, Zitouni; PLUVINAGE, Guy**. Evaluation of impact fatigue damage in glass/epoxy composite laminate. *International Journal of Fatigue*, February 2010, vol. 32, i. 2, p. 443-452.

[50] **TAYLOR, David**. Measuring fracture toughness in biological materials. *Journal of the Mechanical Behavior of Biomedical Materials*, January 2018, vol. 77, p. 776-782.

[51] **YANG, Wen, et al.**. Structure and mechanical properties of Saxidomus purpuratus biological shells. *Journal of the Mechanical Behavior of Biomedical Materials*, October 2011, vol. 4, i. 7, p. 1514-1530.

[52] **O'NEILL, M.; CAFISO, D.; MALA, R.; LAROSA, G.; TAYLOR, D**. Fracture Toughness and Damage Development in Limpet Shells. Submitted to *Theoretical and Applied Fracture Mechanics*, 2018.

[53] **GUPTA Kajal K.; MEEK John L**. A brief history of the beginning of the finite element method. *International Journal for Numerical Methods in Engineering*, November 1996, vol. 39, i. 22, p. 3761-3774.

[54] **ZIENKIEWICZ Olek C., TAYLOR Robert L., Zhu J.Z.**, *The finite element method for solid and structural mechanics*, Edited by Elsevier, 6^{th} Edition, Oxford, UK: Butterworth-Heinemann, 2005. ISBN 0-7506-6320-0.

[55] **ROSTAMI, Sobhan; SHOJAEE, Saeed; SAFFARI, Hamed**. An explicit time integration method for structural dynamics using cubic B-spline polynomial functions. *Scientia Iranica*, February 2013, vol. 20, i. 1, p. 23-33.

[56] **Cressington.com**. Cressington Scientific Instruments. [online]. 2018. [Accessed 2 March 2018]. Available at: `https://www.cressington.com/`.

[57] **Zeiss.com**. Scanning electron microscope -SEM. [online]. 2018. [Accessed 2 March 2018]. Available at: `https://www.zeiss.com/microscopy/int/products/scanning-electron-microscopes.html`.

[58] **CABRAL, Joao P**. Shape and growth in European Atlantic Patella limpets (Gastropoda, Mollusca). Ecological implications for survival. *Web Ecology*, November 2007, vol. 7, i. 1, p. 11-21.

[59] **SUN, Eric Q**. Shear locking and hourglassing in MSC Nastran, ABAQUS, and ANSYS. *MSC Software Users Conference*, 2006, p. 1-9.

[60] **Sharcnet.ca**. Chapter 9: Hourglassing. [online]. 2018. [Accessed 2 March 2018]. Available at: `https://www.sharcnet.ca/Software/Ansys/17.0/en-us/help/ans_lsd/Hlp_L_hour1.html`.

[61] **NOLAN, Conor P**. Size, shape and shell morphology in the Antarctic limpet Nacella concinna at Signy Island, South Orkney Islands. *Journal of Molluscan Studies*, April 1991, vol. 57, i. 2, p. 225-238.

[62] **Hirvonen, J. P., et al**. Wear and Friction of Unio crassus shell in dry sliding contact with steel. *MRS proceedings*, January 2011, vol. 330.

[63] **CAFISO, Diana**, Toughness, damage and repair in limpet shells, Universit degli studi di Catania, Bachelor thesis in Industrial Engineering, academic year 2016/2017.